Magnetic Trapping and Thermal Isolation of NH Molecules Using the Buffer Gas Technique

A dissertation presented
by

Edem Tsikata

to
The Department of Physics
in partial fulfillment of the requirements
for the degree of
Doctor of Philosophy
in the subject of

Physics

Harvard University
Cambridge, Massachusetts
November 2009

Thesis advisor

John M. Doyle

Author

Edem Tsikata

Magnetic Trapping and Thermal Isolation of NH Molecules Using the Buffer Gas Technique

Abstract

Thermal isolation of trapped NH molecules is accomplished. We cool NH molecules to 500 mK using helium vapor buffer gas and magnetically trap them in the 4 Tesla field of an anti-Helmholtz superconducting magnet. The helium is introduced using a fast-acting cryogenic valve, allowing us to abruptly switch off the flow. The buffer gas rapidly exits the trapping region through a large diameter orifice. We trap 10^5 molecules with lifetimes exceeding 20 s. The prospect of extending the loading and trapping techniques to observe atom-molecule collisions is investigated.

Contents

List of Figures

List of Tables

Acknowledgments

The research presented in this thesis represents the collaborative effort of several people. I thank my advisor, John Doyle, for his leadership and guidance on this project. I could not have asked for a kinder or more thoughtful boss.

The intelligence, dedication and unfailing optimism of my coworkers Wes Campbell, Hsin-I Lu, and Matt Hummon made this work possible. I wish them and the rest of the Doyle lab happiness and success.

Finally, I thank my family for their constant support.

Dedicated to my family,

Chapter 1

Introduction

This thesis describes experiments performed to produce samples of molecules, specifically NH, for studies of low temperature collisional processes. This work will describe the design and construction of the experimental apparatus and the application of new techniques to achieving our goal of creating samples of molecules thermally disconnected from their environment.

Chapter 1 provides a motivation for research into cold molecules and an overview of techniques currently employed to produce them.

Chapter 2 is an introduction to buffer gas cooling and low temperature collisions. The physical mechanisms behind trap loss processes are also described in this chapter.

Chapter 3 describes the cryogenic apparatus used in the experiment. It also contains a description of the pulsed buffer gas reservoir, a critical piece of equipment constructed to extend the capabilities of the experiment.

Chapter 4 presents experimental results.

Chapter 5 outlines possible future directions of research.

1.1 Molecular Utility

Since the advent of John Dalton's atomic theory[1] in the early part of the 19th century, advancement in our understanding of nature has been achieved in part through the study of atoms, the fundamental units of matter. The development of atomic beam techniques[2] facilitated experiments that provided basic insight into gas kinetic theory, quantum mechanics[3] and nuclear theory[4]. The invention of the laser in 1958 led to bright, coherent light sources for spectroscopic investigations of atoms, allowing experiments of greater precision and sophistication to be performed. More recently (1980 - present), cooling and trapping of dilute atomic vapors have culminated in the creation of Bose-condensed [41] and Fermi degenerate [44, 23] systems, demonstrating control of the quantum and motional states of matter. As knowledge and control of atomic systems have increased, atoms have been harnessed as tools to gain insight in all areas of physics [41, 25].

Molecules, with their vibrational and rotational structure, possess a complexity not present in atoms. Electronic, vibrational and rotational transitions in molecules form an hierarchy of energy scales ranging from the deep ultraviolet to the microwave, spanning some six orders of magnitude. The complexity of molecules, compared to atoms, presents experimental challenges to their control and manipulation, but also provides unique benefits in a number of areas of research.

The typical rotational energy splitting of a molecule corresponds to a tempera-

[1] Dalton posited that matter was composed of indivisible units he termed "atoms" [81, 19].

[2] Dunnoyer produced the first thermal beams of atoms in 1911 [78].

[3] Stern, Gerlach, Frisch, Estermann and others (1922-1950)

[4] Rabi and others (1938)

ture of a few Kelvin (or, equivalently, radiation at Gigahertz frequencies). Rotational states of opposite parity can be mixed using external electrical fields, resulting in the orientation (or polarization) of the molecular sample. The relatively small rotational spacing (compared to atomic electronic splittings) means that modest fields (1 kV/cm), realizable in the laboratory, can be used to achieve full polarization. Polarized molecules may have a variety of uses, including as bits in a quantum computer [24] and as probes in sensitive spectroscopic searches for the permanent dipole moment of the electron [25, 30].

The small rotational energy scale also means, unfortunately, that a multitude of rotational states are populated at room temperature. For many applications it is desirable to have molecules in the ground rotational state or in a small number of states near the ground level. Cooling molecules helps achieve high purity in the desired rotational states and allows molecules to be confined using external electromagnetic fields. High ground state molecule densities and long interaction times, made possible through trapping, also make cold molecules ideal for high precision spectroscopy.

1.1.1 High Precision Spectroscopy

The interaction of atoms and molecules with electromagnetic radiation provides information about their energy levels and internal structure. Light can be used to selectively place them in specific energy states, and by monitoring the emission or absorption of radiation, we can gain insight into physical processes that cause shifts in these energy levels. Small shifts, or equivalently weak interactions, require long observation times and a large number of particles resonant with the probing field to

be detected; cooling and trapping can help us to achieve both.

At room temperature, atoms and molecules travel at high speeds. Their spectral lines are broadened by this thermal motion, and the short interaction time of the particles with the radiation field further reduces experimental sensitivity ("transit time broadening" [26]). Cooling the species reduces Doppler broadening, increases interaction times and leads to a narrower distribution of molecular rotational states, facilitating the performance of sensitive measurements.

Cold molecules are of particular benefit to spectroscopic searches for the electric dipole moment (EDM) of the electron. The electric dipole moment of the electron is a stringent test of theoretical models of particle physics [5, 57]; a value only a few orders of magnitude below the current experimental limit of 1.6×10^{-27} e-cm [80] is predicted by some extensions of the Standard Model [17]. A more sensitive experimental limit would either reveal the need for augmentation of the Standard Model or would invalidate a class of potential extensions.

Current limits on the electron EDM have been derived from Thallium beam experiments [1]. A number of polar molecules (YbF [52], PbO [25, 30], ThO [16, 69]) have been proposed as test species in a new generation of experiments. If external electric fields are applied to polarize these molecules, extremely large internal fields can be created in them, greatly enhancing the experimental sensitivity by enlarging the EDM-induced energy shift $\vec{d}_{edm} \cdot \vec{E}_{int}$ ($\vec{d}_{edm}$ is the EDM and $\vec{E}_{int}$ is the internal molecular electrical field, which can be GV/cm in strength).

Cooling the molecules allows them to be interrogated for longer durations. If the molecules are created in a beam, the interaction time is proportional to the

reciprocal of the beam velocity; if the molecules are held in a trap, the trap lifetime sets the observation time. A precision measurement involves repeatedly recording an experimental value in highly controlled circumstances. Long interaction times in cold beams (and possibly traps) allow more rapid and more efficient attainment of the desired sensitivity.

1.1.2 Quantum Computation

Quantum computation refers to the use of the quantum properties of matter to perform logical operations. Quantum phenomena, particularly the superposition of quantum states, allow some calculations to be performed more efficiently with quantum systems than with classical computation methods

Polar molecules have been proposed as bits in quantum computation schemes [24]. Such proposals envision using polar molecules aligned with ($|0\rangle$) or against ($|1\rangle$) an external electric field to represent the logical states of a computer. Conditional logical operations can be performed by coupling neighboring molecules via the long range electric dipole-dipole interaction.

The strength of the interaction between electric dipoles is

$$E_{dd} = \frac{\vec{d_1} \cdot \vec{d_2} - 3(\vec{d_1} \cdot \hat{r})(\vec{d_2} \cdot \hat{r})}{R^3} \tag{1.1}$$

For electric dipoles of moment 1 Debye (the typical size of a molecular dipole moment) separated by 1 micron, the interaction energy corresponds to a temperature of approximately 1 μK. For strong coupling of the dipoles, the polar sample must have a thermal energy below this energy.

A fundamental requirement of a quantum computational system is control of the state of each bit, with the simultaneous ability to perform conditional logic operations using pairs of (adjoining) bits. In the molecular dipole scheme proposed above, addressability of the individual bits can be attained by superimposing a field gradient over molecules organized in an optical lattice array. The spatial variation of the electrical field would create a unique resonance frequency for molecules at each lattice site, and bitwise operations could be performed by tuning external (microwave frequency) fields. Optical traps currently available for molecules are typically below 1 mK in depth, so the polar sample must be cooled to microKelvin temperatures for successful confinement.

The speed of a quantum processor is determined by the speed at which CNOT logic operations can be performed; it has been demonstrated that all other logical operations can be decomposed into a series of two-bit CNOT operations [76]. The speed of the CNOT gate is in turn tied to the energy resolution of the experimental system - Heisenberg uncertainty implies that with an energy resolution of ΔE, a time interval of $\tau = \hbar/\Delta E$ is required to accomplish the logic operation. In the proposed polar molecule computer, the 1×10^{-30} J energy difference in energy between the states $|0\rangle|0\rangle$ and $|1\rangle|1\rangle$[5] (where the first ket represents the control bit and the second ket the target bit) determines the minimum time for each gate operation, 50 μs. This energy difference arises from the dipole-dipole interaction between pairs of polar molecules; the strength of the dipole-diple interaction thus fundamentally determines the capabilities of such a quantum processor.

[5]More precisely, we have to be able to distinguish between transitions $|0\rangle|0\rangle \Leftrightarrow |0\rangle|1\rangle$ and $|1\rangle|0\rangle \Leftrightarrow |1\rangle|1\rangle$, representing incorrect and correct execution of the controlled-not operation, respectively.

1.1.3 Quantum Gases

The observation of quantum degeneracy in dilute bosonic gases has provided researchers with experimental systems that can elucidate the physics of higher temperature condensed matter systems. Bose-Einstein condensation is a quantum phase transition of particles with integral spin, characterized by their macroscopic occupation of the system ground state. When Bose particles are cooled to very low (typically microKelvin) temperatures, their thermal de Broglie wavelength $\lambda_{dB} = (2\pi\hbar^2/mk_BT)^{1/2}$ becomes comparable to the interparticle spacing. Below a critical transition temperature T_c, the particles exhibit a collective behavior which favors a large proportion of them occupying the ground energy state.

Condensates are typically created in harmonic traps; in stable condenstates, the trap confinement is balanced by a repulsive isotropic mean-field interaction. Bose-Einstein condensation has been achieved in dilute vapors of alkali metals, metastable noble gases, hydrogen and several other atomic systems. Condensates of chromium [40], a strongly paramagnetic atom ($6\mu_B$), are of special interest because of the magnetic dipole-dipole interaction between the atoms. The interaction between two magnetic dipoles is given by

$$V_{dd} = \frac{\mu_0}{4\pi}\frac{\vec{\mu_1}\cdot\vec{\mu_2} - 3(\vec{\mu_1}\cdot\hat{r})(\vec{\mu_2}\cdot\hat{r})}{R^3}. \tag{1.2}$$

This interaction is anisotropic, in contrast to the mean field interaction. At ultracold temperatures, the interaction energy is comparable to the thermal energy.

Polar molecules, oriented in an electric field, would experience an interaction similar in form, but with the magnetic dipoles replaced by electrical ones. Two elementary

electrical charges of opposite sign, separated by a Bohr radius, create a dipole moment of approximately 2.54 Debye. Two such dipoles, separated by a micron, interact with an energy corresponding to about a microKelvin in temperature. In contrast, a pair of 1 μ_B magnetic dipoles interact with an energy smaller by a factor of $1/\alpha^2 = 137^2$ ($\alpha = e^2/4\pi\epsilon_0\hbar c$ is the fine structure constant). The interaction of the electric dipoles would be tunable by external electric fields. Dipolar molecular condensates are of considerable theoretical and experimental interest, potentially providing novel systems to study collective effects.

1.2 Production of Cold Molecules

The potential advantages offered by cold molecules have motivated research into techniques for creating them. While optical techniques have successfully been used to create samples of atoms at ultracold (1 μK) temperatures [68], these methods are of limited utility for cooling molecules. Species suitable for laser cooling must possess electronic transitions sufficiently closed that each atom can scatter thousands of photons before it enters states that are dark to the laser light. The energy level structure of these atoms must also be so simple that atoms in the dark states can be transferred back to the cycling transition using a relatively small number of repumping beams. Laser cooling has thus been applied to cool alkali metals, alkaline earth metals and some metastable noble gases, all of which have strongly closed optical transitions and relatively simple hyperfine structure.

Electronic transitions in most molecules are insufficiently closed for them to be easily laser cooled. Molecules are transferred to non-resonant vibrational and rotational

states after scattering only a few hundred photons [95, 11], and the experimental complexity of plugging the vibrational and rotational holes becomes prohibitive.

The cooling rate in a laser cooling experiment is proportional to the spontaneous emission rate of the excited level: the spontaneous decay rate sets how quickly cycles of excitation and emission can occur. In molecules, the long-lived vibrational and rotational states, with millisecond spontaneous lifetimes (compared to nanosecond lifetimes in atomic electronic states) decay too slowly to provide useful cooling transitions.

Twofold strategies have been adopted to produce cold molecules. Molecules can be formed from laser cooled atomic samples by using magnetic field dependent (Feshbach-Fano) resonances or laser light. These techniques will be termed indirect. Other methods, which start with the molecules of interest at elevated temperatures and cool them using collisions [32, 11, 92], electrical fields [7] or mechanical means [42], are classed as direct techniques. Stark deceleration and buffer gas cooling are two direct cooling techniques that will be discussed in this chapter.

1.2.1 Indirect Techniques

Molecules can be assembled from cold precursor atoms by binding the atoms together with lasers or by sweeping them through a Feshbach resonance. Photoassociative production of molecules occurs when a pair of free atoms is illuminated with laser light and promoted to a molecular bound state. The rate of this transfer is determined by the wavefunction overlap between the bound state (a vibrational energy level in the molecular potential) and the free particle states. For this reason, photoas-

sociated molecules are typically produced in highly excited rovibrational levels, which have short lifetimes. To obtain more durable molecules, the excited molecules can be coherently transferred to more deeply bound levels. Photoassociation has successfully produced homonuclear alkali molecules and the bialkali species KRb [66, 91], NaCs [45], LiCs [59] and RbCs[56].

In the Feshbach resonance technique, an external parameter (the magnetic field) is adiabatically tuned to transfer colliding atoms from continuum states to a bound molecular level. The free and bound states possess different energies in the external field because they typically have differing magnetic moments; by varying the external field, the total kinetic energy of the free atoms can be precisely matched to a molecular bound state. If this is done near a scattering resonance, the Feshbach resonance, the cross-sections for the molecular formation process can be extremely large, and efficient transfer is obtained. As in the case of photoassociation, Feshbach molecules are typically produced in short-lived excited states, but coherent population transfer to the absolute ground state has been achieved for $^{40}K^{87}Rb$ [75]. Bialkali species produced by the Feshbach technique include $^{6}Li^{87}Rb$ [22] and $^{6}Li^{23}Na$ [84].

The molecules derived from these direct techniques are typically extremely cold: Feshbach molecules are at nanoKelvin temperatures, while photoassociated molecules can be produced at microKelvin temperatures. Both methods yield around 10^5 molecules.

1.2.2 Direct Techniques

Indirect molecular production techniques can be used to obtain a variety of homonuclear and heteronuclear bialkali species. Several potential benefits of polar molecules, particularly their suitability in EDM searches, are strongly tied to intrinsic physical properties of particular molecules. For this reason, direct cooling methods, which have so far yielded molecules at substantially higher temperatures, are of considerable importance. Stark slowing techniques are particularly well suited for decelerating light polar molecules. Buffer gas cooling is an even more general technique and is applicable to cooling virtually any molecule that can be created in the gas phase.

Polar molecules can be brought to a standstill using a Stark decelerator [89, 38, 37, 51, 6]. A polar molecule experiences a force $\vec{\nabla}(\vec{d} \cdot \vec{E(r)})$ in an electrical field. If high voltages are applied to a linear array of cylindrical electrodes, a series of potential hills and troughs can be created. By precise switching of the fields, a portion of the molecules from a beam source can be made to ascend the hilly portions of the potential, losing energy at each stage until the packet is brought to rest. A typical polar molecule has an electric dipole moment of 1 Debye (3.34×10^{-30} C m in S.I. units). The largest laboratory electric fields are 100 kV/cm, so each stage of a Stark decelerator can extract energy equivalent to about 2 K of temperature. Approximately a hundred Stark stages are required to bring a polar molecule to rest in the lab frame. Around 10^5 molecules (NH_3, CO, OH and YbF) at milliKelvin temperatures have been created with this method.

Hot molecules can also be cooled to cryogenic temperatures by colliding them with cold helium vapor [67, 93, 11, 94]. This technique, termed buffer gas cooling,

can be applied to cool a range of atoms and molecules. If hot molecules, generated by laser ablation of solid precursors or propagating as a beam, are injected into a cold cell filled with helium, the thermal energy of the molecules (in the translational and rotational degrees of freedom) is efficiently dissipated by collisions with the cold gas. When buffer gas cooling is combined with deep magnetic traps, large numbers of paramagnetic molecules can be trapped and studied. Buffer gas cooling has produced 10^8 trapped CaH and NH molecules at temperatures of a few hundred mK. The use of this technique to produce cold NH molecules is the subject of this thesis.

The difficulty of cooling molecules with optical techniques has already been discussed in this work. Despite the aforementioned challenges, a recent proposal by Jun Ye and others [85] considers applying the laser cooling technique to cool a specific class of molecules. A brief discussion of the ideas in this proposal is included here.

The imperfect closure of electronic transitions in molecules results in the "leakage" of molecules to non-resonant rotational, vibrational and hyperfine states after several cycles of excitation. This problem can be partially ameliorated by careful choice of the molecules to be cooled. For a few molecules, the excited state possesses a total angular momentum smaller than that of the ground state. The selection rules for electric dipole allowed transitions dictate that $\Delta J = 0, \pm 1$. This rule restricts the decay of excited state molecules to a single channel : $J' = 0$ (excited state) $\rightarrow J'' = 1$ (ground state)[6]. The effect of this restriction is to plug the rotational leakage channel. Furthermore, if the molecule is chosen to have good Franck-Condon overlap between the ground and excited vibrational levels and to possess no hyperfine

[6] $J' = 0 \rightarrow J'' = 0$ is forbidden by angular momentum conservation.

structure (by picking molecules composed of atoms with no nuclear angular momentum), the remaining radiative holes can be partially sealed as well. A number of molecules, including TiO, TiS and ThO, satisfy all the listed criteria and are candidates for laser cooling. TiO, for instance, is predicted to undergo 3300 cycles of excitation before becoming dark to the excitation laser. A potential experimental path to milliKelvin polar molecules may be to employ buffer gas cooling to generate a beam of 4 K molecules, and then apply laser cooling as a bridge between the Kelvin and milliKelvin temperature ranges. These laser cooled molecules may be confined in modified magneto-optical traps that employ pulsed electrical fields[7] in addition to lasers and magnetic fields [85].

1.3 Trapping

Particle speeds at room temperature are typically hundreds of meters per second. Laser detection volumes are only a few cubic millimeters in size, meaning that particles in thermal beams can interact with laser fields for only a few microseconds[8]. Traps for neutral particles lengthen the duration of field interaction and allow different processes, spanning many temporal decades, to be monitored.

Inhomogeneous magnetic and electric fields can be used to confine atoms and

[7]The electrical fields enforce the mixing of the magnetic sublevels, to ensure that the molecule can always absorb light from a laser field that provides a restoring force and viscous drag, as in a standard MOT.

[8]Multipass laser cavities effectively increase interaction volumes by allowing laser light to intersect the beams at several points. Ramsey's separated oscillatory field technique is an even more elegant solution to the problem of time of flight broadening. In this technique, particles in a beam interact with multiple spatially separated phase-coherent electromagnetic fields [26]. The spectral resolution is limited by the (long) free flight time, not the (short) field interaction time.

molecules to regions of free space, out of physical contact with the walls of the experimental region. Trapping may be performed to enable the manipulation of the particles with external fields (like laser light), to allow collisional processes to occur [73, 74] and to permit the monitoring of processes, like radiative decay, which can happen on timescales smaller than the trapping time [12].

Static traps are of particular importance to studies of molecules and will be discussed in this section. Motion in a trap is characterized by periodic transfer between potential and kinetic energy. To confine a sample of particles, the internal energy states of the particles must be coupled to an external field in such a way that the potential energy barrier the particles experience is deeper than their thermal energy.

1.3.1 Trapping in Static Magnetic Fields

In a magnetic field, a magnetic dipole experiences a force

$$\vec{F}(\vec{r}) = \vec{\nabla}(\vec{\mu} \cdot \vec{B}). \tag{1.3}$$

The magnetic moment, $\vec{\mu}$, is a constant quantity that depends on the internal state of the particle. The trap, therefore, is created by the interaction of the dipole with a spatially varying magnetic field. Free space magnetic field maxima cannot exist as a consequence of Gauss's law [54], so a magnetic trap confines particles in states whose potential energy increases with field strength. Such particles are termed low field seekers.

A magnetic moment of 1 μ_B has a value of $9.274{\times}10^{-24}$ J T^{-1}. In a field of 1 T, it possesses an energy that corresponds to a temperature of around 1 K. To trap

such a particle, it must be cooled to a temperature substantially below 1 K. A figure of merit for how well a particle is confined is the ratio of the potential energy barrier to the particle's thermal energy:

$$\eta = \frac{\mu B}{k_B T}, \tag{1.4}$$

where B represents the depth of the trap, T is the temperature and k_B is the Boltzmann constant. Superconducting magnets can produce traps a few Tesla deep; molecules can be loaded into them if they are cooled with helium gas to temperatures below a Kelvin. Room temperature magnets produce traps that are substantially shallower (1 mK trap depth) and have been used to confine molecules created at microKelvin temperatures from ultracold atoms.

1.3.2 Electrostatic trapping

Electrostatic traps have been used to confine molecules that have been decelerated with Stark slowing. An electric dipole trapped in an inhomogeneous electric field experiences a restoring force $\vec{\nabla}(\vec{d} \cdot \vec{E}(\vec{r}))$ where $\vec{d}$ is the dipole moment and $\vec{E}(\vec{r})$ is the electric field strength. The typical dipole moment of a polar molecule is 1 Debye, which is equivalent to 3.34×10^{-30} Cm in SI units. Fields of 1 kV/cm strength are routinely created in laboratories (state of the art is two orders of magnitude higher). Electrostatic traps thus have depths of a few milliKelvin per kV/cm. They have been used to hold Stark-decelerated OH [89] and deuterated ammonia (ND_3) molecules [6] for several seconds.

1.4 This Work

This thesis describes experiments performed to cool and trap NH molecules in a magnetic field, using the buffer gas technique. To extend the molecule lifetime, we reduce the buffer gas density in the trapping region and observe molecules persisting for tens of seconds. The long molecule lifetimes should allow us to measure collisional loss rates of molecules interacting with each other and with various co-trapped species.

Chapter 2

Buffer Gas Theory

With one exception (atomic hydrogen [28]), particles which come into contact with cold (1 K) surfaces stick to them. For this reason, atoms and molecules cannot be cooled by direct contact with cryogenic cells. To cool these particles we can, however, inject them into a cold cell filled with an inert "buffer" gas. The gas inhibits the transport of the target species to the walls by enforcing diffusive motion, while acting as a link that allows the atoms and molecules to thermalize to the wall temperature.

2.1 Thermalization and Diffusion

The buffer gas technique relies on elastic collisions between a cold gas and a target species. At 4 K and below, only the isotopes of helium (helium-3 and helium-4) Fig.[2.1] have substantial vapor pressures. Hydrogen and neon are other potential buffer gases, suitable for producing samples at temperatures above 15 K [77].

The thermalization of a molecule proceeds by the exchange of kinetic energy and

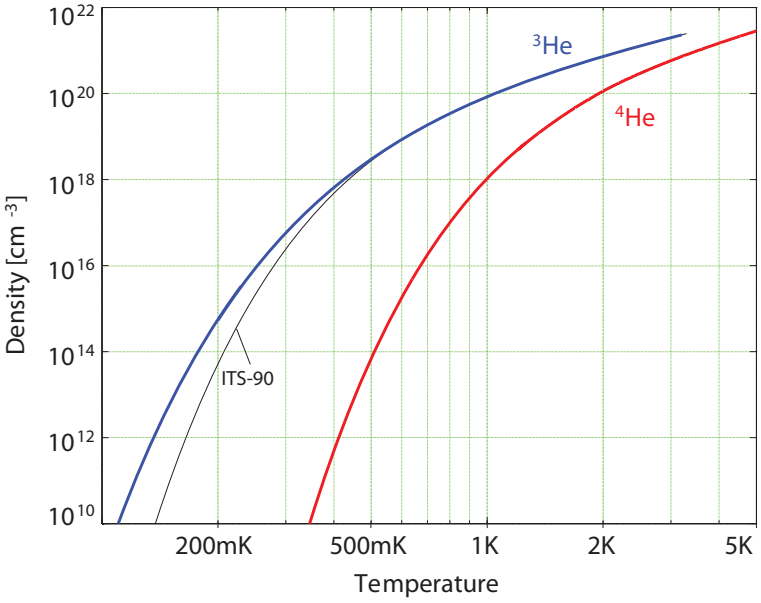

Figure 2.1: Saturated vapor density curves for helium-3 and helium-4 below 5 K. The curve for helium-4 is obtained from ITS-90 standard, Ref. [79]. The curve for helium-3 is from Ref. [50].

momentum with the buffer gas. The fractional energy exchange in each collision is determined by the mass mismatch between the two species; a lighter molecule will give up more of its energy after a collision with helium, a light atom. The rate of this energy exchange is $n_b \sigma_d v_{rel} \epsilon(m_b, M)$ [58], where n_b is the buffer gas density, σ_d is the elastic collision cross-section (more accurately, the thermal transport cross-section). v_{rel} is the relative velocity between the colliding species and

$$\epsilon(m_b, M) = \frac{2 m_b M}{(m_b + M)^2} \tag{2.1}$$

is the mass factor. m_b is the mass of the buffer gas atom and M is the mass of the target to be cooled.

A lighter molecule like NH (mass number 15) requires only about forty collisions

to be cooled from 1000 K to below 1 K; europium [58](a heavy atom, mass number 152) requires around two hundred collisions.

In the buffer gas thermal bath, the motion of the molecule is diffusive [48]. In our experiments, the collision of the molecule with the cell always results in loss, so the evolution of the particle density can be modeled with boundary conditions that produce destruction at walls. Temporal evolution of the particle density is governed by the following equation:

$$\frac{\partial n}{\partial t} = D\nabla^2 n(\vec{r}) \tag{2.2}$$

The diffusion constant, D, is equal to [48]

$$D = \frac{3\pi}{32}\frac{\bar{v}_{rel}}{n_b \sigma_d}. \tag{2.3}$$

The solution to this equation is a set of eigenfunctions, written as the product of time and spatially dependent parts:

$$n(\vec{r}, t) = \sum_i n_i(\vec{r}) e^{-\frac{t}{\tau}} \tag{2.4}$$

In cylindrical coordinates, the spatial functions for diffusion in a cell of radius R and length L are

$$n(\vec{r}) = n(0) J_0\left(\frac{j_{01} r}{R}\right) \cos\left(\frac{\pi z}{L}\right) \tag{2.5}$$

$J_0(r)$ is the zeroth-order Bessel function of the first kind; j_{01} is its first root[1].

[1]We have implicitly assumed that diffusive behavior is dominated by the most slowly decaying eigenmode of the system, the zeroth-order eigenmode.

The time constant τ, which characterizes the rate of particle loss can be expressed as

$$\tau_0 = \frac{n_b \sigma_d}{g_{cyl} \bar{v}_{rel}}, \tag{2.6}$$

where

$$g_{cyl} = \frac{3\pi}{32}\left(\frac{j_{01}^2}{R^2} + \frac{\pi^2}{L^2}\right). \tag{2.7}$$

Superimposing a magnetic trap on the diffusion volume modifies the motion of the species by creating a mean drift velocity towards the trap center for particles in low field-seeking states [92], slowing their rate of diffusion to the wall.

A quadrupole trap potential, similar to those produced by our magnets, takes the form

$$U = \mu B' \sqrt{r^2 + 4z^2} = \frac{\eta k_B T}{R}\sqrt{r^2 + 4z^2} \tag{2.8}$$

and produces a modification to the trap lifetime exponential in the parameter η:

$$\tau_{cyl}(\eta) = \frac{n_b \sigma_d}{g_{cyl} \bar{v}_{rel}} e^{0.31\eta + 0.018\eta^2} [9]. \tag{2.9}$$

This expression represents a numerically derived approximation to the diffusion lifetime in a trapping field. The theses of Brahms [9] and Weinstein [92] offer detailed treatments of drift-diffusion.

2.1.1 Buffer Gas Loading and Trapping

Buffer gas cooling refers the use of an inert gas to thermalize an atom or molecule to cryogenic temperatures. The species-buffer gas elastic cross-section (typically 1×10^{-14} cm^2) and the buffer gas vapor pressure (see Fig.2.1), a bulk physical property of the buffer gas, determine the physical scale of our experiments. Typical loading densities of between 10^{14} and 10^{16} cm^{-3} allow us to cool particles in volumes that measure a few centimeters on a side. Diffusion times in these cells are typically a few milliseconds. In buffer gas trapping, paramagnetic species are buffer gas cooled in the presence of a static magnetic trap. With modern superconducting technology, traps as deep as 4 Tesla can be constructed. Particles with one Bohr magneton magnetic moments can thus be trapped for seconds in 100 mK cells. Confinement times may be limited by inelastic interactions between the trapped species and the buffer gas or by collisions which promote the trapped particles to untrapped trajectories.

2.2 Inelastic Collisions

Atoms and molecules may ejected from a trap by a number of processes. Inelastic collisions refer to collisions which result in a change in the energy state of the trapped species. Processes which cause inelastic loss include spin-exchange, Zeeman relaxation, Feshbach resonances, shape resonances and dipolar loss. Sufficiently high rates of inelastic loss may preclude trapping or limit the attainable particle density. Understanding the physical mechanisms behind these processes is thus crucial.

2.2.1 Spin Exchange

As suggested by its name, the process of spin exchange [90] refers to the exchange of angular momentum by colliding particles. When paramagnetic atoms or molecules collide in an external magnetic field, their spin states will be preserved if the collision partners are in maximally stretched Zeeman sublevels. If the partners are in non-fully stretched magnetic states, all exit channels that preserve the total spin projection $m = m_a + m_b$ (where m_a and m_b are the spin projections of the colliding particles) are accessible.

$$|S_a, m_a\rangle|S_b, m_b\rangle \rightarrow |S = S_a \oplus S_b, m = m_a + m_b\rangle. \tag{2.10}$$

The transition of a low field seeking particle to a lower magnetic sublevel leads to more rapid diffusion out of the trap.

Helium-4 possesses no orbital, spin or nuclear angular momentum. A paramagnetic particle colliding with helium-4 cannot undergo spin-exchange. The nuclear spin of the helium-3 permits spin exchange collisions to occur, mediated by the direct hyperfine interaction, $\mathbf{S} \cdot \mathbf{I}$ ($\mathbf{S}$ is the spin of the paramagnetic particle, $\mathbf{I}$ is the nuclear spin of helium-3). Spin exchange rates with helium-3 are typically slow (the rate coefficient of rubidium-helium-3 collisions is $1{\times}10^{-19}$ cm^3 s at 300 K [15]) and this mechanism is not a significant inelastic channel in our system.

2.2.2 Resonantly Enhanced Collisional Loss: Shape Resonances

A shape resonance occurs when free particles are bound together without a coupling of their internal states. Centrifugal barriers in higher-order partial wave scattering may support the existence of quasi-bound energy levels. When particles at low temperatures collide with energies matching that of the quasi-bound state, a shape resonance results. The quasi-bound state can facilitate the short-distance interaction of the particles by allowing tunneling through the centrifugal potential barrier. The particles cling together as transient, weakly-bound molecules and then fly apart. The increased interaction of the particles at close distances, due to the shape resonance, may lead to enhanced inelastic loss rates.

2.2.3 Zeeman Relaxation

If paramagnetic atoms and molecules are placed in a magnetic field, the external field breaks the degeneracy of the Zeeman (magnetic) sublevels. States whose energies increase with field strength are known as low field seeking states, and particles in these states can be trapped in static magnetic fields. Collisions (with helium or with other particles) can cause the transfer of particle populations between different sublevels [35].

Buffer gas trapping has been applied to S-state atoms and Σ-state molecules, which nominally have isotropic electronic distributions. For most non-S-state atoms and non-Σ-state molecules [65], the interaction with helium is predicted to cause loss rates (transitions from low field seeking states to untrapped states or more weakly trapped

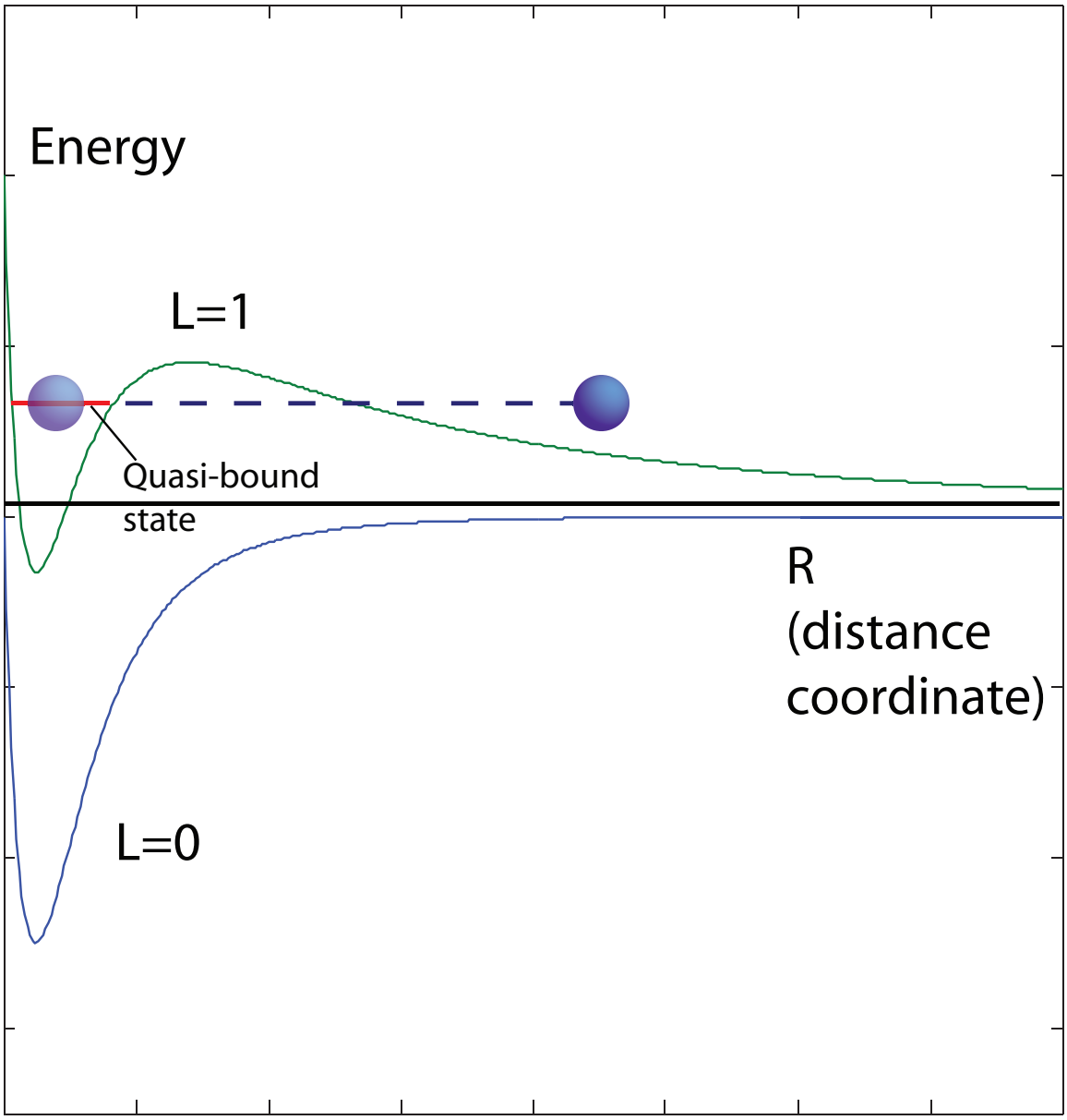

Figure 2.2: The occurrence of a shape resonance. The collision energy exactly matches the energy of a quasibound state in the $L = 1$ partial wave. This resonance may lead to tunnelling and close approach of the collision partners, enhancing inelastic loss rates.

states) large enough to preclude trapping. Successful trapping typically requires an elastic to inelastic collision ratio on the order of 1000; species with anisotropic electron clouds suffer elastic and inelastic collisions with near equal frequency [60, 83, 8].

Krems and Dalgarno theoretically elucidated the mechanisms behind the Zeeman-relaxation of $^2\Sigma$ and $^3\Sigma$ molecules [64, 61]. The cartoon model of the molecule-helium interaction depicts the collision partners as hard sphere scatterers; in reality, the collision with helium can cause a distortion of the molecule's rotational wavefunction, effectively mixing in contributions from excited rotational levels. The coupling of the rotational angular momentum in these excited states to the electronic spin drives the spin relaxation of Σ-state molecules. Collisional distortion of the rotational wavefunction accounts for inelastic loss in $^2\Sigma$ molecules. $^3\Sigma$ molecules and molecules of higher spin multiplicity also suffer intrinsic wavefunction asymmetry because of perturbations arising from the interactions of their spins. Inelastic loss for these molecules scales as

$$\Gamma_{SS} = \frac{\lambda_{SS}^2}{B_e^2}, \tag{2.11}$$

where Γ_{SS} is the spin-spin loss rate, λ_{SS} is the spin-spin coupling constant and B_e is the rotational spacing.

For $^2\Sigma$ molecules, the loss rate scales differently:

$$\Gamma_{SR} = \frac{\lambda_{SR}^2}{B_e^4} \tag{2.12}$$

where Γ_{SR} is the spin-rotation loss rate and λ_{SR} is the spin-rotation coupling constant.

Two-body loss rates for trapped paramagnetic atoms

Atom	**Ground State**	$\mathbf{g}_{2b}$ [$\mathbf{cm^3 s^{-1}}$]	Ref.
Molybdenum	$^7S_3$	1.2×10^{-12}	[46]
Dysprosium	$^5I_8$	1.8×10^{-12}	[73]
Holmium	$^4I_{15/2}$	0.72×10^{-12}	[73]
Chromium	$^7S_3$	5×10^{-14}	[74]
Manganese	$^6S_{5/2}$	0.38×10^{-12}	[74]
Manganese-Chromium	$^6S_{5/2}$,$^7S_3$	0.15×10^{-12}	[74]

Table 2.1: Two-body loss rates for trapped paramagnetic atoms

2.2.4 Dipolar Loss

Inelastic loss may also be triggered by the magnetic interaction between paramagnetic species [21]. The relative motion of the magnetic dipoles can induce disorientation of the trapped particles by effectively tipping over the spins in the external field. The rate of molecule-molecule dipolar loss depends on the square of the particle density; at the densities in our experiments we do not yet expect to observe this. We are, however, attempting to co-trap atomic and molecular samples with atomic densities high enough to observe dipolar loss. Such loss will strongly determine the feasibility of evaporative cooling or sympathetic cooling schemes for paramagnetic molecules.

Two-body relaxation measurements have been recorded for several paramagnetic atoms at temperatures of a few hundred milliKelvin, Table[2.1]. Typical loss rates are around 1×10^{-12} $\mathrm{cm^3 s^{-1}}$. Theoretical calculations are currently underway to determine these rates for nitrogen-NH collisions.

2.2.5 Resonantly Enhanced Collisional Loss: Feshbach Resonances

Two free particles may be associated into a bound state via a coupling of their internal degrees of freedom. When particles at low temperatures collide in a magnetic field, bound molecular states may possess energies near the collision energy. For specific values of the external magnetic field, exact coincidence may occur. If the bound and free states are coupled together (for instance, linked by a hyperfine interaction), transitions between them may be resonantly enhanced by the resonance. Such a resonance is termed a Feshbach-Fano resonance [34, 71, 18, 53]. The scattering cross-section at these resonances may become extemely large, leading to increased rates of inelastic loss and molecule formation. Feshbach resonances are routinely used to form molecules from ultracold, optically-cooled atoms. The field dependence of the resonance allows precise external control of the rates of molecule formation in these experiments.

A Feshbach resonance is predicted to occur in collisions of NH with helium-3 [62] and may partially account for the rate of inelastic loss measured experimentally [13].

2.3 Elastic Background Collisions

A reduction in the buffer gas density leads to a decrease in the rate of loss arising from inelastic collisions with helium. The reduction in this loss rate does not lead to infinite trapping times, however, as elastic collisions can also result in the ejection of trapped molecules.

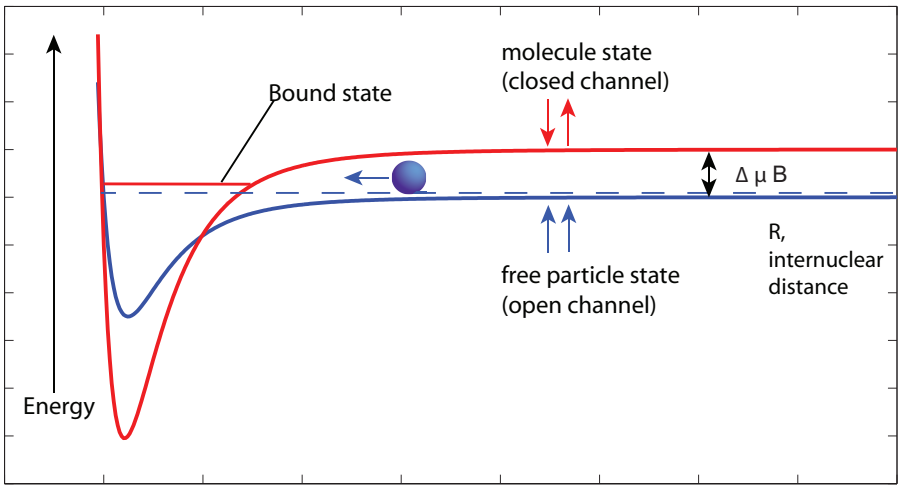

Figure 2.3: The occurrence of a Feshbach resonance. Free particles (open channel) collide with an energy close to that of a bound molecular state. The position of the bound state can be tuned by adjusting the external field B.

When the mean free path of the molecules is much smaller than the linear dimension of the cell, the diffusive treatment of molecular motion is valid. Buffer gas cells are typically a few centimeters in diameter. With typical particle-Helium elastic cross-sections around 1×10^{-14} cm^2, diffusion remains a good model for particle behavior at buffer gas densities exceeding 10^{15} cm^{-3}:

$$\lambda = \frac{1}{n_{He}\sigma_d} = 0.1\ cm \approx \frac{1}{30} r_{cell}. \tag{2.13}$$

The mean free path at a density of 10^{14} cm^{-3} is comparable to a cell radius. At this density, collisions with the buffer gas are too infrequent to enforce diffusive motion, yet are frequent enough to maintain thermal contact with the trapping cell. The loss of the diffusion enhancement of the lifetime leads to a reduction in the trapping duration. The buffer gas can still impart energy to the trapped molecule, however,

and collisions can transfer the molecule to untrapped trajectories. If the buffer gas density is decreased further, collisions become less frequent, and the molecule lifetime lengthens.

A technical challenge arises from this background loss. When the bulk of the buffer gas is extracted from the experimental cell, a helium film persists on the walls and desorbs at a slow rate. The desorbing film holds the buffer gas densities at levels where elastic loss is high. This thesis will describe our attempts to circumvent this problem.

2.4 Buffer Gas Trapping in Our Experiment

The conceptual simplicity of buffer gas cooling belies its technical challenges. To trap molecules in our experiment we must integrate our room temperature source with our helium-3 fridge and other cryogenic equipment. We must introduce buffer gas into the trapping region to load molecules and then extract it, to thermally isolate the trapped molecules. The design and construction of the experimental apparatus is described in the following chapter.

Chapter 3

Apparatus

Buffer gas trapping experiments employ magnetic traps to confine paramagnetic species and cryogenic refrigerators to attain temperatures low enough for effective trapping. Our experiment differs from all others in that we work with molecules produced as a supersonic beam.

Our molecules are created at room temperature and are initially too hot to be held in our 4 T deep trapping field. To trap them, we have to dissipate their energy without losing them to the walls or to chemical reactions. Helium retains a high vapor pressure at low temperatures and can provide a thermal link between the molecules and a cryogenic cell. To thermally isolate the trapped molecules, we must remove the helium from the cell without excessive loss of the molecules. Because residual helium can cause evaporative loss of molecules, we have developed a cryogenic reservoir for helium delivery that gives us greater control of the background gas density in our system.

The physical structure of the experiment can be divided into the molecular beam

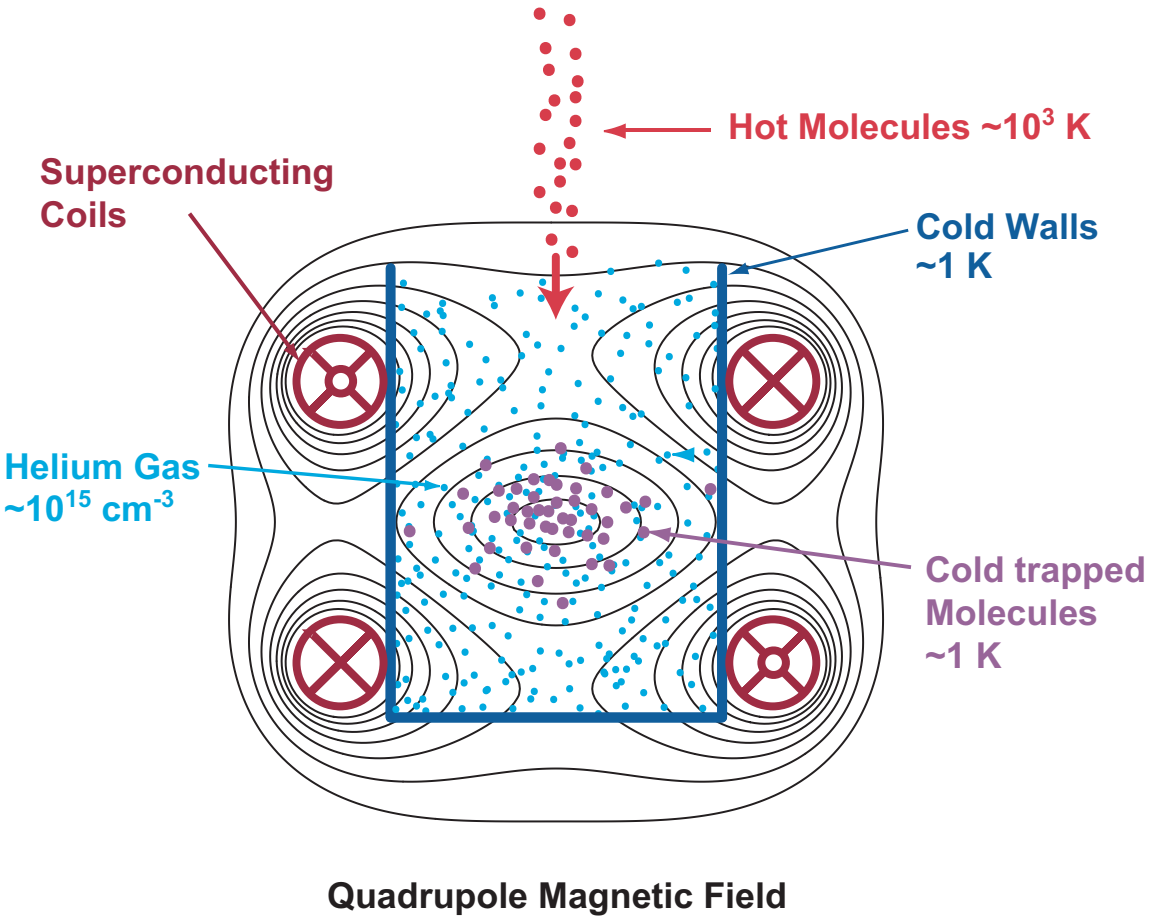

Figure 3.1: Cartoon view of buffer gas loading. Hot molecules are injected in to a cold cell filled with helium gas. The collisions with helium thermalize the molecules to the cell temperature, and they are loaded into a quadrupole trap created by superconducting coils in an anti-Helmholtz configuration.

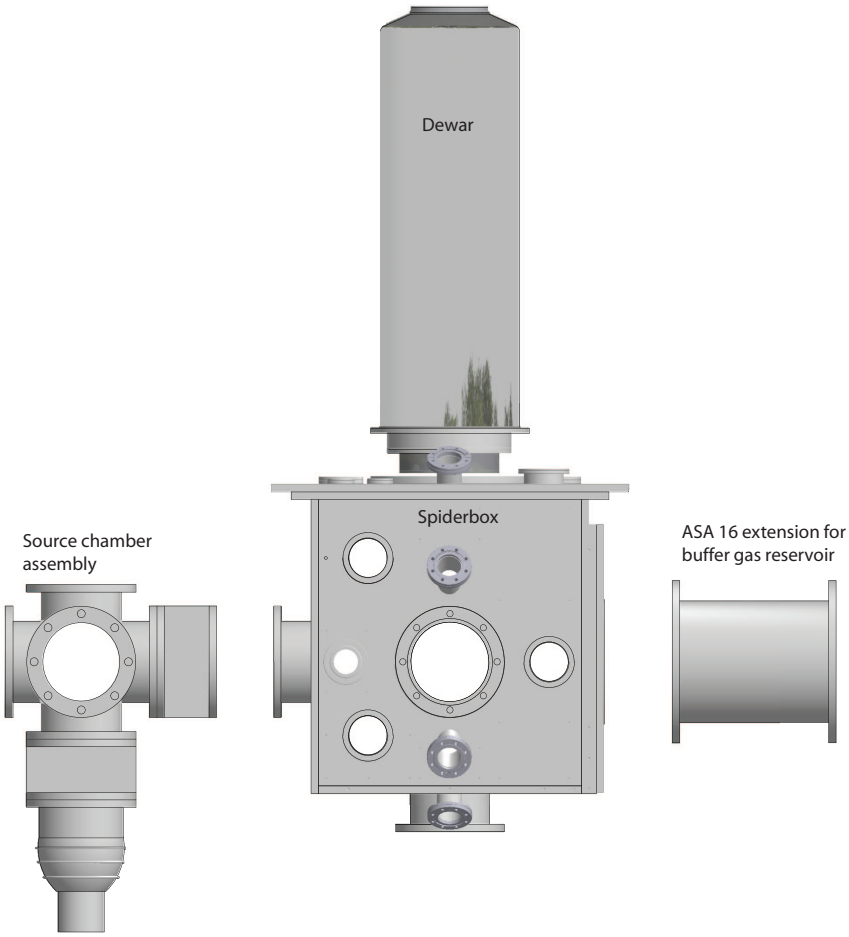

Figure 3.2: Experiment showing the positions of the source chamber, spiderbox and ASA-16 extension for the buffer gas reservoir assembly.

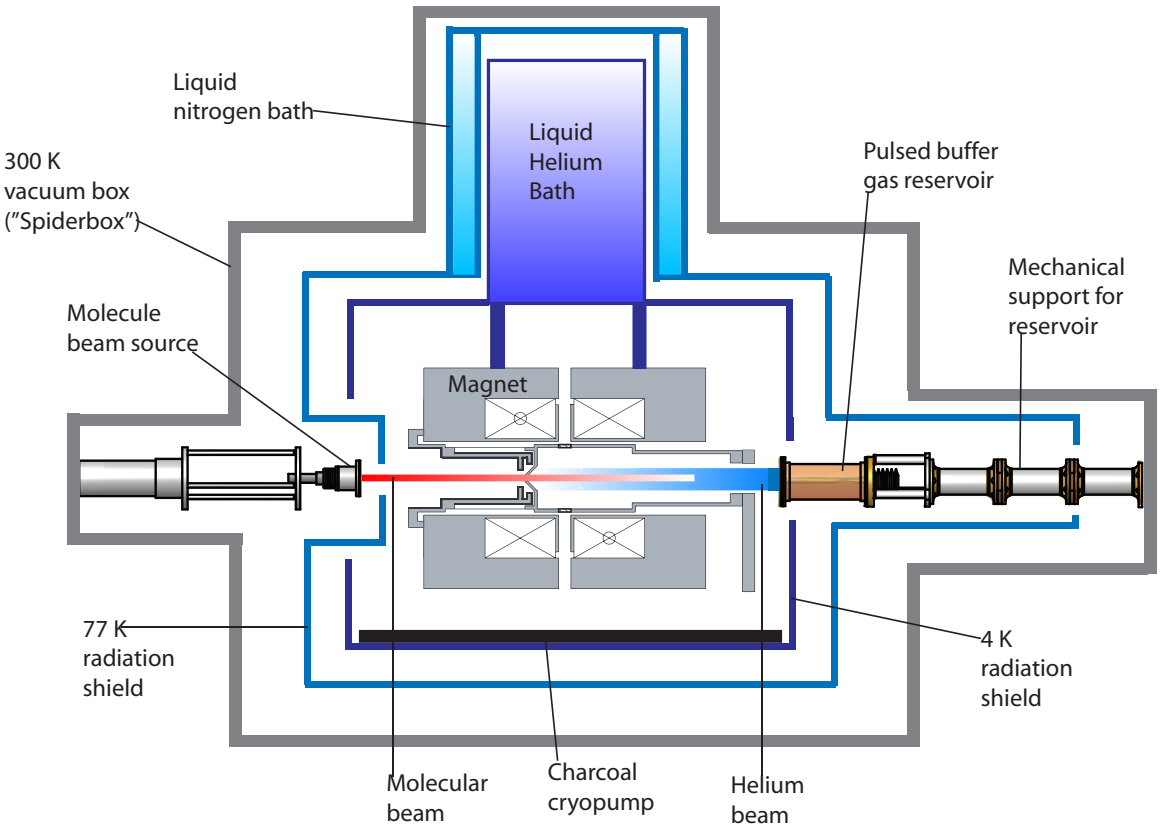

Figure 3.3: Schematic drawing of the experimental apparatus. The molecule beam propagates through the vacuum space to enter the cell, housed in the bore of the trapping magnet. Buffer gas, supplied by the pulsed reservoir, fills the cell and allows the molecules to thermalize to the cell temperature. The molecules are detected with laser light that passes through ports in the magnet midplane. Visible in this drawing are thermal connections that connect the magnet to the liquid helium bath.

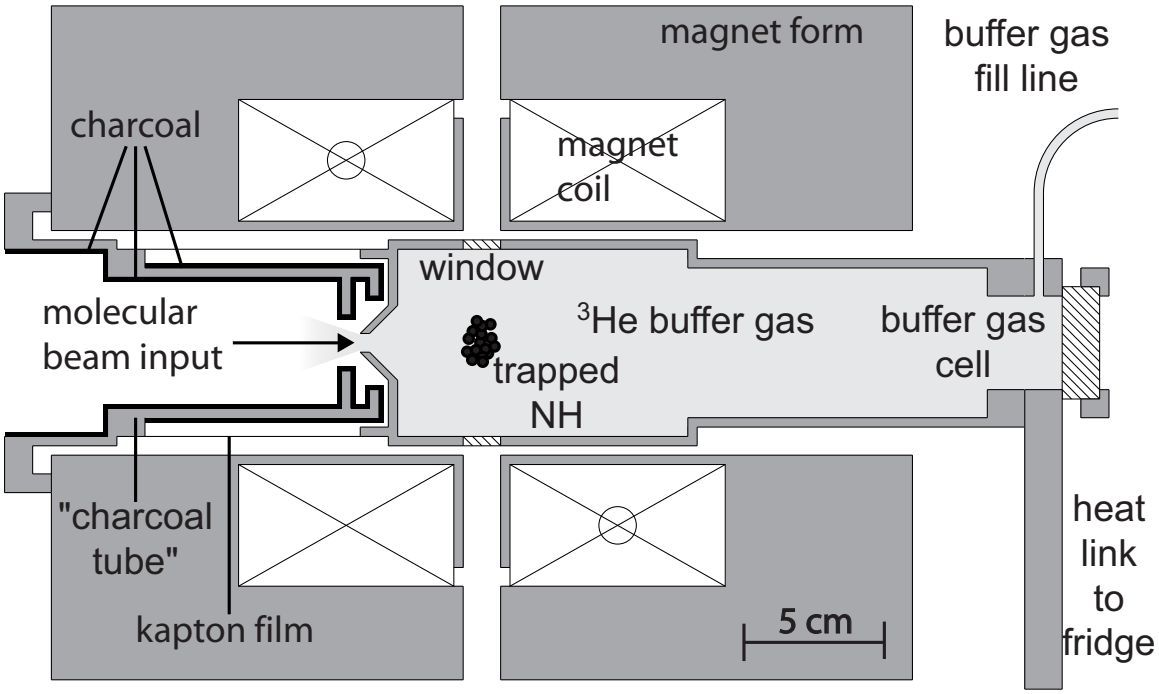

Figure 3.4: Schematic view of the superconducting magnet and the cell. Molecules enter the cell through the 1 cm diameter front aperture; helium enters through the fill line. We place the charcoal tube (a copper cylinder with charcoal epoxied to it) outside the cell to pump away helium. High helium densities in the region in front of the aperture could scatter molecules from the beam before they enter the cell and create a thermal link between the 500 mK cell and the 5 K magnet. The Kapton film further reduces the likelihood that helium escapes into the bore of the magnet. Laser light for detection (336 nm) enters through windows coincident with the magnet midplane. In the experiments to measure the Zeeman-relaxation of NH in collisions with helium, a steady flow of buffer gas creates a fixed density in the cell. In the thermal isolation experiment, the rear cell window is removed to allow the buffer gas to be injected with the cryogenic reservoir. The large rear aperture also allows the buffer gas to exit the cell more rapidly (40 ms, compared to 500 ms with the front aperture alone).

source, the main vacuum chamber and the pulsed buffer gas reservoir. The molecular beam source is a room temperature vacuum chamber, backed by a diffusion pump, in which the NH molecules are created. The main vacuum chamber (the "spiderbox") houses the cryogenic guts of the system - the superconducting magnet, pulsed tube cooler, helium-3 fridge and cell. The pulsed buffer gas reservoir has the external appearance of an ASA-16 flange mounted onto the spiderbox; several internal thermal connections allow us to accomplish the task of turning room temperature helium flow into discrete gusts of cold vapor in the cell. These three parts of the experiment will be discussed in the following two chapters.

3.1 The NH molecule

The molecule we study is NH, also known as imidogen or nitrogen monohydride. The selection of this molecule and preliminary studies with it are discussed elsewhere [11, 31]; the properties that make it useful to us will be summarized here.

NH is a $^3\Sigma$ ground state molecule, meaning that it possesses two unpaired electrons and no orbital angular momentum. The achievable magnetic trap depth (4 T) and temperature (0.5 K) in our experiment allow us to trap $^3\Sigma$ molecules and molecules of higher spin multiplicity; to trap molecules with a single unpaired electron, we require colder cell temperatures, necessitating the use of a dilution refrigerator instead of the helium-3 fridge we employ. NH also possesses a strong optical transition at 336 nm [86, 87, 10, 27, 4], which we use for detection. Theoretical models of molecular spin relaxation [64, 63] indicate that molecules with large rotational energy splittings are more resistant to spin-depolarizing collisions. NH has a rotational splitting of 16.34

cm^{-1} (corresponding to a temperature of around 24 K), which is among the largest in any molecule. NH also has gas-phase precursors (ammonia or nitrogen-hydrogen mixtures), allowing us to produce it in the form of a supersonic beam.

Zeeman Effect in NH

NH is a $^3\Sigma$ molecule in its ground state. Its two unpaired electrons produce a magnetic moment of $2\mu_B$. The coupling of the molecular electronic spin to the orbital angular momentum is weak, making NH an example of a Hund's case (b) molecule [49]. In Hund's case (b), molecules have a magnetic moment given by the formula

$$\mu_{(b)} = 2m_s + \frac{\Lambda^2 m_N}{N(N+1)}\mu_B, \tag{3.1}$$

Where m_s is the spin magnetic sublevel, Λ is the projection of the orbital angular momentum on the molecular axis and N is the sum of the orbital and rotational angular momenta. Ground state NH possesses no orbital angular momentum and $\Lambda = 0$.

In the ground rotational level of the electronic excited state (the $A^3\Pi$ state), $N = |\Lambda| = 1$. Using angular momentum addition rules, the electronic spin and orbital angular momentum sum to create total angular momentum states $^3\Pi_J = {}^3\Pi_2$, $^3\Pi_1$ and $^3\Pi_0$.

In the $^3\Pi_2$ state, the spin and orbital angular momenta must be aligned. Herzberg's formula for the magnetic moment produces a value of $2.5\mu_B$ in this state.

In the $^3\Pi_1$ state, the total angular momentum $J = 1$ can be derived from states

which have either the spin or the orbital angular momentum aligned with the molecular axis; the other angular momentum projects no component on the molecular axis. Specifically, the ($J = 1$,$m_J = 1$) state is composed of superpositions of the states $|m_S = 1, \Lambda = 0\rangle$ and $|m_S = 0, \Lambda = 1\rangle$. Evaluating Herzberg's formula for each of the superposition states, we derive a magnetic moment of $1.25\mu_B$ in this state.

By similar arguments, $^3\Pi_0$ state is composed of states where the orbital and spin angular momenta contribute projections opposed along the molecular axis. The ($J = 0$,$m_J = 0$) state is obtained from the states $|m_S = 1, \Lambda = -1\rangle$, $|m_S = -1, \Lambda = 1\rangle$ and $|m_S = 0, \Lambda = 0\rangle$. The magnetic moment in this state is 0 μ_B.

The magnetic moments of the sublevels of interest to our experiment can now be explicitly enumerated:

$$In\ the\ ^3\Sigma\ state,\ \mu = \{-2\mu_B, 0, 2\mu_B\} \tag{3.2}$$

$$In\ the\ ^3\Pi_2\ state, \mu = \{-2.5\mu_B, -1.25\mu_B, 0\mu_B, 1.25\mu_B, 2.5\mu_B\} \tag{3.3}$$

Molecules in the ($^3\Sigma, m_J = 1$) level are loaded into our trap from a supersonic beam. Laser light at 336 nm addresses the R_1 transition, promoting molecules to the $^3\Pi_2$ excited state. Decay from this level is detected on a PMT.

3.2 Molecule beam source

An earlier version of this experiment demonstrated the successful loading of a molecular beam into a buffer gas cell [29]. Building on that work, we trapped NH

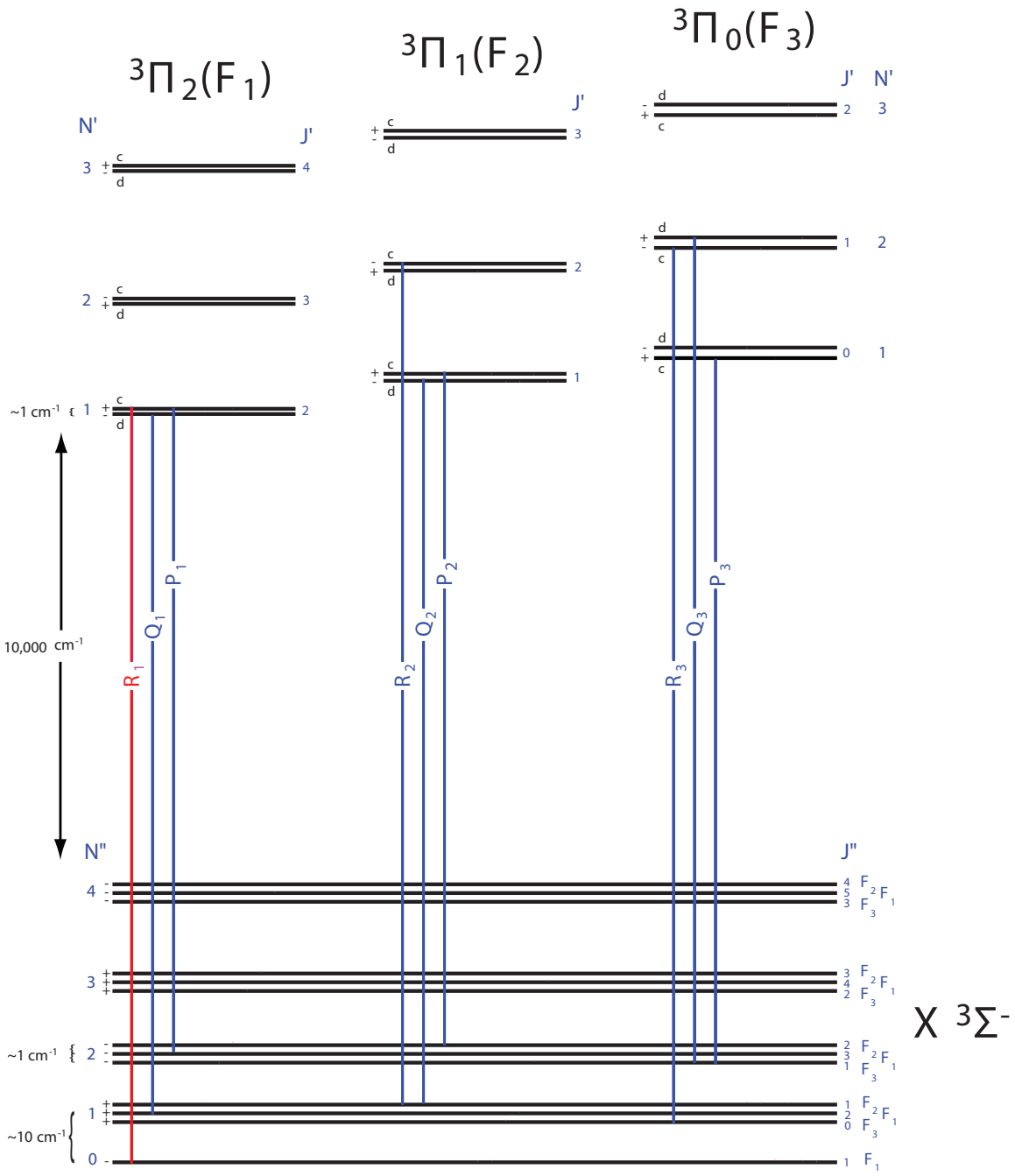

Figure 3.5: Optical detection of NH. We use 336 nm laser light to excite the $X^3\Sigma^- \rightarrow A^3\Pi_2(R_1)$ transition. Fluorescence from the excited state is detected by a PMT.

molecules by using the bore of an anti-Helmholtz magnet as our buffer gas cell. The pulsed valve (Parker Hannefin General valve P/N 9-1646-900) had to be shielded from the field gradients of the trapping magnet by a "compensation coil" to accomplish this [31]. The compensation coil is a length of copper tubing wound into the shape of a solenoid. At the position of the pulsed valve, it creates a magnetic field that cancels the residual field from the magnet. Without the coil, the residual field holds the valve in the open position, leading to the leakage of process gas into the chamber.

The molecule source in the current experiment still uses the compensation coil to null the field at the position of the pulsed valve, but the entire valve assembly (pulsed valve, compensation coil, water lines for cooling the compensation coil) can be translated in the X, Y and Z directions. X and Y translation allow us to align the molecular beam with the front orifice of the cell. The Z position determines how close the pulsed valve is to the cell; we typically try to place the valve as close as possible (18 cm) to optimize the solid angle capture of the beam [1].

The electrical, water and gas lines for the pulsed valve fit within the 5 cm diameter bore of a stainless steel tube. To translate the pulsed valve in the Z-direction, the stainless steel tube slides through two ultratorr fittings welded into conflat flanges. The conflat flanges and a conflat tee mount onto a 15 cm by 15 cm stainless steel plate, which slides with respect to the ASA flange of the source chamber. The translation of this plate permits X and Y alignment. An O-ring between the plate and the ASA flange accomplishes the vacuum seal.

[1] We can place the molecular source no closer than 18 cm from the cell because we must accommodate a charcoal cryopump in front of the cell. Without the cryopump, helium exiting the cell can reach a density high enough to scatter the majority of the molecules out of the beam before they reach the trap.

The weight of the conflat assembly is sufficient to pry open the O-ring seal, so the assembly is supported by a spring hanging from the ceiling. To further ensure the integrity of the seal, the plates which translate the steel plate in the Y dimension also apply a clamping force in the Z-direction.

3.3 Cryogenic Vacuum-Compatible Magnet

Our magnet consists of two coils of NbTi wire wound around a titanium alloy frame (Grade 6 Ti: Ti 92.5%, Al 5%, Sn 2.5%). At full current, the coils repel each other with a force of 27 tons, so the mechanical strength of this frame is a critical design parameter.

With an operating current of 140 A in both coils, we produce a 4 Tesla deep trap in the region between them. The magnetic field increases linearly in all directions, with the axial gradient twice as large as the radial gradient. The equal field contours are thus pancakes flattened in the axial dimension.

To keep the magnet in a superconducting state, it is thermally anchored to a bath filled with liquid helium.

3.3.1 High Temperature Superconducting Leads

To supply current to our magnet we use leads made from a high temperature superconductor. The leads are rated for currents up to 250 A and have been tested up to 82 K. The top portion of the leads is kept below the superconducting transition

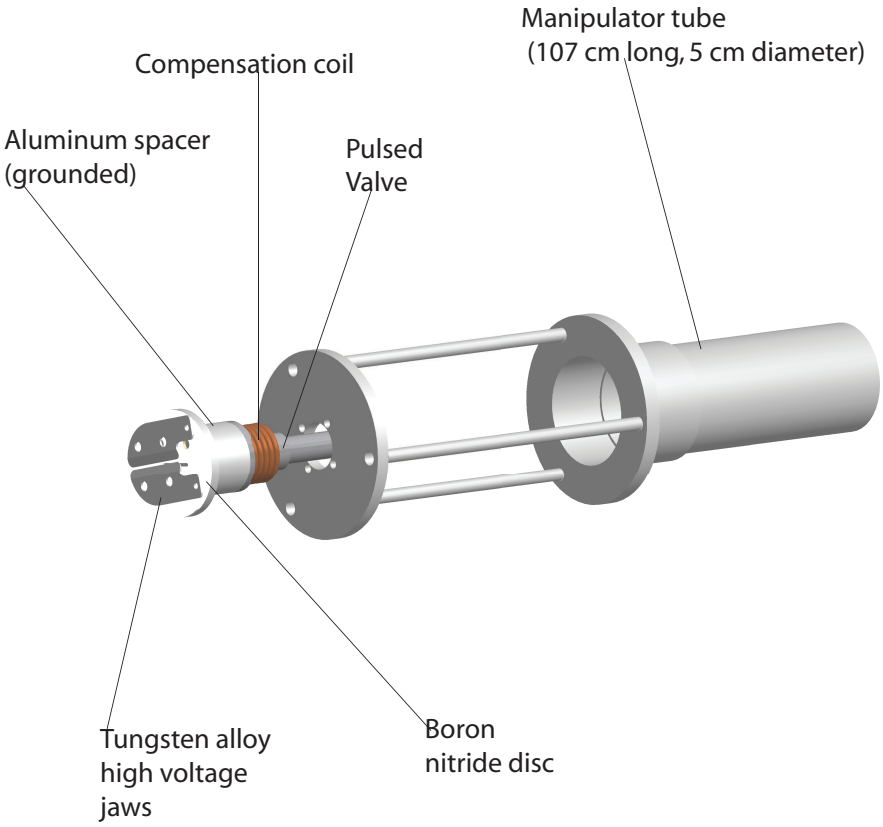

Figure 3.6: Molecular beam source. A Parker-Hannefin supersonic valve is used to produce our NH beam. Our precursor gas (ammonia or a mixture of nitrogen and hydrogen) dissociates in the electric field between two tungsten alloy jaws held at high voltage. The beam propagates through vacuum and enters the trapping cell. Residual fields from our magnet interfere with valve actuation, so we place a copper compensation coil around the body of the valve to null them out. Not shown are water, electrical and gas lines that fit within the manipulator tube.

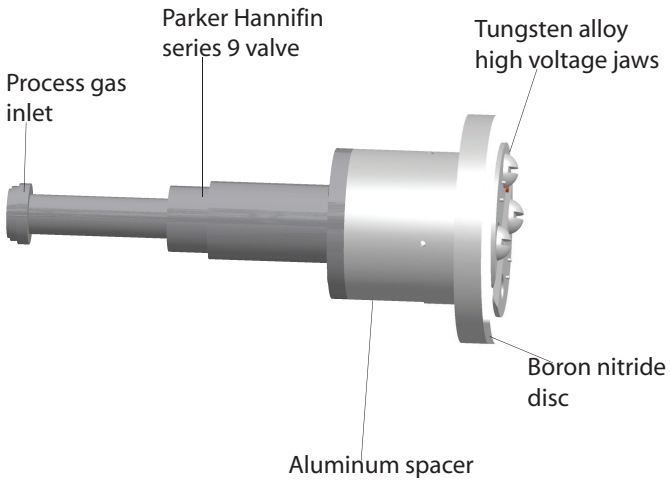

Figure 3.7: Close-up view of molecular pulsed valve.

temperature by the cooling power of the first stage of the pulsed tube cooler[2]. The bottom of the leads is cooled by connection to the magnet. At the magnet's full current of 140 A, the temperature of top of the leads rises by around 10 K, from the base value of 63 K to 73 K, due to resistive heating of copper parts of the lead assembly.

3.4 Helium and Nitrogen baths

Our magnet is cooled by anchoring it to bottom of the helium bath via copper bars. The bath contains around 30 L of helium and has a hold time of around 24 hours when we're not operating the helium-3 fridge. Running our helium-3 fridge requires operation of the 1 K pot[3] and the cooling of the fridge sorb with helium

[2]The pulsed tube cooler is a cryogenic refrigerator. Its operation is briefly discussed at a later point in this thesis.

[3]The 1 K pot is an auxiliary fridge with a base temperature of 2 K. It has a cooling power of about 1 mK/mW [11]. It is essentially a can of helium-4, continually replenished by sipping from

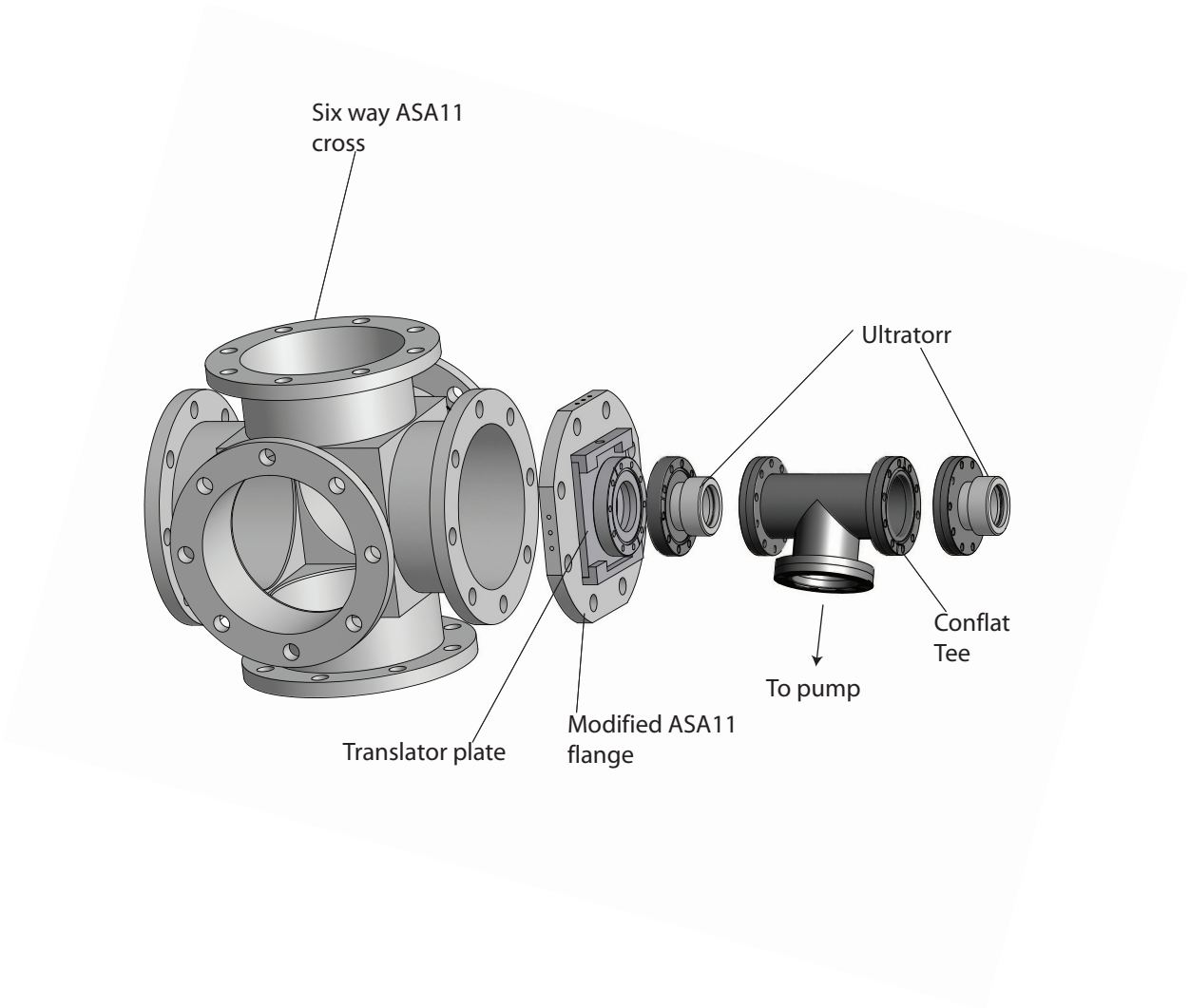

Figure 3.8: Exploded view of part of the molecular beam source assembly. The manipulator tube slides through the ultratorr fittings to move the pulsed valve into the correct Z-position; the pulsed valve assembly moves from inside the ASA cross to within the main vacuum chamber. To align the pulsed valve with the cell aperture, the translator plate slides parallel to the modified ASA-11 flange. The volume defined by the outer surface of the manipulator rod, the ultratorr fittings and the conflat tee is evacuated by a pump so that translation of the manipulator tube does not introduce gas into the vacuum chamber.

vapor, imposing an additional heat load that halves the hold time. The helium bath is surrounded by a nitrogen jacket that also cools the 77 K copper shields.

3.5 Pulsed Tube Cooler

To maintain various parts of the experiment at their operating temperatures, we must periodically supply cryogens. The running experiment consumes approximately 40 L of helium a day, and with helium priced at around $6 a liter, this amounts to a considerable expense during runs of several months duration. Our operating costs have been reduced by installing a cryocooler, a device, running on electricity, which creates a refrigeration cycle that rejects heat at various points in the experiment. We employ an orifice pulsed tube cooler, a version of cryocooler particularly suited to our work because of its reliability and the lack of vibration at the cold points. The unit provides two anchoring points: the first stage can provide 35 W at 45 K and the second 1 W at 4.2 K. The 4 K radiation shield is anchored to the latter stage and sits at 5 K when cold. The top sections of the high temperature superconductor leads are anchored to the first stage and stay below 77 K when the magnet is at full current.

3.6 Cell

Trapping occurs in a copper cell housed in the magnet bore. We desire cell temperatures lower than operating temperature of the magnet (5 K), so the cell is held

the bath, and pumped on by a room temperature pump. The evaporation of the helium reduces the temperature of the bulk liquid. It provides a condensation point for the helium-3 fridge and a thermal anchoring point for the pulsed buffer gas reservoir.

out of thermal contact with the magnet by a system of G10 rings and kevlar threads, commonly referred to as a lasso. Early versions of the cell had a single front orifice that allowed the entry of the molecular beam. Steady helium flow through the fill line and out of the cell via the front orifice established a fixed buffer gas density within it. Thermal anchoring of the cell to the helium-3 fridge occurred through welded copper braids that linked an annealed copper plate on the back of the cell to another plate positioned on the top of the fridge evaporator. Three radial sapphire windows and a fused silica window at the back aperture provided optical access to the trapped species. The mounting of the windows is a critical procedure; leaks can create a helium path between the cell and magnet, imposing an intolerable heat load on the cell.

The thermal isolation experiment required the removal of the helium fill line and the window that capped the back of the cell. A trickle of helium through the fill line is sufficient to keep the molecules in thermal contact with the cell. The open back aperture allowed the injection of buffer gas using the cryogenic reservoir and facilitated a rapid pumpout of the helium once flow is stopped.

3.7 Helium-3 Fridge

To attain temperatures cold enough to trap NH, we constructed a helium-3 fridge. The fridge is essentially a can of liquified helium-3, pumped on by a charcoal sorb. As the hotter atoms evaporate from the bulk helium-3, the temperature of the remaining liquid drops. The fridge evaporator typically sits at 400 mK during a run, and when we link it to the cell via copper braids, we can hold the cell at approximately 500

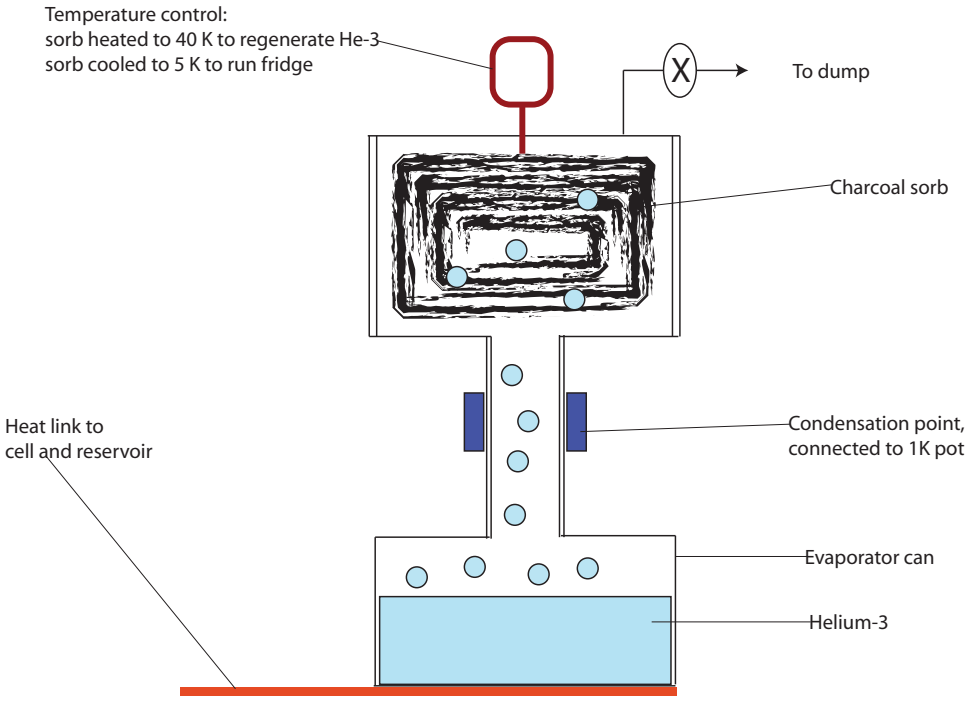

Figure 3.9: Schematic view of the helium-3 fridge. To run the fridge, the charcoal sorb is cooled to 5 K and pumps on the liquified helium-3. The evaporation of the helium reduces the temperature of the bulk liquid.

mK. The fridge is single shot, meaning the helium-3 is not continuously regenerated. The hold time is eight hours; regeneration proceeds by heating the sorb to make it release the helium and condensing the vapor to liquid by using a 1 K pot. After the liquid is condensed, the sorb can be cooled down to 5 K and the run commences.

3.8 Thermal Isolation using the Pulsed Buffer Gas Reservoir

The apparatus described above, Fig.[3.4], allows us to trap molecules cooled to the cell temperature of 500 mK. The buffer gas density in the cell remains high ($\sim 10^{14}$

cm^{-3}) even when room-side flow is shut off because the gas trickles through the small conductance fill line. To create a low background gas density in the cell after loading molecules, we remove the rear cell window and load the buffer gas into the cell with the cryogenic reservoir, the subject of the next section.

Cryogenic valves in various forms have been used in the experiments of our group [9, 70]. Creating a trapped sample of atoms or molecules out of thermal equilibrium with the surrounding cell necessitates a reduction in the density of the buffer gas present during loading. The canonical approach to achieving this has been to rapidly pump out the buffer gas through a large conductance valve, while simultaneously freezing the helium film that persists to the cell wall by dropping the cell temperature.

The theses of Michniak [70] and Brahms [9] discuss in detail the use of cryogenic valves to thermally isolate atomic species. In these experiments, the atoms were created by YAG ablation of metallic targets; we load our species from a molecular beam. This difference has consequences for the starting conditions of our experiment: we typically load at buffer gas densities nearly an order of magnitude below those of ablation experiments.

In the ablation experiments, the buffer gas in the cell is removed by a charcoal sorbtion pump when the cryogenic valve is opened. The cryogenic valve switches in the pump, and the rate of pumpout is limited by the valve conductance. The open geometry of our experiment allows us to exploit the vacuum of our chamber to remove the bulk of the buffer gas. The reservoir serves to regulate the buffer gas density for a brief period of time (20 ms), and when the flow is stopped, the pumpout rate is determined by the conductance of the cell apertures (and the desorption from the

wall).

Two other modes of operation are possible. When the reservoir is held open continuously, we can directly simulate the conditions of a cell loaded through a fill line. To permit the injection of helium using the reservoir, the cell back window is removed, creating an aperture that is ten times larger than the front cell aperture. The cell conductance is ten times larger, and the buffer gas flow rate must be correspondingly increased to reach the same densities.

The reservoir can also be used simply as a means to apply a film of helium to the walls of the cell. Indeed, it is in this mode that we obtain our longest lifetimes. To load molecules into the trap, we fire a pulsed YAG laser to desorb the helium coating the walls. Helium exits through the apertures, as well as sticking back on to the cell wall as the cell cools. The change in buffer gas density is thus determined by the aperture conductances and the cooling rate of the cell.

Most of our attempts to achieve long molecule lifetimes employed helium-3 as the buffer gas. While we have successfully demonstrated trapping molecules with helium-4, the superfluidity of this isotope make its use in the experiment problematic. The reservoir is not a perfect seal for a superfluid, and the flow of helium through tiny scratches in the sealing surfaces is sufficient to create a continuous flux of vapor into the cell. Much to our surprise, when we use Helium-4 we are able to load molecules with a nominally closed reservoir.

3.8.1 Design

The technical challenges involved in making a working cryogenic reservoir will be described in this section.

The design of the cryogenic reservoir entails accommodating thermal and mechanical constraints. The lowest attainable cell temperature in our experiment is around 500 mK. One technique for attaining a good cell vacuum involves raising the cell temperature 200 mK above its base value, and then allowing the cell to cool. This "cryogenic bakeout" binds the remaining film more tightly to the cold cell surface. However, thermalization of molecules with helium at 700 mK proceeds less efficiently than with helium at 500 mK. The benefit of better vacuum is partially nullified by the reduced molecule signal. To have long-lived molecules, we must make the cell both cold and clean.

The installation of the reservoir must therefore not add a significant conductive heat load to the cell, and the gas the reservoir supplies should be as cold as possible. The heat deposited on the cell can be controlled by careful material selection and assiduous heat sinking. The materials chosen for their thermal properties must also withstand mechanical stresses that occur from the static mounting of the reservoir and from its actuation.

Thermal Constraints

Our starting point for thermal design of the reservoir is the power curve for the cell, obtained by applying heat to the cell and observing the difference between the cell and evaporator temperatures. From this plot, Fig.[3.10], we can obtain the heat

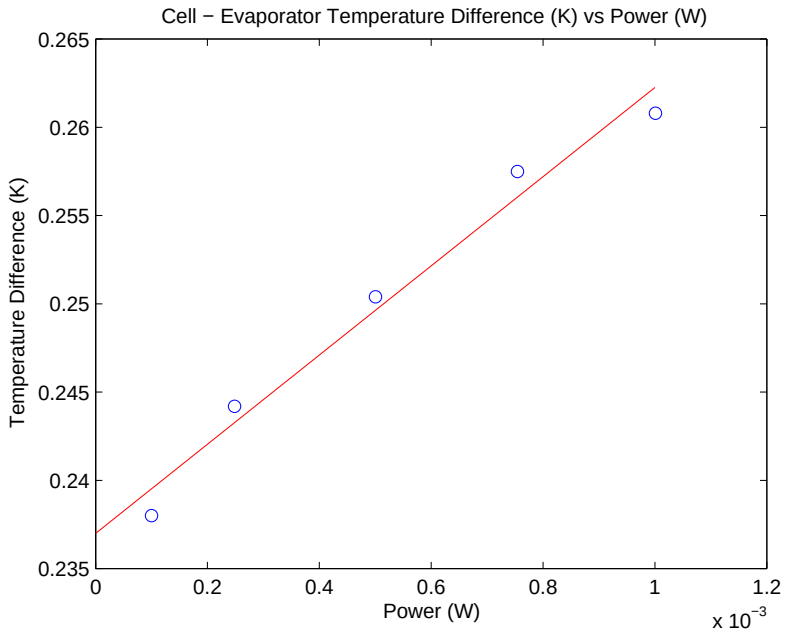

Figure 3.10: Cell - Evaporator temperature difference vs applied power. This graph gives us heat load on the cell when no power is applied and the sensitivity of the cell temperature to an external heat load.

load on the cell with no applied power - 9.4 mW - and the sensitivity of the cell to an external heat load - 25.2 $\frac{mK}{mW}$. If we are willing to tolerate a 3 mK rise in the cell temperature, we see that we must restrict the heat flowing from the reservoir to the cell to around 100 μW.

To minimize the heat flowing to the reservoir and cell, we chose to make the support rod for the reservoir, Fig.[3.13], out of Alloy 304 stainless steel (0.25 mm wall thickness, 3.80 cm outer diameter, 30 cm total length), a material mechanically strong and poorly conductive of heat. The rod was divided into three equal length sections and assembled in the following way. One section was mounted mechanically to a plate at 300K on one end and thermally anchored to 100K at the other. The next section had ends at 100 K and 4 K, and the last had ends at 4 K and 2 K. Between

each section was a 0.635 cm thick copper plate that served as a cold baffle, preventing blackbody radiation from being piped to the reservoir and providing a cold point for effective pinning of the section end temperatures.

The maximum deflection of a beam loaded at one end with the other end fixed is [39]

$$D = \frac{Wl^3}{3EI} \tag{3.4}$$

where D is the deflection, W is the weight of the load, l is the beam length, I is the moment of inertia and E is the elastic modulus of the beam material. A 3.81 cm diameter tube, 0.025 cm wall thickness, loaded with 1 kg, produces a deflection of 0.7 mm over 30 cm. This deflection is acceptable.

As a final thermal disconnect, the reservoir was stood off from support tube by three 7.62 cm long 1.27 cm diameter tubes with 0.025 cm wall thickness. The heat deposited on the reservoir by its mechanical support is 32 μW; the heat flowing to the cell from the reservoir will be even less. We can thus work to achieve the coldest possible reservoir by directly heat-sinking it to the cell via five 101 Alloy copper (99.99 % min Cu purity) braids (12.7 cm long).

To prevent thermal gradients, the reservoir body was constructed from 101 Alloy copper. The reservoir is sealed by a teflon disc ("the boot") pressing against a brass surface ("the seat"). Both surfaces are polished to mirror-like flatness. The idea behind soft-hard surface seals is reduce leak paths (created by dust or surface imperfections) by tolerating a small amount of deformation of the soft surface. Teflon, Kel-F and several other polymers retain a degree of plasticity at low temperature,

and are the materials most often used in such applications. Brass and alumina have successfully been used as seat materials because they maintain a high polish.

A Vespel SP22 shaft threads into the boot and slides through a guide bushing (also made of Vespel SP22) to open and close the reservoir. Friction between the shaft and the bushing leads to heating of the buffer gas each time the reservoir is actuated; Vespel SP22 (the version of Vespel with the highest graphite content) is chosen to minimize this. The top of the shaft is shaped like a hemispherical dome and is captured within a G10 (a fiberglass-epoxy composite material) assembly known as the "cage". Pulling on the top of the cage compresses a phosphor bronze spring and lifts the shaft. In the closed position, the spring presses down on the hemisphere via the top plate of the cage and thus transmits force to the boot. The "cage" design is chosen to prevent improper sealing of the reservoir due to canting of the boot with respect to the seat. The point contact between the cage and shaft hemisphere ensures that the boot sits flat against the seat when the reservoir is closed.

The reservoir spring is phosphor bronze and provides 57.8 $\frac{N}{cm}$ closing force. Spring compression is matched by the extension of a bellows - the bellows, flanges and main valve body form the enclosed volume for the buffer gas. The opening force is transmitted through a steel thread to the bellows flange.

3.8.2 Shield Modifications

The addition of the reservoir to the experiment compelled us to make changes to the main vacuum box and the radiation shields. We require forces of around 50 N (provided by the spring) to seal the reservoir and 100 N (provided through the steel

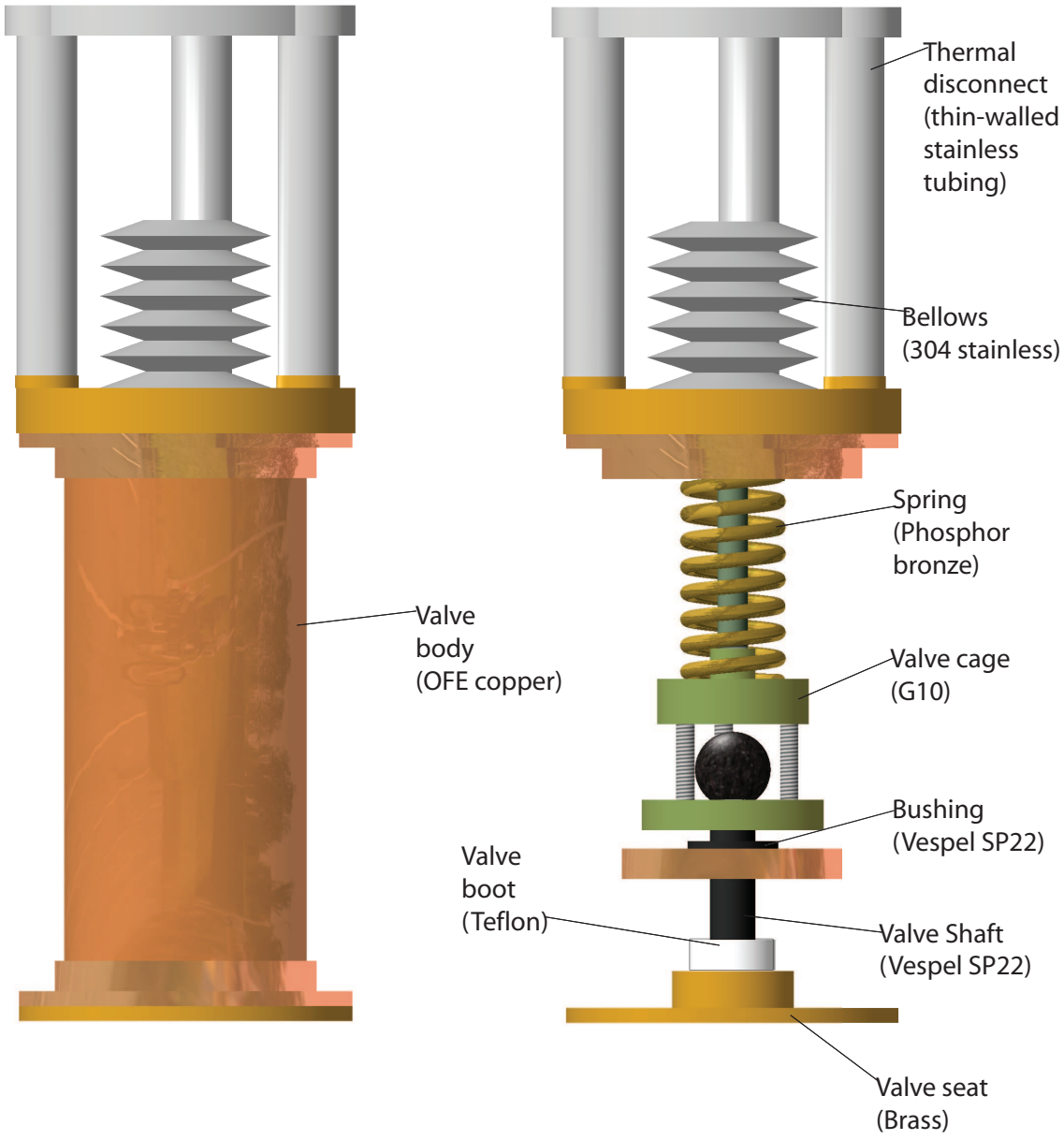

Figure 3.11: External and internal views of pulsed buffer gas reservoir.

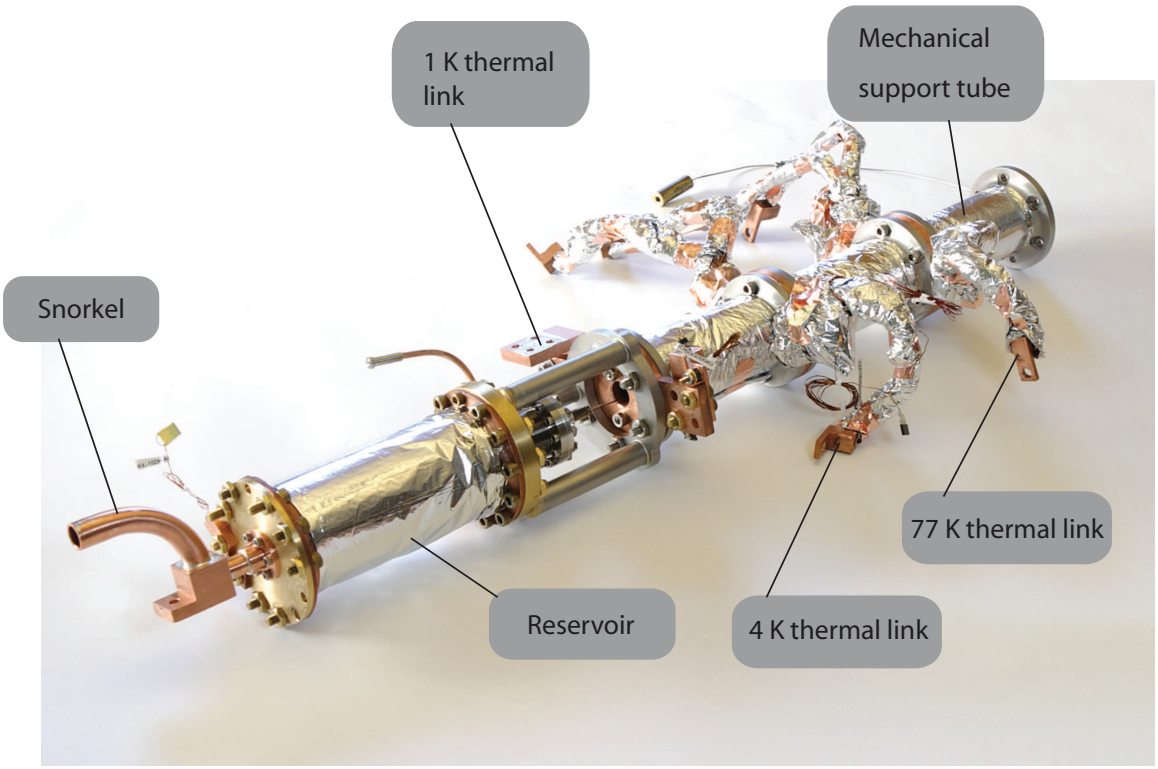

Figure 3.12: Fully assembled pulsed buffer gas reservoir

thread) to open it. The direct application of the opening force to the radiation shields is likely have a host of unfortunate consequences, including the optical misalignment of our probe laser and the catastrophic opening of various indium seals in the system. To avoid these problems, tubular extensions were created for the radiation shields and the spiderbox. The shield extensions also serve as intermediate thermal anchoring points, so their thermal properties were of considerable importance. The extensions are centered around the magnet axis and are designed to nest within each other, in a manner reminiscent of Matryushka dolls.

4 K Extension

The 4 K extension is a 27.9 cm long tube of 20.3 cm diameter extruded 6063 Alloy aluminum. Eighteen flexible tabs with holes are machined at each end of the extension. The holes align with holes in two end flanges; the tabs flex to maintain good contact to the flanges through thermal cycling. The tube wall thickness is 0.32 cm.

Consider the blackbody heat on the extension from a radiation shield at 120K:

$$Power = A\sigma T^4 = 2.5\ W \tag{3.5}$$

A is the shield area, σ is the Stefan-Boltzmann constant and T is the temperature of the blackbody source. For a range of materials we can calculate the temperature rise we expect at the far end of the tube, if we anchor its base to a 4 K shield that sits at 5 K. With 2.5 W on the tube extension,

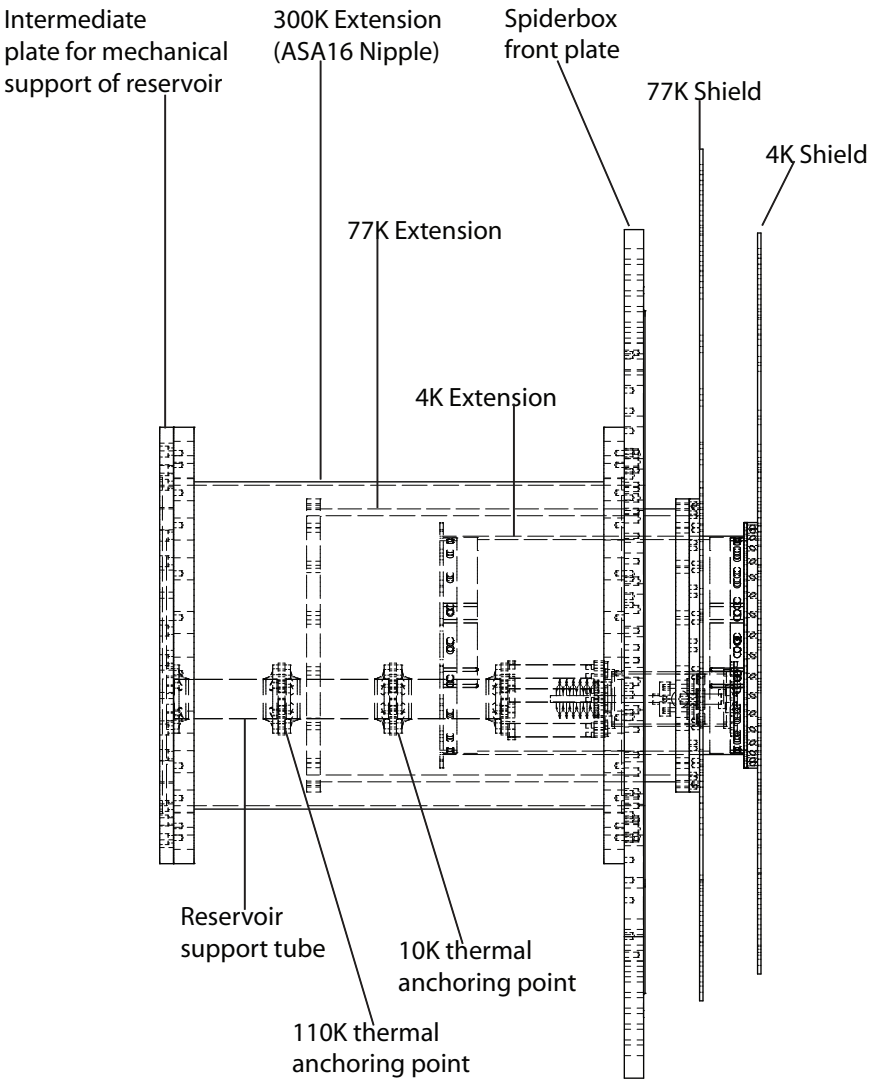

Figure 3.13: View of the cryogenic shield assembly, modified to incorporate pulsed buffer gas reservoir.

$$T_{Cu} = 5.2\ K \tag{3.6}$$

$$T_{Al_{6063}} = 10.2\ K \tag{3.7}$$

$$T_{Al_{6061}} = 15.6\ K \tag{3.8}$$

The copper tube has far superior performance, but the 6063 aluminum alloy is acceptable.

77 K Extension

The 77 K extension is 35.5 cm long and 27.3 cm in diameter. The external diameter of the original tube stock is reduced from 27.3 cm to 25.4 cm over the middle 33 cm to create two flanges at the ends. It is made from 6061 alloy aluminum. 6063 alloy aluminum is a better conductor of heat than 6061 alloy but was not available at the size we required. By making the flanges part of the tube, rather than separate pieces, we eliminated two boundaries and thus improved the thermal performance of the extension.

The blackbody heat load on the 77 K extension is approximately 150 W. With the base of the extension anchored to the 77 K shield (90 K), the end of the extension would rise to 140 K.

For both the 77 K and 4 K extensions we can reduce the absorbed blackbody by wrapping them in layers of superinsulation (aluminized mylar foil). With six layers

of mylar wrapped around each extension, the 4 K extension sits below 10 K and the 77 K extension below 110 K.

300 K Extension

The extension of the spiderbox is a 41.9 cm long ASA-16 nipple. The nipple mounts directly to the spiderbox. An intermediate plate, made from aluminum, bolts onto the end of the extension for mechanical support of the reservoir. The vacuum space of the spider box is closed by an ASA flange with windows and ports for pumping and reservoir actuation.

3.8.3 Reservoir Actuation

To open the reservoir, approximately 100 N of force is transmitted through steel cable to the top flange of the reservoir. The flange sits atop a bellows, so the opening force causes extension of the bellows and compression of the sealing spring. The opening force is provided by an actuator assembly located outside the spiderbox, so we have to accomplish a transition from vacuum to atmospheric pressure as we transmit this force. A stainless steel bellows is again used to achieve this. To ensure tautness of the actuation cable, the bellows fits on the end of a 1.91 cm diameter tube that slides through an ultratorr fitting. As the tube slides outwards, the room-side bellows is compressed and the actuation cable loses its slack. The tube position is maintained by a stop, so the initial mechanical conditions are precisely defined. A displacement of the actuating piston is reciprocated by internal motion of reservoir.

Kevlar is an alternative to stainless steel as a material for the actuation cord. It

is a poorer conductor of heat than stainless steel, and thus would impose a smaller heat load on the reservoir. Unfortunately, for our application, Kevlar or any other aramid fiber would have had a number of disadvantages. While steel cable can be brazed or welded to flanges that can mate to other parts via threads, Kevlar must be glued (or braided to other Kevlar). The glued fiber has a failure mode in which the epoxy-Kevlar composite cracks when it is subjected to cycles of high stress. Kevlar also undergoes a slow extension when subjected to stress, as the fibres settle into more compact configurations. This would result in a degradation of the actuation performance, as the cord loosened over time.

A pneumatic actuator provides the force required to open the reservoir. The main actuator component is a barrel, which is divided into two chambers by the piston. Each chamber can separately be filled with pressurized air. Differential air pressure in the chambers places a net force on a piston, which moves back and forth within the barrel. We modify a commercial actuator for our experiment. The chambers have NPT tapped holes drilled in them to accommodate ports that permit (1) air to be introduced, (2) air to be vented and (3) air pressure to be measured. Air inlet and exit are regulated by a pair of solenoid valves for each of the two chambers. The piston is coupled to bellows by a length of steel cable. The displacement of the piston is mechanically limited and damped by sorbethane pads; we require a throw of about 3 mm to fully open the reservoir.

3.8.4 A Note on the Reservoir

At room temperature, only the mechanical response of the reservoir can be tested. The seal quality of the boot, the gas delivery to the cell and the thermal heat load applied to the cell must all be investigated at cryogenic temperatures to determine if the experimental system performs within specifications. It is to be noted that use of the reservoir to supply helium does not guarantee thermal isolation; the reservoir merely allows us to start and stop buffer gas flow on demand. The reservoir does not address the desorption of the helium film from the cell surface.

The following chapter will present experimental results illustrating successful use of the reservoir to trap molecules in a cell with a low background gas density.

Chapter 4

Results

The goal of our experiment is to create a system where the dynamics of trapped molecules are not determined by the presence of the buffer gas used to load them. To that end, we sought to decrease the background gas density in the cell and concomitantly achieve a longer trapped molecule lifetime. We have been able to increase the molecule lifetime by two orders of magnitude, from 400 ms to above 20 s.

The results of our experiment are presented here. This chapter will cover the calibration of the buffer gas density in the original apparatus and trapping measurements performed there. It will also cover our techniques for attaining enhanced trap lifetimes with the pulsed buffer gas reservoir and the open cell, a cell with a high conductance aperture.

4.1 Buffer Gas Density Calibration

The density of the buffer gas is a critical parameter in our experiment. Elastic collisions with helium allow us to cool the species of interest from its initial temperature (300 K) to temperatures where it can be confined by our magnetic trap (1 K). Collisions with helium also determine the molecule lifetime by setting the rates of evaporation and inelastic loss, as well as the degree of lifetime enhancement through diffusion. To establish the feasibility of using the buffer gas technique for cooling the molecule and to understand various loss processes that govern the trapping duration we require a determination of the absolute buffer gas density in our system. A few challenges are inherent in this density determination.

If two reservoirs at high and low temperatures are connected, the ideal gas equations do not always produce accurate results for the pressures in the vessels. In particular, thermal transpiration leads to the equality of the quantity $P\sqrt{T}$, where P is the pressure and T is the temperature, when the particle mean free path is long, rather than the equality of pressure expected in the short mean free path regime [55]. The surface properties of fill lines also affect flow and add further ambiguity to our knowledge of the buffer gas density. The thesis of Wesley Campbell [11] discusses low temperature barometry in some detail, and the reader is directed to this reference for further insight. We establish a fixed buffer gas density in our cell by maintaining a steady flow through it. The quantity of gas flowing out of the cell (throughput Q) is proportional to the product of the gas density and the conductance of the cell aperture

$$Q = n_{He} C_{cell}, \tag{4.1}$$

where n_{He} is the buffer gas density and C_{cell} is the cell aperture conductance. A determination of the cell conductance allows us to associate a buffer gas density with a room temperature flow rate; we can thus remove the uncertainty transpiration and other effects introduce.

In the molecular flow regime, where the mean free path between particles exceeds the orifice dimensions, the aperture conductance is [82]

$$C_{mol} = \frac{A\overline{v}}{4}. \tag{4.2}$$

$$C_{mol} = \frac{A}{4}\sqrt{\frac{8Tk_B}{\pi m_{He}}} = 2.10A\sqrt{T} \tag{4.3}$$

A is the aperture area in cm^2 and $\overline{v}$ is the mean particle velocity. C_{mol} is measured in liter/s.

When the mean free path between gas particles is short, the flow from one vessel to another depends on the pressures within the vessels. In this regime, the regime of viscous flow, the conductance of an aperture can be expressed in terms of the upstream and downstream pressures as [82]

$$C_{visc} = \frac{9.13A}{1 - P_{down}/P_{up}} \left(\frac{P_{down}}{P_{up}}\right)^{1/\gamma} \left(\frac{2\gamma}{\gamma - 1}\left(\frac{T}{M}\right)\left[1 - \left(\frac{P_{down}}{P_{up}}\right)^{(\gamma-1)/\gamma}\right]\right)^{1/2}. \tag{4.4}$$

As the pressure ratio decreases, the flow velocity and conductance reach a maximum at a critical ratio given by

$$r_c = \frac{P_{down}}{P_{up}} = \left[\frac{2}{\gamma+1}\right]^{\gamma/\gamma-1}. \tag{4.5}$$

γ is the ratio of the heat capacity at constant pressure C_P to the heat capacity at constant volume C_V. $\gamma = \frac{C_P}{C_V} = \frac{5}{3}$ and r_c is 0.49 for helium.

Flow at pressure ratios below this value is "choked" and thus the gas throughput is

$$Q_{choked} = C_{c,visc} P_{up}. \tag{4.6}$$

$C_{c,visc}$ is the conductance at the critical flow ratio.

$$C_{c,visc} = 3.73A\sqrt{T}. \tag{4.7}$$

To determine the conductance of the cell orifice, we measured the pumpout rate of helium with a sensitive, fast-acting gauge, a Fast Ion Gauge. The gauge response time is 5 μs and the useful measurement range is from 10 milliTorr to 10 nanoTorr.

The pumpout measurement is performed by abruptly switching off helium flow and monitoring the pressure at a point just outside the cell. Correcting for the pumpout time of the fill line (20 s), we obtain a cell aperture pumpout time constant of 6.2 $\pm$ 0.7 s.

Helium flow at room temperature is measured using a mass flow meter. To verify the accuracy of the nominal flow setting, the flow meter is calibrated by recording the pressure rise over time in a fixed volume.

The cell aperture conductance is measured to be 110 $\pm$ 10 cm^3/s for an orifice 3 mm in diameter. For the enlarged aperture (10 mm diameter), the conductance is

approximately 1220 cm^3/s. A flow of 1 sccm of helium creates a density of

$$n_{He} = \frac{f_{sccm}}{\sqrt{T}} \times 2.92 \pm 0.3 \times 10^{15} \frac{\sqrt{K}}{sccm} cm^{-3} \tag{4.8}$$

in a 3 mm aperture cell. The corresponding density with a 10 mm diameter aperture is $\frac{f_{sccm}}{\sqrt{T}} \times 2.65 \pm 10\% \times 10^{14} \frac{\sqrt{K}}{sccm} cm^{-3}$.

The measured value of the conductance agrees well with the calculated value of an aperture in the molecular flow regime.

The conductance measurements and calculations inform our construction of the pulsed buffer gas reservoir. To obtain a more rapid decrease in the buffer gas density after we stop flow, we decided to open the back of the cell to the vacuum space, creating an aperture 3.81 cm in diameter. The cell back aperture permits helium to be pumped out of the cell with a characteristic time constant of 40 ms, if we neglect film desorption.

Aperture Diameter: 0.3 cm - front aperture, first cell design

	Conductance (L/s)	Pumpout time (s)
C_{mol}	0.115	6
C_{visc}	0.186	3.71

Aperture Diameter: 1 cm - front aperture, second cell design

	Conductance (L/s)	Pumpout time (s)
C_{mol}	1.28	0.54
C_{visc}	2.27	0.30

Aperture Diameter: 3.81 cm - back aperture, for reservoir

	Conductance (L/s)	Pumpout time (s)
C_{mol}	16.9	0.041
C_{visc}	30.1	0.023

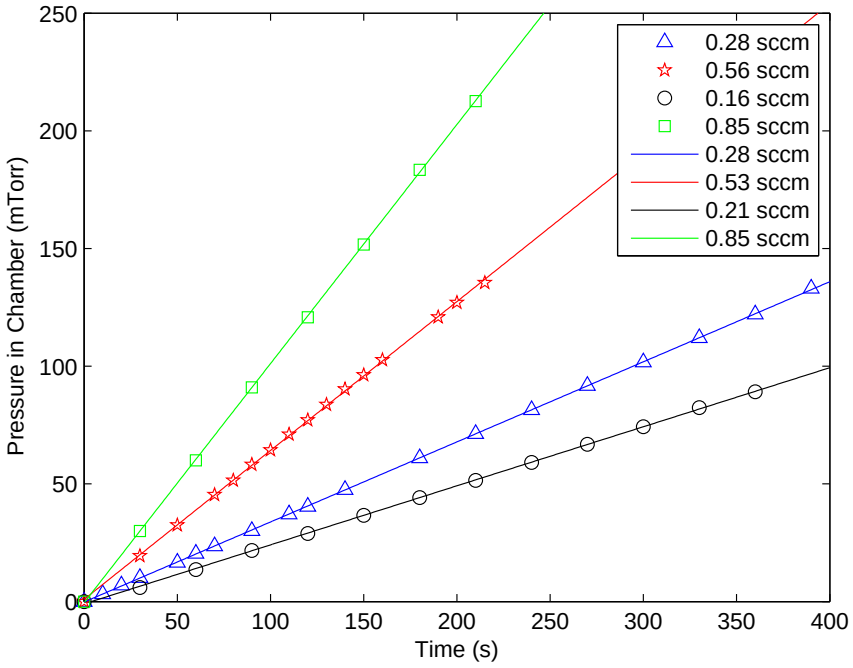

Figure 4.1: Buffer gas flow calibration. Data points represent the flow determined by filling a fixed volume. Lines represent the nominal flow, as recorded by a mass flow meter.

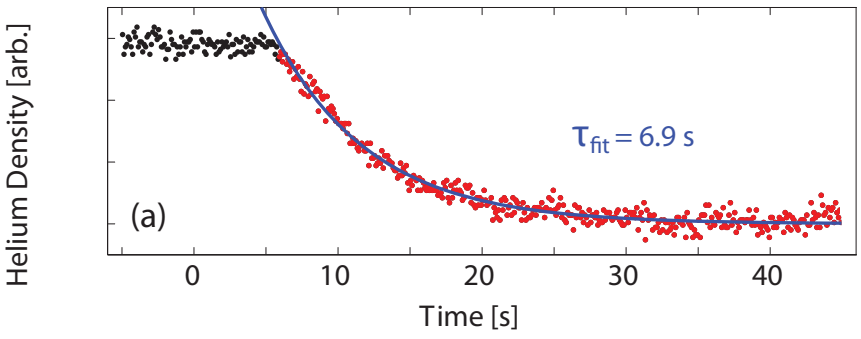

Figure 4.2: Pumpout of buffer gas from a cell with 3 mm diameter aperture, as measured by a Fast Ion Gauge (FIG).

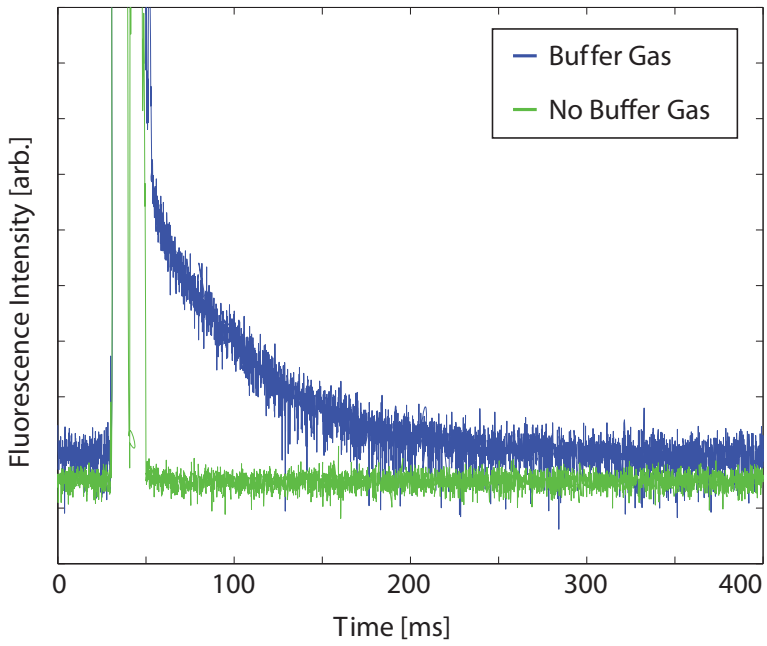

Figure 4.3: Fluorescence signal, with and without buffer gas.

4.2 Loading and Trapping

The trapping of atomic, molecular and ionic species may be defined as increasing the observation/interaction time of the sample by using external fields.

Even though we can bring the molecular beam to a standstill using only helium, we do not consider this trapping. To trap, we place the molecules in a magnetic potential many times deeper than their mean energy. For a trap depth ten times deeper than the mean molecular energy ($\eta = 10$ for T = 500 mK, B = 4 T), for instance, we can extend the molecule lifetime by a factor of 100, from 3 ms to 300 ms.

Loading of molecules is verified by recording the fluorescence signal in the presence and absence of the buffer gas Fig.[4.3].

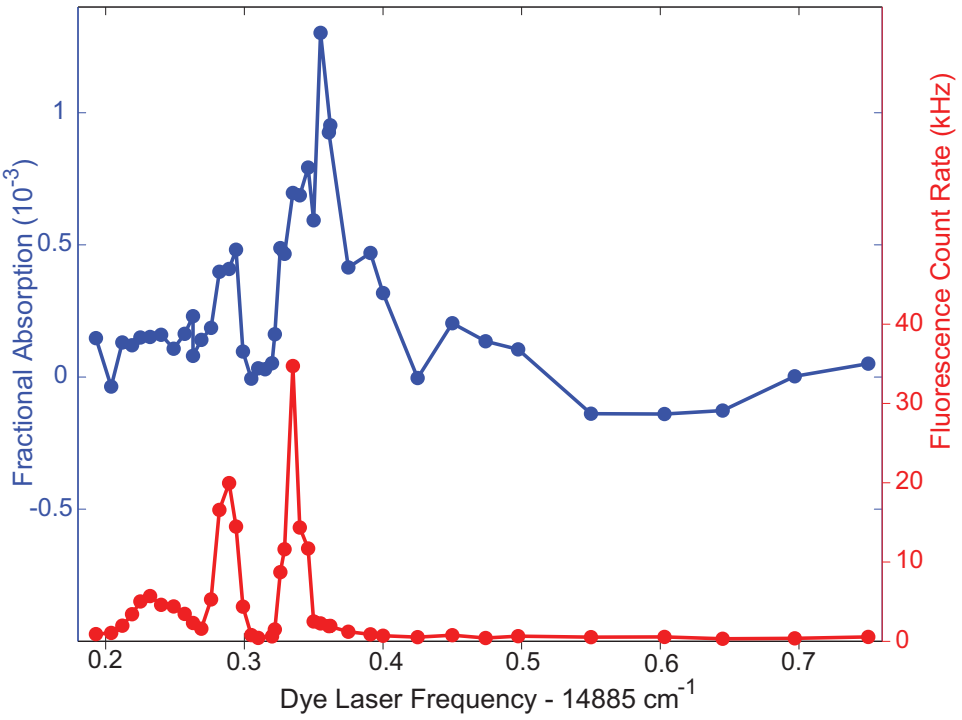

Figure 4.4: Molecular spectra, taken in fluorescence and absorption. The wavenumbers are recorded with respect to a 14885 cm^{-1} dye laser frequency.

To demonstrate the correct identification of the species, we scan the frequency and record molecular spectra in fluorescence and absorption Fig[4.4].

As discussed by Jonathan Weinstein [92] and others, from the variation of the lifetime with η (the ratio of trap depth to mean energy) we can determine the elastic cross-section of the molecule with helium (^{3}He) Fig.[4.6] (inset), calculated in our experiment to be 2.7 $\pm$ 0.8 $\times$ 10^{-14} cm^2. Using the cross-section value obtained, we can further determine the rate of Zeeman-state changing collisions by recording the variation of trapping times with the buffer gas density Fig.[4.6]. The Zeeman relaxation cross-section is $3.8 \pm 1.1 \times 10^{-19}$ cm^2 and the Zeeman relaxation rate, k_{ZR}, at 700 mK is $3.0 \pm 0.9 \times 10^{-15}$ cm^{3}s^{-1}. One Zeeman state changing collision occurs for every 70,000 elastic collisions with helium [14].

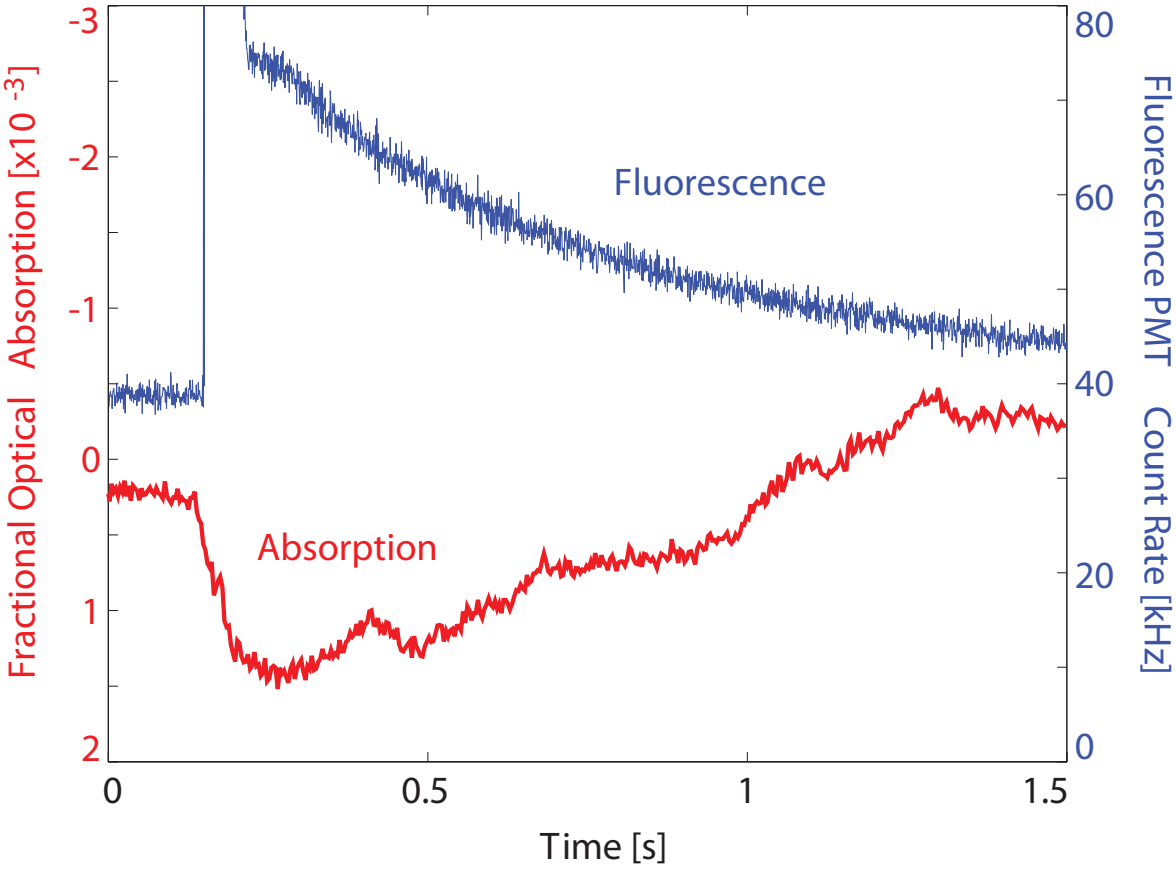

Figure 4.5: Fluorescence calibration. By recording the decay of the molecular signal in absorption, we obtain an absolute determination of the trapped molecule number [11]. If we simultaneously record fluorescence spectra, we can convert the fluorescence signal to a molecule density.

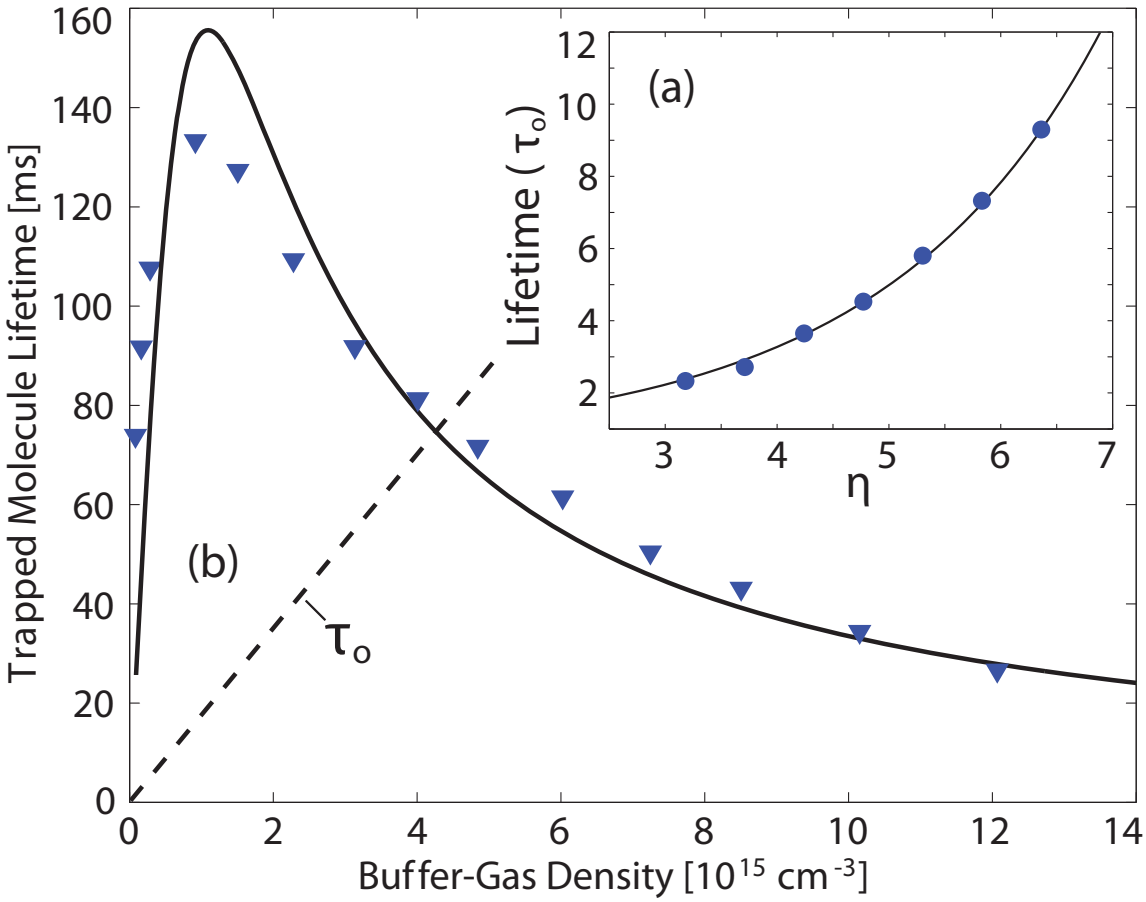

Figure 4.6: Variation of molecular lifetime with buffer gas (^{3}He) density. The buffer gas temperature is 710 mK. Inset shows the variation of the molecule lifetime as we change the trapping parameter η by changing the magnetic trap depth. The buffer gas temperature is fixed at 690 mK and the buffer gas density is set to 8.5×10^{14} cm^{-3}

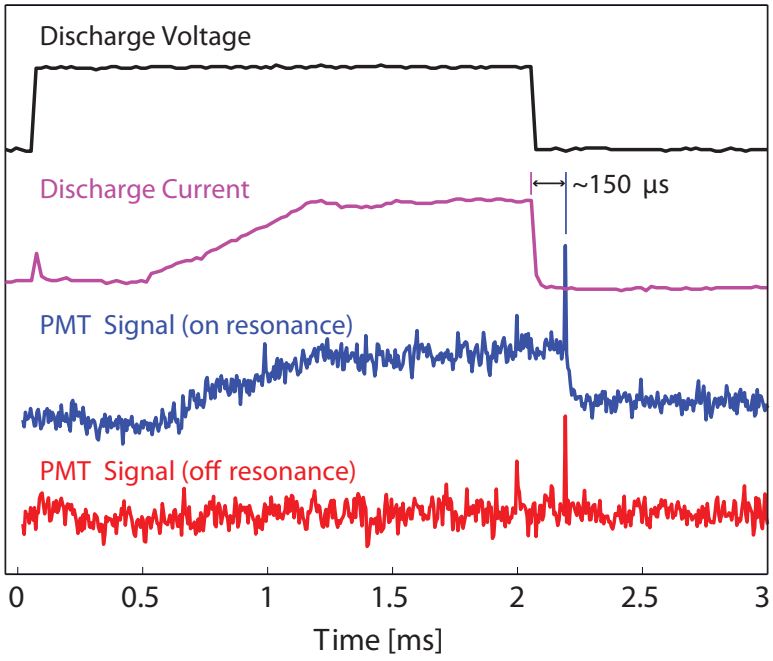

Figure 4.7: Time profiles of the high voltage used to generate NH molecules, the discharge current and the free flight molecule signal.

4.2.1 Cross-Section Calculated from Beam Loading

The molecular beam propagates through vacuum and enters our trapping cell. When the cell is filled with buffer gas, we can dissipate the forward momentum and stop the molecular packet within the cell. If we can stop the beam in the presence of a trapping field, a portion of the molecules (corresponding to a particular velocity class) will be brought to rest at a spatial position coinciding with the trap minimum. These molecules will be loaded into the trap. The combination of buffer gas and trap thus act as a very crude velocity selector for the molecules.

From our data, Fig.[4.7], we see that the molecular beam propagates at approximately 1190 m/s, corresponding to a forward temperature of 1200 K. To thermalize the beam from a temperature of 1200 K to a temperature of 550 mK (within 10% of

the base temperature), we require a total stopping distance of 4.6 cm and approximately 34 collisions with helium. The stopping distance is measured from the front orifice of the cell to the position of the magnetic trap center. This definition assumes a low gas density in the region immediately outside the cell, where we have a charcoal cryopump. Our data, Fig.[4.8], shows that a helium density of 2.65×10^{14} cm^{-3} thermalizes the class of molecules at the most probable velocity. Using these numbers, we can obtain an approximate value for the elastic cross-section of the molecules with helium.

$$N_{stop} = \sigma_d n_{He} L_{stop} \tag{4.9}$$

N_{stop} is the number of collisions required for thermalization, σ_d is the elastic cross-section and L_{stop} is the stopping distance.

The cross-section derived from this data is $2.2\times\ 10^{-14}$ cm^2, consistent with the value calculated previously. A point to note is that a degree of error is inherent in this simple calculation because we have ignored the fact that the molecular beam velocity is many times the speed of sound in helium at these temperatures (50 m/s) [72]. The error supersonic beam propagation may introduce is briefly discussed below.

The cell can crudely be represented as a pipe with one open end. The supported pressure eigenmodes [36] have nodes at the closed end ($x = 0$ cm) and antinodes at the open front orifice ($x = L = 22$ cm). They are of the form

$$p(x,t) = p_0 sin(k_n x) cos(\omega_n t) \tag{4.10}$$

The boundaries impose the constraint that $k_n L = \frac{2n-2}{2}\pi$. The temporal frequency

of the pressure variation is

$$\omega_n = \frac{n\pi}{L}\left(\frac{T}{m}\right)^{1/2}, \tag{4.11}$$

where T is the gas temperature and m the helium mass.

While the mean free path at the buffer gas density (3 mm) is smaller than the scale of the pressure fluctuations, the fluctuations are of a length comparable to the distance required to stop the molecules (5 cm). The injection of the molecular beam, at a velocity twenty times the sonic speed, leads to the propagation of shockwaves through the gas [72] . Sonic shock will activate a number of pressure eigenmodes in the buffer gas, resulting in pressure variations on the centimeter scale. The mean buffer gas density is unchanged, but the inhomogeneity of the pressure in the cell might change the density at which molecules with the most probable velocity come to rest at the trap position.

4.2.2 Towards Thermal Isolation

The maximal lifetime we observe in the cell with the 10 mm aperture is around 400 ms with a steady state flow of 500 mK buffer gas. To increase the lifetime we can employ "cold loading", where we stop buffer gas flow to the cell and generate sufficient helium to load molecules by desorbing it off the walls. To desorb the helium, the heat may be delivered by a YAG laser or a resistive heater or come from the molecular beam itself, as it sticks to the rear cell window. Using cold loading, we can obtain lifetimes just below 1 s (940 ms). Even though cold loading thins the film, most of the helium readsorbs back onto the walls. This helium desorbs slowly, and, due to

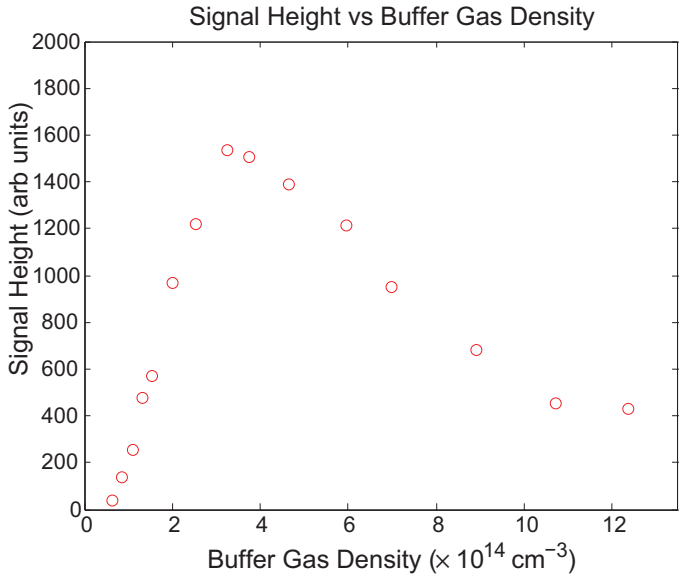

Figure 4.8: Variation of loaded NH signal (arbitrary units) with buffer gas density (cm^3).

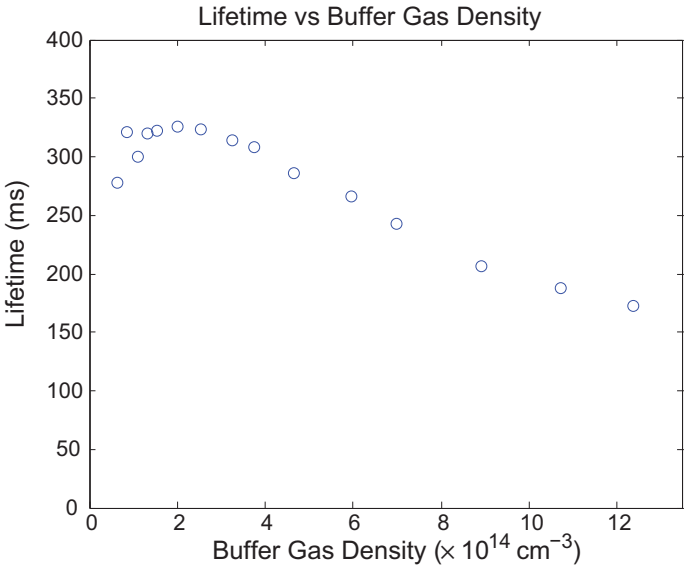

Figure 4.9: Variation of NH trap lifetime with buffer gas density.

the small conductance of the orifice, maintains a density in the cell high enough to keep us in thermal contact.

To achieve thermal isolation the cell design was modified. In addition to the front aperture, we created a large diameter (3.81 cm) aperture in the back of the cell. The pumpout time of the cell with the larger back aperture is around 40 ms, an order of magnitude smaller than a typical trap lifetime. As the buffer gas density decreases from a typical loading density of 10^{15} cm^{-3}, we expect the lifetime to decrease initially (as we lose the diffusion enhancement of the lifetime) and then to increase, as inelastic loss and evaporation over the trap edge shut off at the lower densities.

In the new cell, we also removed the small conductance fill line that previously supplied helium. To load buffer gas into the cell, we actuate the pulsed buffer gas reservoir; this will be termed "reservoir loading".

The transition to low buffer gas densities as the buffer gas exits the cell results in changes to the trap lifetime, since the rates for different processes (diffusion, evaporation) change. In the experiments with steady helium flow through the cell, we obtained excellent agreement to one-body fits for the entire trap duration. In contrast, the changes in the helium density due to pumpout will lead to changes in the trap lifetime and poor agreement to one-body fits Fig.[4.10].

The molecule lifetime observed with reservoir loading is still fairly short ($\sim$ 400 ms). The likely culprit is the helium film on the walls. To overcome the limit the film sets on our lifetime, we can employ a variation of the cold loading technique to load molecules into the trap. We actuate the pulsed buffer gas reservoir, wait a time interval for the film to thin and then fire a diffuse YAG laser beam to desorb helium

from the walls.

A less intense YAG pulse can produce buffer gas at a lower temperature, but does not generate sufficient gas density to thermalize the beam. The competing factors of density and temperature limit the YAG energy we can use to approximately 4 mJ. The density and temperature of the desorbed helium are not well known at this time[1]

If we fire the YAG laser and molecular beam 10 s after reservoir actuation, the trap lifetimes we observe are on the order of 5 s, Fig.[4.11]. If we delay the molecule and YAG pulses even further (45 s), to allow for even more film thinning, we observe lifetimes exceeding 20 s, Fig.[4.12]. The lifetime of 20 s indicates that the helium density in the cell is below 10^{12} cm^{-3}. For the sake of comparison, we note that to load the molecules with a steady state flow of buffer gas, we require a density of around 10^{14} cm^{-3}; the lifetime we measure with a background gas density of 10^{14} cm^{-3} is approximately 400 ms, at a temperature of 500 mK.

4.3 Simulation

Background evaporation is treated using a Monte Carlo simulation [9, 70]. Mass, temperature, elastic cross-section and the trapping parameter η all determine molecule lifetime in the long mean free path regime.

The Monte Carlo simulation randomly extracts molecules from a Maxwell-Boltzmann distribution at the cell temperature and tracks their motion in the trapping field.

[1]One potential way of obtaining this information is to trap a more paramagnetic species, like chromium, and then monitor how the atoms are expelled from the trap as laser power and trap depth vary. The rate of energy transfer from the desorbed gas to the trapped sample can be used to infer the transient density created in the cell.

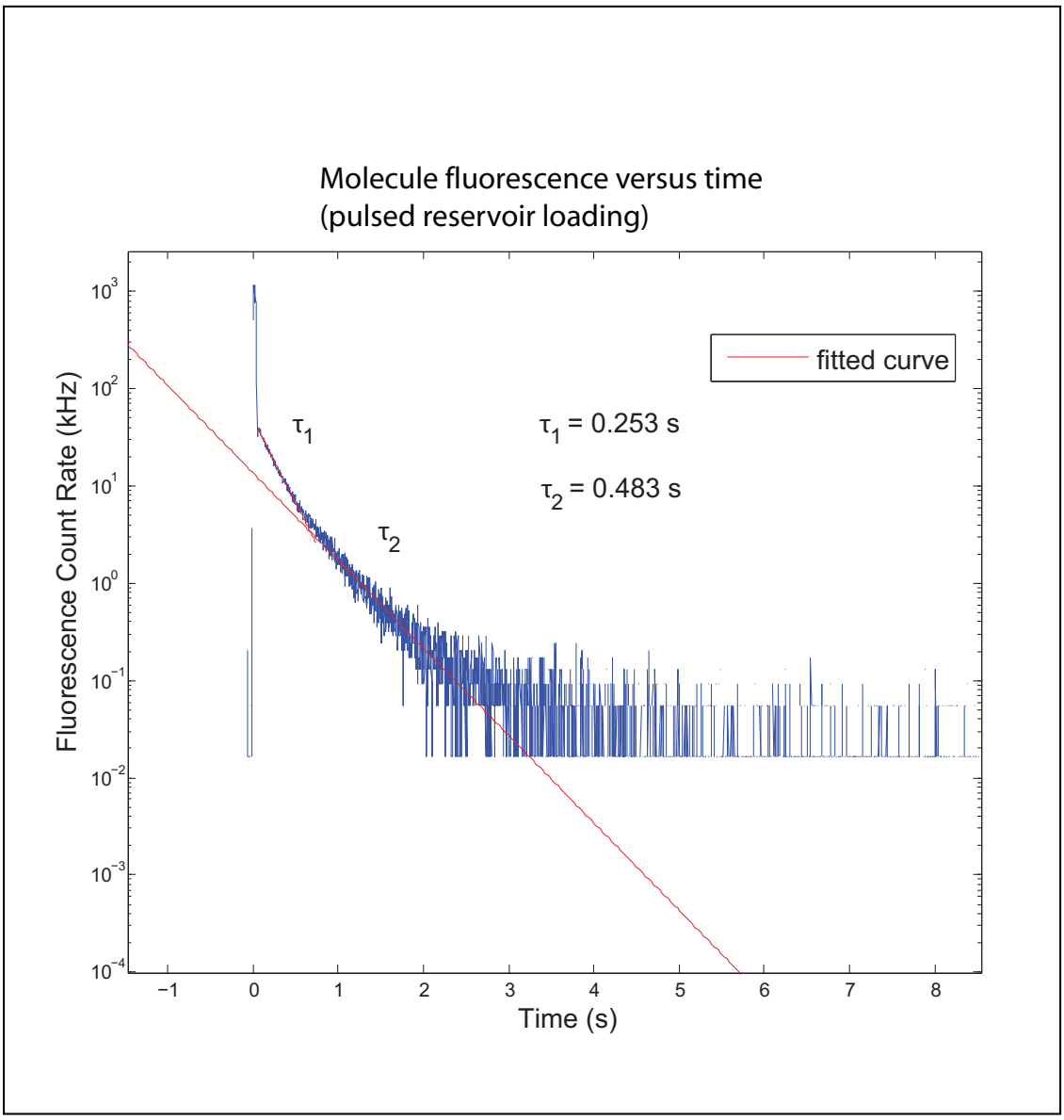

Figure 4.10: Decay of molecular fluorescence signal. At early times (0 s - 1 s) the molecule lifetime fits well to 0.25 s. At later times the lifetime lengthens to 0.48 s.

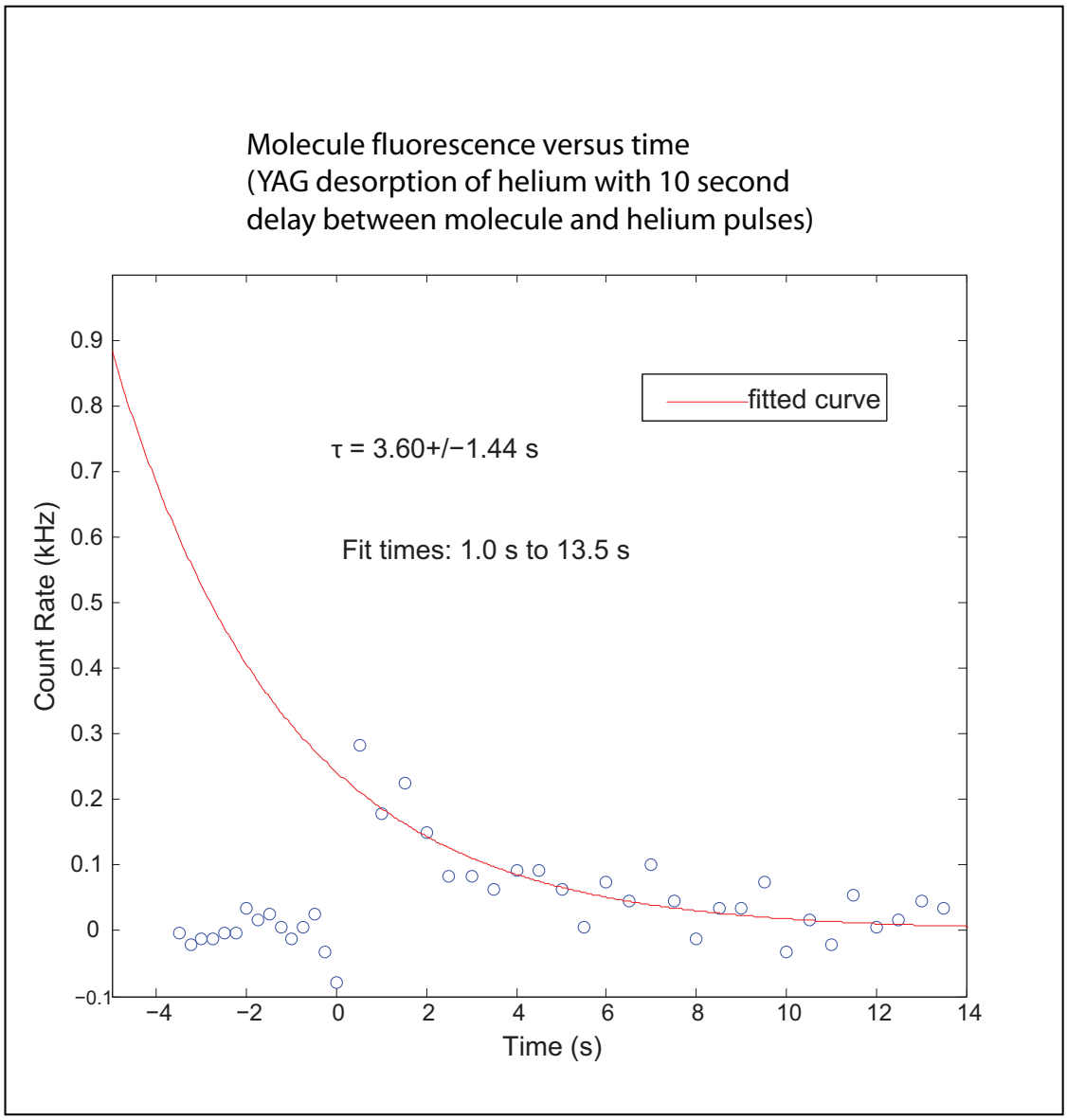

Figure 4.11: Decay of molecular fluorescence signal with YAG loading. The YAG laser pulse is fired 10 s after the pulsed buffer gas reservoir coats the cell with helium. The molecule lifetime is approximately 4 s, suggesting a high residual helium background.

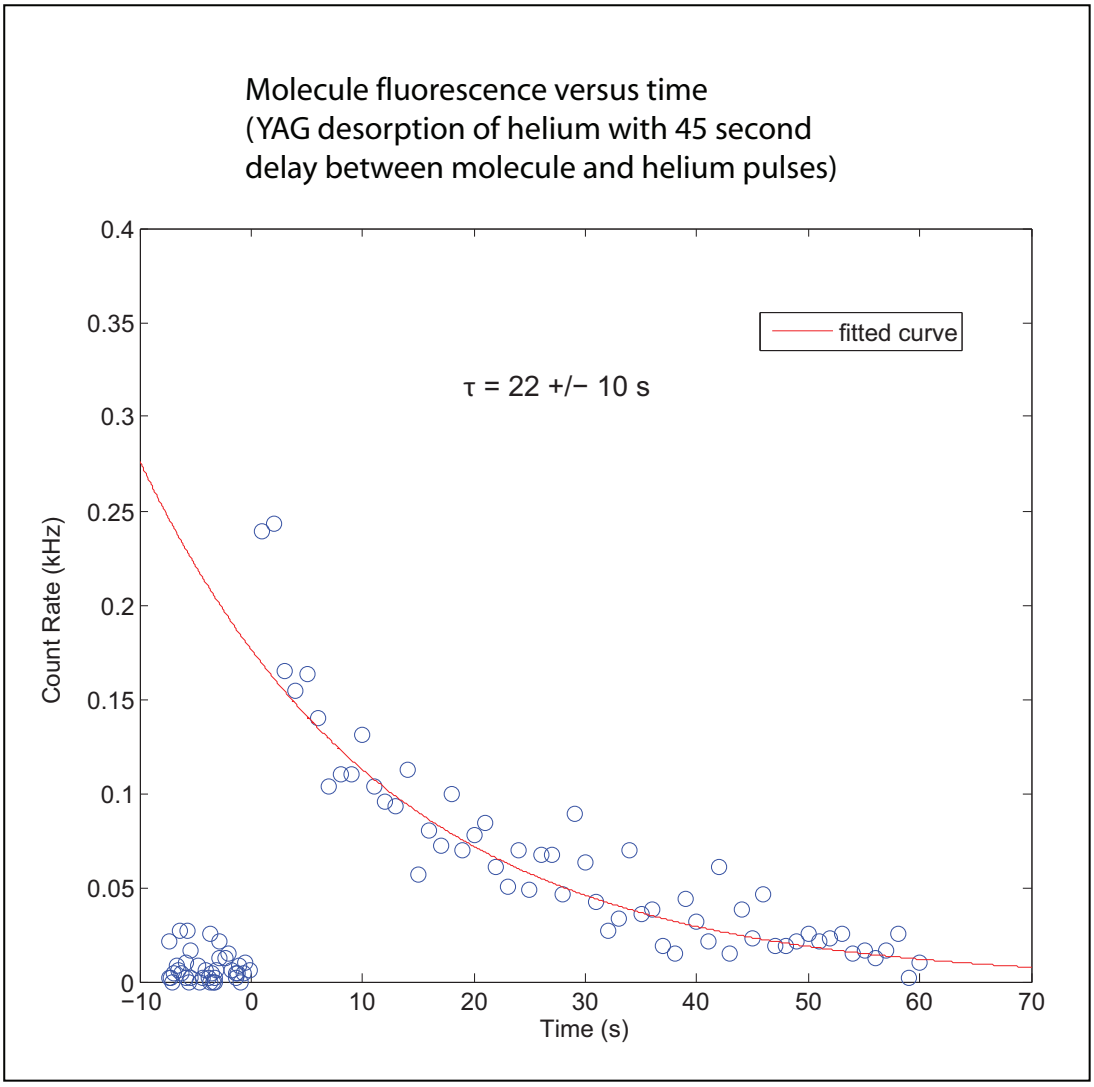

Figure 4.12: Decay of molecular fluorescence signal with YAG loading. The YAG laser is fired 45 seconds after the pulsed buffer gas reservoir coats the cell with helium. The longer lifetime indicates a lower background gas density.

Variation of mean free path with buffer gas density

Buffer Gas Density (cm^{-3})	λ, Mean Free Path (cm)	$\frac{\lambda}{R_{cell}}$
10^{15}	0.017	0.005
10^{13}	1.7	0.5
10^{11}	170	50

Table 4.1: Variation of mean free path with buffer gas density

Collisions with helium can change the velocities, energies and orbits of the trapped particles and can produce evaporative loss from the trap.

The diffusive model of molecular motion in a background gas is only valid when the mean free path is small compared to the cell dimension. For long mean free paths, the Monte Carlo simulation is essential to understanding the trap dynamics.

In several experiments we perform, we have limited knowledge of the elastic cross-section of the species with helium. We use the value of 1×10^{-14} cm^2 in calculations as a guide; in previous work, measured cross-section values have deviated from this by small factors of unity.

In our experiment, we have been able to empirically measure the elastic cross-section of NH with helium; we can use the Monte Carlo simulation to further investigate the effect of varying the cross-section on the rate of background loss. Our simulation, Fig.[4.15], indicates that the onset of diffusion enhancement occurs at a lower density for large cross-sections. A smaller cross-section also correlates to a longer lifetime at lower densities, as evaporation becomes less likely.

The Monte Carlo lifetime only reflects diffusion and evaporation; inelastic loss is excluded. In the presence of spin relaxation, the measured lifetime will be determined by both elastic and inelastic trap loss processes. τ_{eff}, the effective lifetime (a value

that would be measured in an experiment), is related to the Zeeman relaxation lifetime $\tau_{ZR} = 1/(n_b k_{ZR})$ and the elastic lifetime τ_{MC} in the following way:

$$\tau_{eff} = \left(\frac{1}{\tau_{MC}} + \frac{1}{\tau_{ZR}}\right)^{-1}. \tag{4.12}$$

At a buffer gas density of 10^{15} cm^{-3}, $\tau_{MC} = 3$ s and $\tau_{ZR} = 1/3$ s. $\tau_{eff} = 300$ ms, in close agreement with what we measure.

The curves in Fig.[4.14] show the lifetimes for identical η but at different temperatures. The evaporation fraction of a molecular distribution is a function of η [20], so the temperature dependence of the evaporation rate seen in the figure arises solely from the change in the collision frequency at the different temperatures. For a given buffer gas density, the trap lifetimes at the colder temperature (250 mK) are forty one percent longer than those at the higher temperature (500 mK). This difference is fully accounted for by the difference in the mean relative speeds of the collision partners.

The Monte Carlo simulation appears physically self-consistent and accurately reproduces the molecule lifetimes for densities we can control (around 10^{15} cm^{-3}). Using the simulation and measured molecule lifetimes, we estimate that the residual buffer gas density in our cell after cold loading is between 10^{11} cm^{-3} and 10^{12} cm^{-3}, Fig.[4.15].

The desorption of the film can also be modeled numerically [70]. The thickness of the film on the cell $d(t)$ is coupled to the equilibrium helium density $n_{He}(t)$ by the following differential equations:

$$\dot{n_{He}} = \frac{n_{He}}{\tau} + \frac{Af}{V}\left[P_0 exp\left(\frac{-\alpha}{Td(t)^3}\right)\frac{1}{k_B T} - n_{He}\right] \tag{4.13}$$

$$\dot{d} = -\frac{d_0}{N_0} f A \sqrt{\frac{k_B T}{2\pi m}}\left[P_0 exp\left(\frac{-\alpha}{Td(t)^3}\right)\frac{1}{k_B T} - n_{He}\right]. \tag{4.14}$$

- $d(t)$ is the film thickness (d_0 is its initial value).
- $n_{He}(t)$ is the buffer gas density.
- A is the cell surface area.
- V is the cell volume.
- $f = 0.75$ is the sticking probability of helium.
- α is the van der Waals coefficient of helium, which measures the binding energy between the helium atoms and the surface.
- N_0 is the number of atoms in a monolayer of helium.
- τ is the cell pumpout time, the cell volume divided by the aperture conductance.

The helium density profile that solves this equation is characterized by very rapid initial pumpout, Fig.[4.16] (as the gas leaves through the cell apertures), followed by a slow decrease, as the film thins from the wall and exits the cell. After twenty seconds, the residual buffer gas density is determined to be 10^{12} cm^{-3}. If we incorporate a time dependence in the cell temperature, to simulate cooling after a YAG fire, the buffer gas density decreases more quickly, as the film becomes more tightly bound to the cooling cell.

We fire the YAG laser 45 seconds after coating our cell with helium to "cold load" molecules. After the initial spike in gas density from YAG induced desorption, the numerical solution suggests that the background density falls below 10^{12} cm^{-3}, as helium driven from the film pumps out through the cell aperture.

The long molecule lifetimes and low background gas densities suggest the possibility of observing collisions between NH molecules and trapped paramagnetic atoms. If molecules and atoms can be trapped at sufficiently high densities, inelastic collisions between them will be manifested as a change in the molecule lifetime correlated to the atomic density. The chapter that follows discusses this potential direction of our experiment.

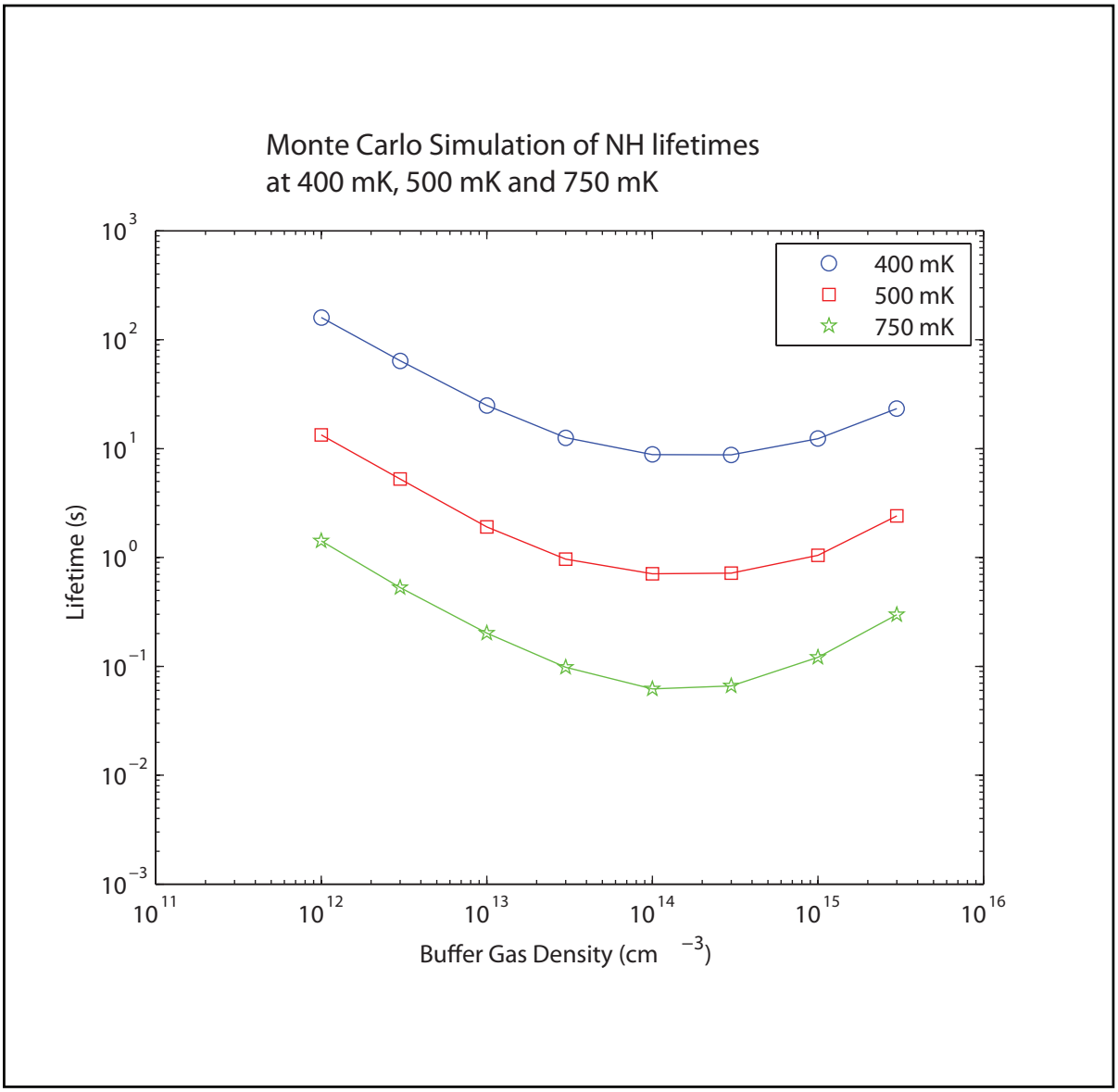

Figure 4.13: Simulation of the variation of molecule lifetime with buffer gas density at different temperature.

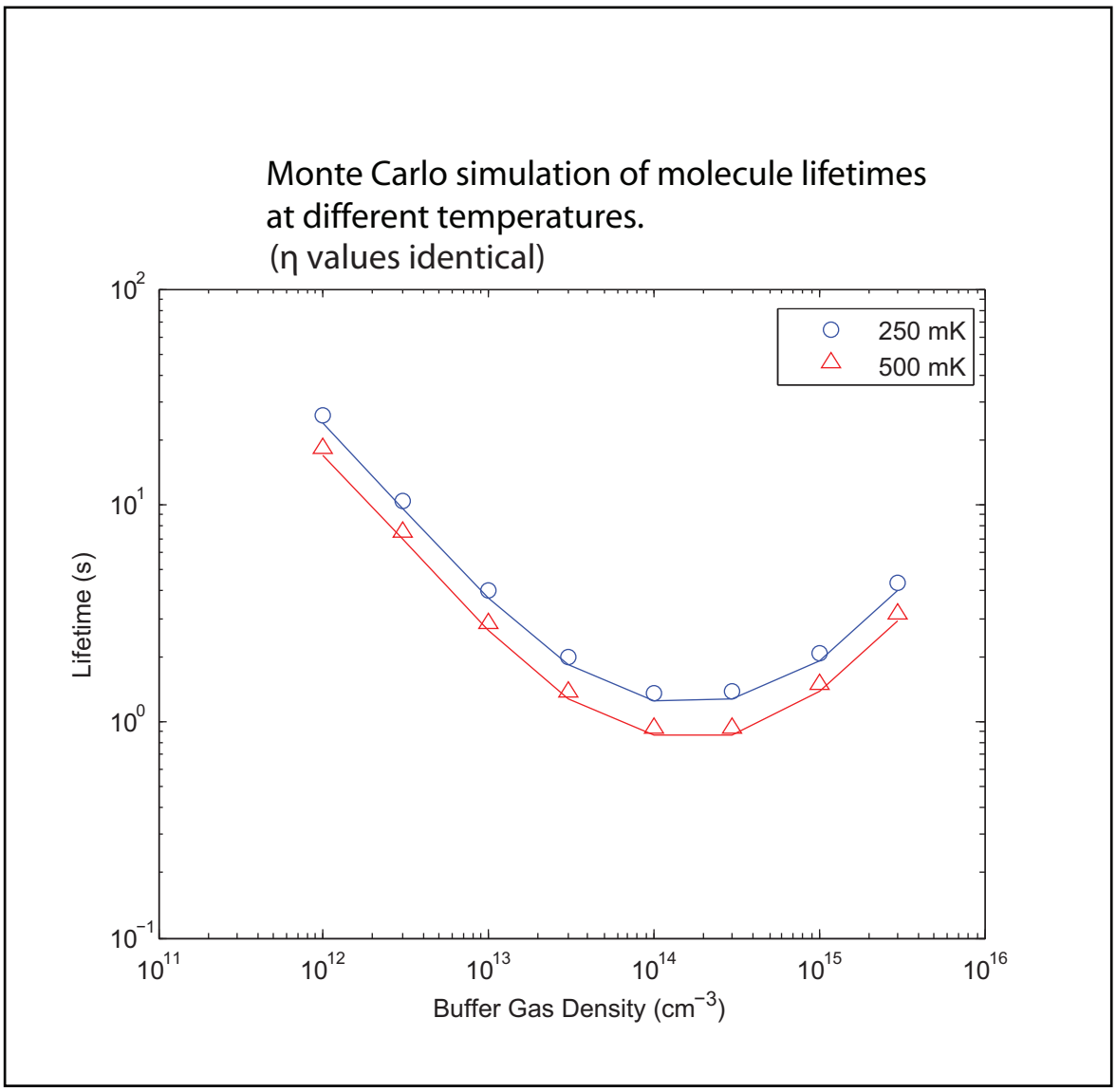

Figure 4.14: Variation with molecule lifetime with buffer gas density, identical η values, different temperatures

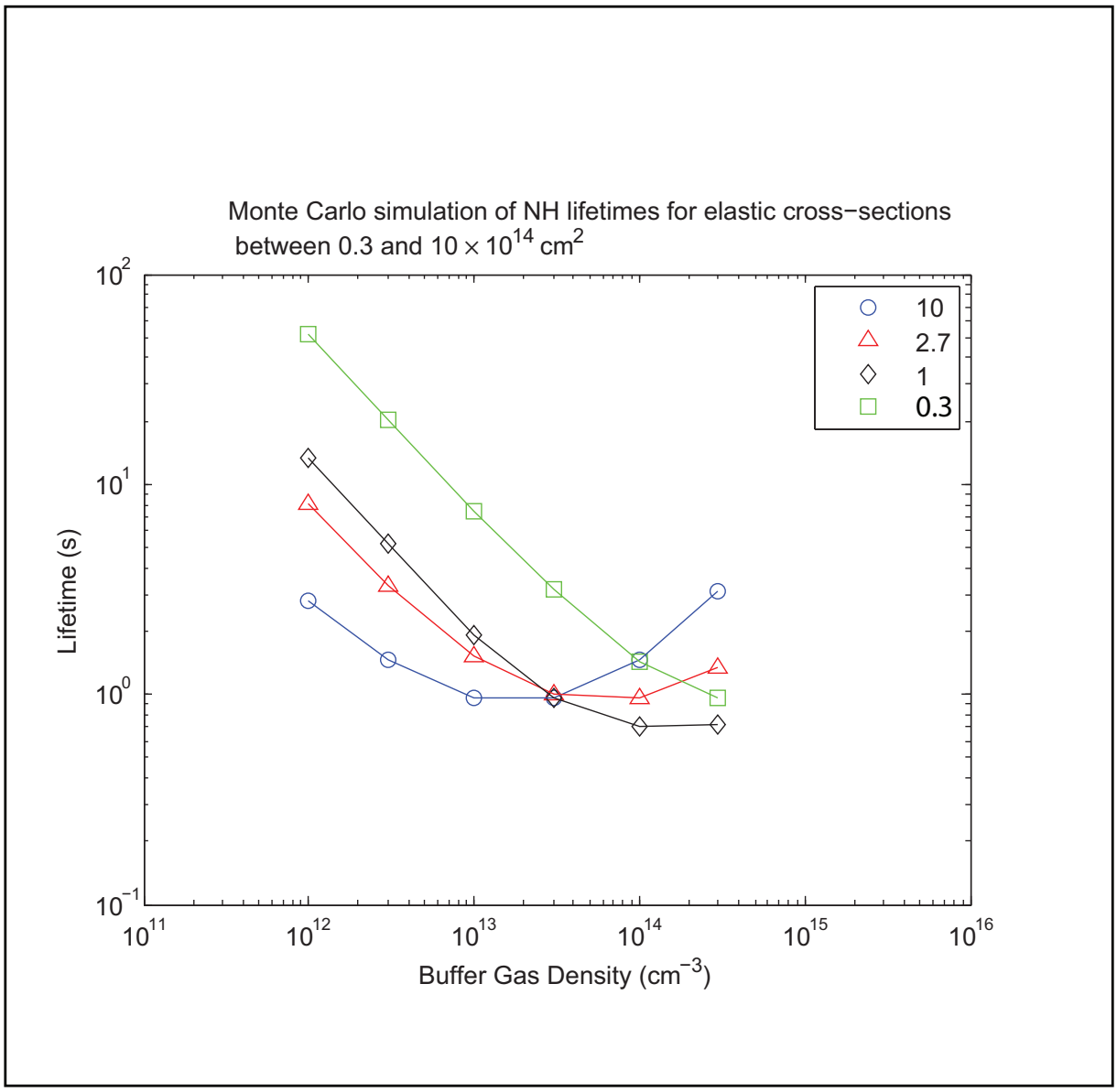

Figure 4.15: Variation of molecular lifetime with buffer gas density for different NH-He elastic cross sections.

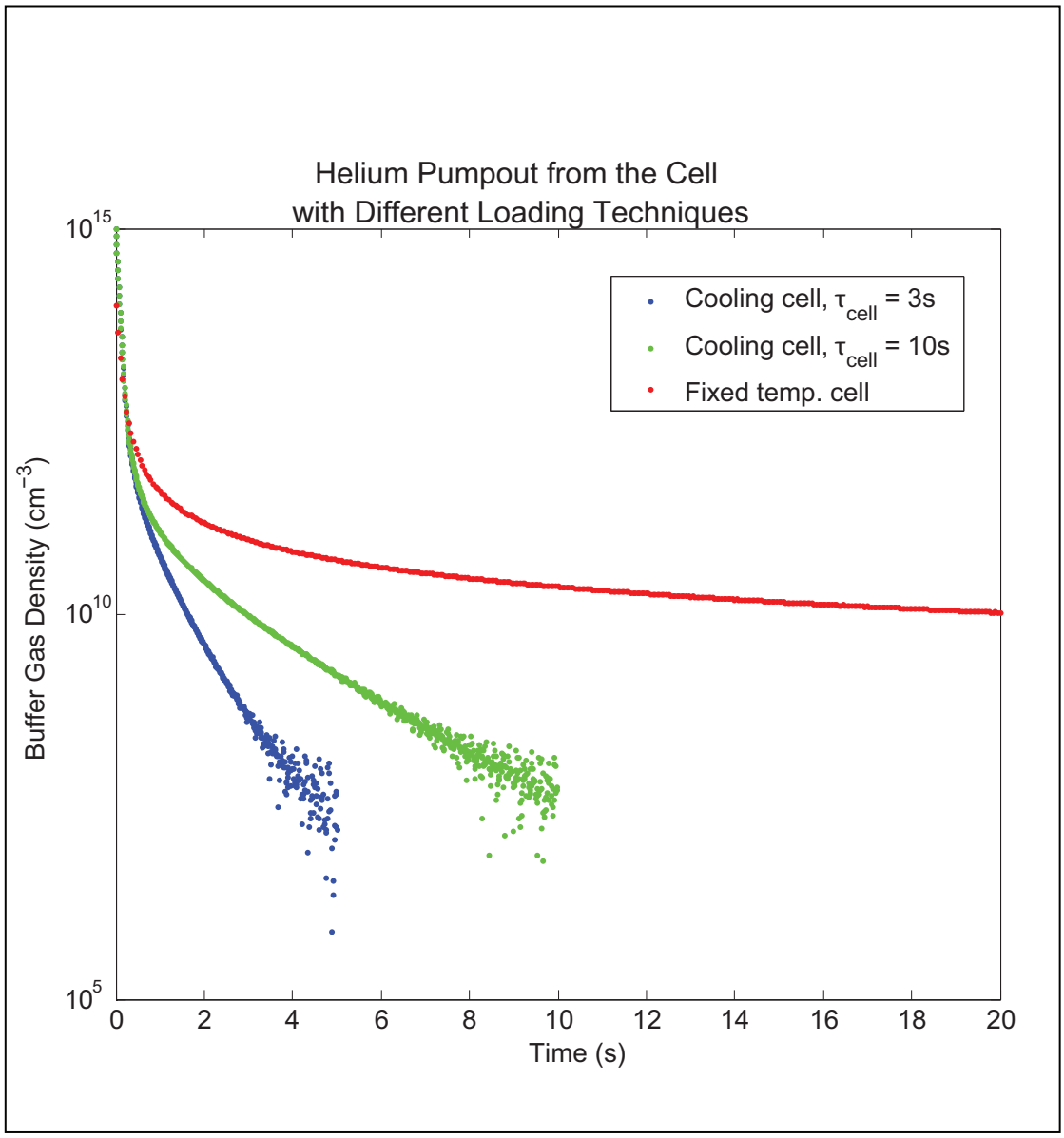

Figure 4.16: Buffer gas pumpout from a cell in various situations. τ_{cell} refers to the characteristic cooling time of the cell.

Chapter 5

Future Directions

This chapter discusses possible future directions of the experiment. The long term goal of our project is to obtain high densities of molecules at ultracold temperatures. On the road to this target, we hope to develop a more detailed understanding of atom-molecule and molecule-molecule collision processes. This research will require new technical developments and new approaches to molecule trapping. A few will be discussed here.

We have demonstrated that we can trap $2\mu_B$ molecules in an environment with a low density of helium vapor. We have trapped 10^5 molecules at a density of 10^8 cm^{-3} and retained them for tens of seconds. To observe molecule-molecule collisions, we believe we must increase the trapped molecule density by several orders of magnitude. Observing atom-molecule collisions should be possible with current molecule densities or with slight improvements to the current densities (because we can generate large atom numbers). However, because evaporative and sympathetic cooling are lossy techniques, creating larger molecular samples is a high priority.

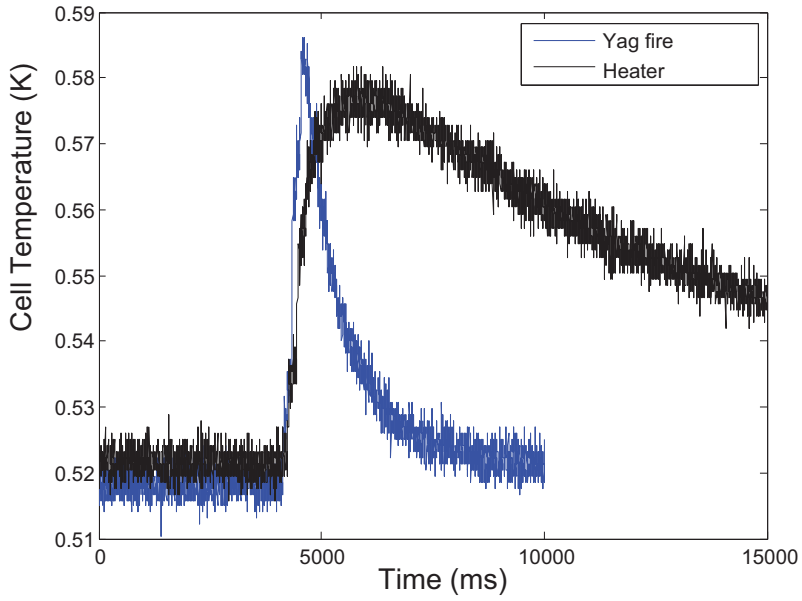

Figure 5.1: Temperature profile of the cell after YAG and resistor heating. After 4 mJ of YAG energy, the cell returns to its base temperature within 5 s. The cell takes about 50 s to recover from the resistive heating.

5.1 Molecule Loading with Colder Cell

One approach to increasing the trapped molecule number is to use the cold loading technique in a cell with a lower base temperature. Our current cell temperature is 500 mK; we can reasonably expect to attain temperatures of around 100 mK using a dilution refrigerator.

The effect of the YAG pulse is to raise the temperature of a portion of the cell (rather than the entire cell); helium from this local region desorbs and thermalizes molecules in the beam Fig.[5.1].

The low temperature specific heat capacity of copper is [79]

$$C_{Cu} = 6.91 \times 10^4 T + 1944 \left(\frac{T}{344}\right)^3 \ J\ mol^{-1}\ K^{-1}. \tag{5.1}$$

T is the temperatures in K. The first and second terms represent the electron and phonon heat capacities of copper, respectively.

We can calculate the heat required to raise the mean temperature of the cell from different starting temperatures. If we set 600 mK as a buffer gas temperature cold enough for efficient loading, we can perform heat load integrals with starting cell temperatures of 100 mK and 500 mK.

$$Q_{0.10K} = 1.22 \times 10^{-4} \frac{J}{mol} \tag{5.2}$$

$$Q_{0.50K} = 3.88 \times 10^{-5} \frac{J}{mol}. \tag{5.3}$$

With a starting temperature of 100 mK, we can deposit approximately 3.1 times as much heat on the cell to raise the mean temperature to 600 mK. The helium will desorb from an area that is approximately $3.1^{2/3} = 2.14$ times larger with the colder cell and generate a transient density that is also 2.14 times higher[1].

Loading from a colder cell has several distinct advantages. The Maxwell-Boltzmann distribution of particle velocities scales as v^2 for small v, so the higher density will stop a velocity class that is roughly four times more populous. The lower temperature will also result in a lower helium background and a slower rate of molecule evaporation.

We estimate that these effects, each contributing order of unity enhancements to the retained molecule number, will increase the molecule density by perhaps an

[1]The exponent 2/3 arises because film desorption is a surface phenomenon

order of magnitude. This increase appears too small to justify the expense and experimental complexity of incorporating a dilution refrigerator. However, a dilution refrigerator might permit loading of molecules by actuating the molecule beam source and the buffer gas reservoir simultaneously ("direct reservoir loading"). This could lead to us retaining a thousand times more molecules in a low background gas density environment[2].

5.2 Molecule Loading with a Cold Beam Source

An alternative means of increasing the loading efficiency would be to attempt cold loading with colder, slower molecules. The cold source envisioned here is a beam of molecules hydrodynamically entrained in gas exiting an orifice [77]. For a neon buffer gas source at 20 K, we estimate that we can produce a beam of molecules travelling at around 100 m/s. A helium based source would produce a molecule beam with a mean speed of approximately 50 m/s. We can compare the loading efficiency from such a source to what we obtain with our current supersonic beam source.

In a beam from a supersonic source [43, 3, 88], the particle velocity is boosted from the mean thermal velocity by an amount determined by the backing pressure and the nozzle geometry. The distribution exhibits a thermal spread around the mean supersonic velocity.

Mathematically, the velocity distribution takes the form

[2]With direct reservoir loading, we can currently trap 10^8 molecules, but film desorption limits the lifetime to around 400 ms.

$$f(v) = A\frac{v^2}{v_0^3}e^{-\frac{(v-v_s)^2}{v_0^2}}, \tag{5.4}$$

where A is a normalization factor, $v_0 = \sqrt{\frac{2k_BT}{m}}$ is the thermal spread in velocity and v_s is the supersonic velocity. In our experiment, the supersonic velocity of our beam is determined to be 1200 m/s.

For a thermal beam, the the velocity distribution is [68, 78]

$$f(v) = A'\frac{v^3}{v_0^4}e^{-\frac{v^2}{v_0^2}}, \tag{5.5}$$

The v^3 factor in this expression reflects the fact that the beam is obtained from a thermal distribution by selecting particles moving in a specific direction. In other words, the beam flux has additional velocity dependence, compared to a thermal distribution.

With a cold source (4K effusive beam, mean thermal velocity of 50 m/s), the narrow velocity spread and slow speed should allow more efficient thermalization with helium desorbed by the YAG pulse. The number of trapped molecules will depend on the properties of the source, so quantitative comparisons with the current loading scheme are difficult at this stage. However, we calculate that thirteen collisions are required to stop the molecules at the most probable velocity for beam at 4 K (compared to 34 for the supersonic beam); we would need to create a helium density of 10^{14} cm^{-3} in the cell. Cold loading yields molecule numbers about 10^3 times smaller than direct reservoir loading (when the molecule beam is fired simultaneously with the pulsed buffer gas reservoir), suggesting that we thermalize molecules present in the tail of the distribution. The smaller number of collisions required with the cold

source means that we might be able to extract molecules from the peak of the 4 K distribution, rather than the tail of the supersonic distribution. With beams of equal flux, the 4 K thermal distribution will also be a hundred times narrower than the distribution produced in the supersonic beam, potentially gaining us an additional two orders of magnitude in molecule number. Further analysis (and the construction and characterization of the source) is required, but a thousandfold increase in the trapped molecule number seems to be an attainable target.

5.3 Elastic Atom-Molecule Collisions

A central goal of our experiment is to develop techniques to study atom-molecule and molecule-molecule collisions. The molecule lifetimes we observe suggest that our cell is clean enough to study collisions between trapped species. With laser ablation, we can produce large numbers (10^{13}) of several paramagnetic atoms - manganese ${}^6S_{5/2}$ [74], chromium ${}^7S_3$ [70, 92] and europium ${}^8S_{7/2}$ [58]. These species are more paramagnetic than our molecule, and will persist for tens of seconds in our trap. Strongly paramagnetic species are also robust against background loss, and once the atoms are loaded into the trap with buffer gas, the cell can be cleaned by firing a series of YAG pulses to desorb helium from the walls. The background helium density can thus be reduced without significant loss of atoms.

If we desire molecules to be trapped without further use of helium, we can consider optical loading of the molecules Fig.[5.3] . This approach exists only as a concept at the current time [33]. By pumping cold molecules between trapped and untrapped states at selected positions in the magnetic field, we believe they can be transferred

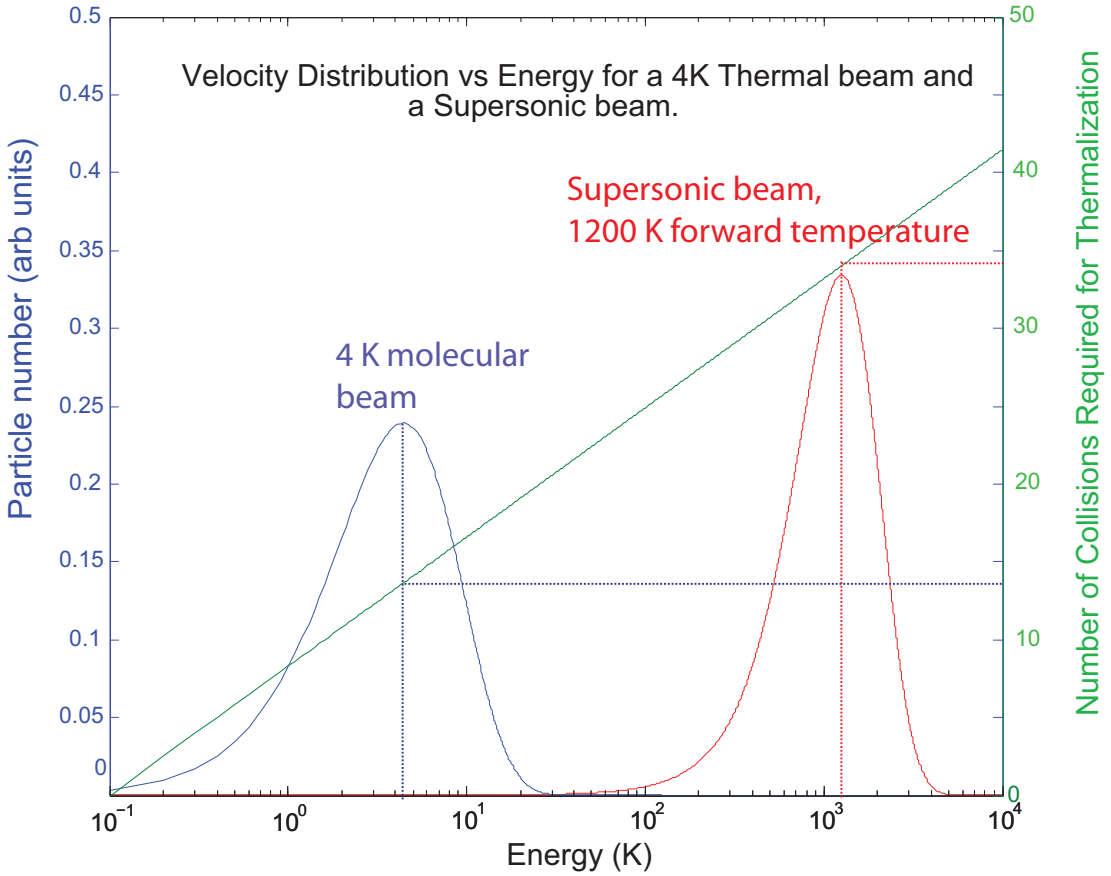

Figure 5.2: Variation of the particle velocity distribution with thermal energy. The blue trace represent the distribution from an effusive 4 K source. The red trace represents the velocity distribution from a supersonic source (velocity 1200 m/s, temperature 300K). The green line show the number of collisions required to thermalize a particle at a given energy. For a 4 K particle, 13 collisions are required. For the supersonic source, approximately 34 collisions are needed.

into the magnetic trap, given sufficient laser power.

Once co-trapping of molecules and atoms occurs, we can attempt sympathetic cooling of the molecules. To reduce the atom temperature, we can force evaporation by using a radiofrequency knife to selectively address and remove the most energetic atoms. Momentarily ignoring inelastic collisions between the atoms and molecules, we can can calculate how heating from residual background gas is balanced by cooling from an atomic sample.

The energy transferred to the molecules by a collision with the buffer gas is

$$dE_{He} = (E_{He} - E_{NH})\epsilon(m_{He}, M_{NH}), \tag{5.6}$$

where

$$\epsilon(m_{He}, M_{NH}) = \frac{2m_{He}M_{NH}}{(m_{He} + M_{NH})^2}. \tag{5.7}$$

E_{He} is the background gas temperature and E_{NH} is the temperature of the molecular sample.

We can write a similar expression for the energy transferred in a collision between a molecule and a trapped atom.

$$dE_{atom} = (E_{atom} - E_{NH})\epsilon(m_{atom}, M_{NH}). \tag{5.8}$$

The heating rate is given by

$$\frac{dQ}{dt} = \quad n_{He}\sigma_{He}\bar{v}_{\mu,He}\epsilon(m_{He}, M_{NH})\langle dE_{He}(1 - f(E_{NH} + dE_{He})\rangle$$

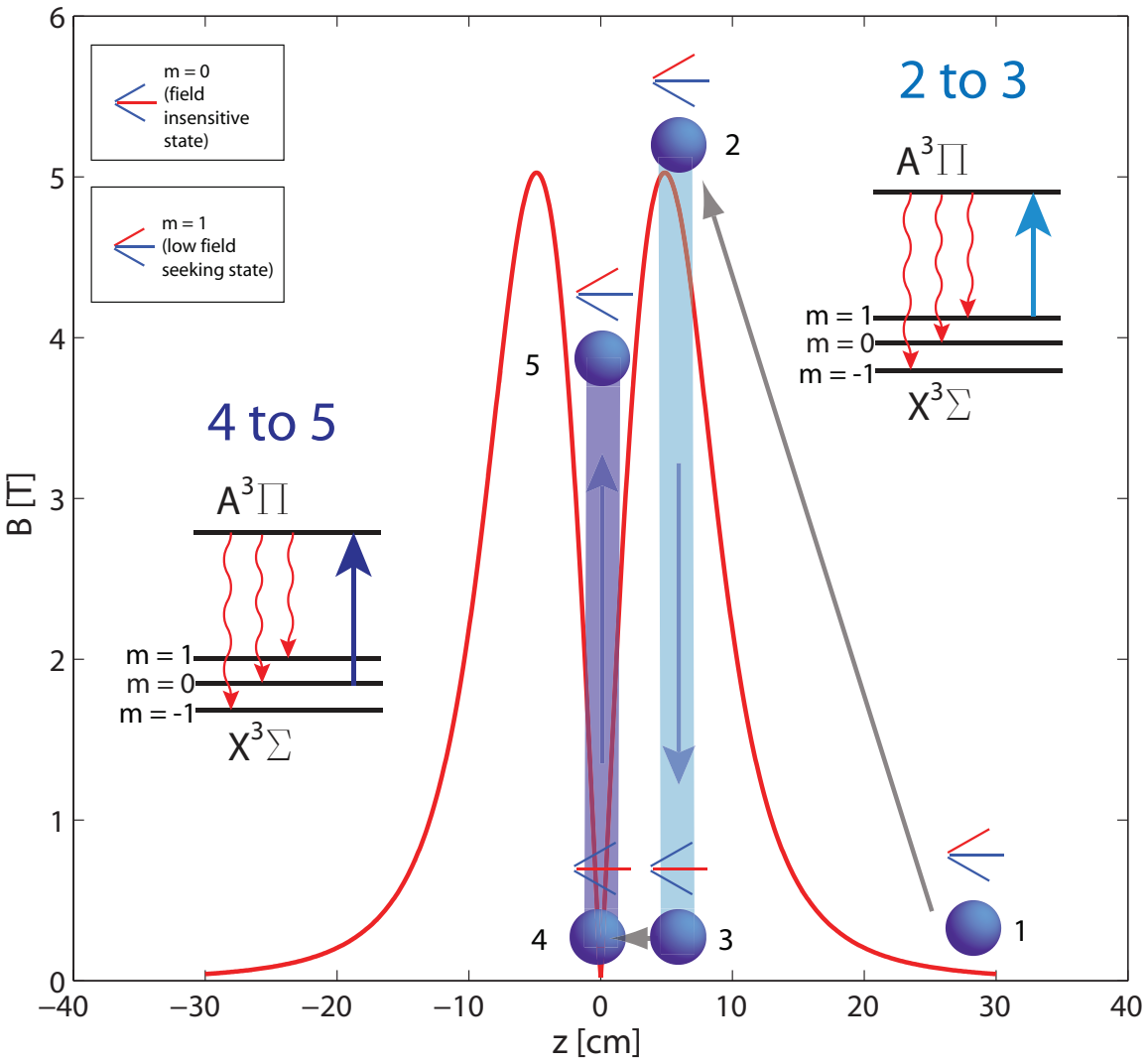

Figure 5.3: Cartoon view of optical loading of NH molecules. (1) Cold molecules in a low-field seeking state (4 K) enter the trapping field. After losing energy by climbing up the potential hill (2), the molecules are pumped with a laser to a field insensitive state (3). The molecules travel to the trap center where they are pumped back up to a low field seeking state (5). Their residual energy is less than the trap depth.

$$+n_{atom}\sigma_{atom}\bar{v}_{\mu,atom}\epsilon(m_{atom}, M_{NH})\langle dE_{atom}(1 - f(E_{NH} + dE_{atom})\rangle.$$

The terms $f(E_{NH}+dE_{He})$ and $f(E_{NH}+dE_{atom})$ reflect the fractions of the molecular distribution evaporated by the transfer of energy from the helium and the trapped atoms, respectively. For large values of η, the evaporated fraction is small. With this assumption, we can rewrite the heating equation:

$$\begin{aligned}\frac{dQ}{dt} \approx \quad & \frac{3}{2}n_{He}\sigma_{He}\bar{v}_{\mu,He}\epsilon(m_{He}, M_{NH})(T_{He} - T_{NH}) \\ & +\frac{3}{2}n_{atom}\sigma_{atom}\bar{v}_{\mu,atom}\epsilon(m_{atom}, M_{NH})(T_{atom} - T_{NH}).\end{aligned}$$

At steady state, the NH molecules would reach a temperature

$$T_{NH} = \frac{\phi T_{He} - T_{atom}}{\phi - 1}, \tag{5.9}$$

where

$$\phi = \frac{n_{He}}{n_{atom}}\frac{\sigma_{He}}{\sigma_{atom}}\frac{\epsilon(m_{He}, M_{NH})}{\epsilon(m_{atom}, M_{NH})}\frac{\bar{v}_{\mu,He}}{\bar{v}_{\mu,atom}}. \tag{5.10}$$

Sympathetic cooling of NH molecules by atoms in the presence of a helium background is thus favored by the following things:

- a close mass match between NH and the atom acting as the reservoir

- a large atom-NH elastic cross-section

- a low background gas density and a high atomic density

- a low atom reservoir temperature.

The close mass match between atomic nitrogen and NH suggests the use of the former as a sympathetic cooling partner. Our knowledge of the elastic cross-section of nitrogen with NH is limited; a sympathetic cooling experiment would be a means of obtaining this number. Other paramagnetic atomic species are less well matched to NH, but might be produced in sufficient numbers (10^{13}) to make them suitable candidates.

5.4 Inelastic Collisions with Atoms

Despite helium possessing a highly isotropic electronic distribution, we still observe inelastic loss in collisions with NH. We expect inelastic loss rates to be higher for NH interacting other atoms, especially paramagnetic ones. In addition to the collisions leading to electrostatic distortion of the molecular rotational wavefunction, we anticipate a direct coupling of the molecular spin to the spin of the atomic species (dipolar loss).

Paramagnetic atoms trapped at high density can undergo loss that depends on the square of their density [21, 20, 47]. If we cotrap NH and an atom, the inelastic atom-molecule interaction would be manifested as a depletion in the molecule number that tracks the decay of the atomic sample. In theory, this loss is easy to distinguish from processes which depend solely on the molecule density.

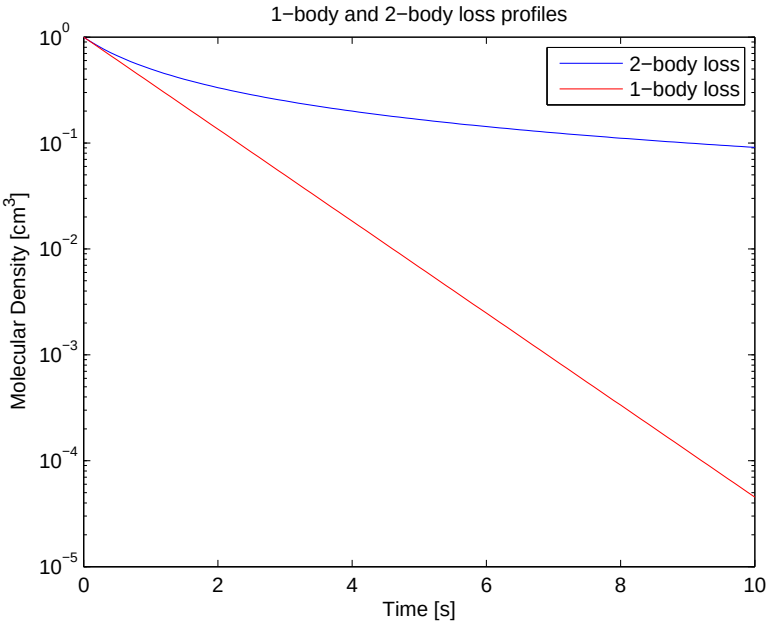

Figure 5.4: 1-body and 2-body decay profiles.

5.5 Cotrapping of NH and N

We have simultaneously trapped NH and atomic nitrogen in a 4 T field. These experiments were performed in the presence of a high buffer gas background, limiting the trapping duration of NH to a few hundred milliseconds. The trapped nitrogen atoms (approximately 10^{11}) decayed with an exponential lifetime of around 10 s.

The success of this experiment further motivated us to pursue thermal isolation of NH. Long trapping times for both species would greatly facilitate the observation of inelastic processes.

5.5.1 Nitrogen Production and Detection

Nitrogen atoms are generated from molecular nitrogen or ammonia by a DC glow discharge. With the appropriate selection of precursor gases, both NH and atomic nitrogen can be produced by the same source. The atoms propagate through the vacuum as a beam and enter the trapping cell.

To detect nitrogen we use two-photon absorption laser induced fluorescence (TALIF) [2]. The nitrogen atoms absorb two photons at 207 nm and emit a photon at 745 nm, detected on a PMT. Approximately 10^{11} molecules are trapped at 500 mK. Fig.[5.6] illustrates the experimental configuration that permits simultaneous detection of NH and nitrogen in fluorescence. The dips in the NH fluorescence signal show how the 207 nm laser light removes trapped molecules from the detection region. Experiments are currently underway to measure elastic and inelastic cross-sections of nitrogen colliding with itself and with NH molecules.

5.6 Conclusion

Our experiment has demonstrated that we can trap molecules in a low background gas environment. Sympathetic cooling of molecules with nitrogen might allow us to span the milliKelvin and microKelvin temperature ranges; we require a deeper understanding of low temperature collisional loss to establish this. Our bifurcated approach to the target of ultracold molecules thus involves generating larger thermally isolated molecular samples, while concurrently determining if collisional methods can be applied to increase our phase space densities and reduce temperatures. The path to

cold molecules may be unclear at the present time, but the rewards are manifold.

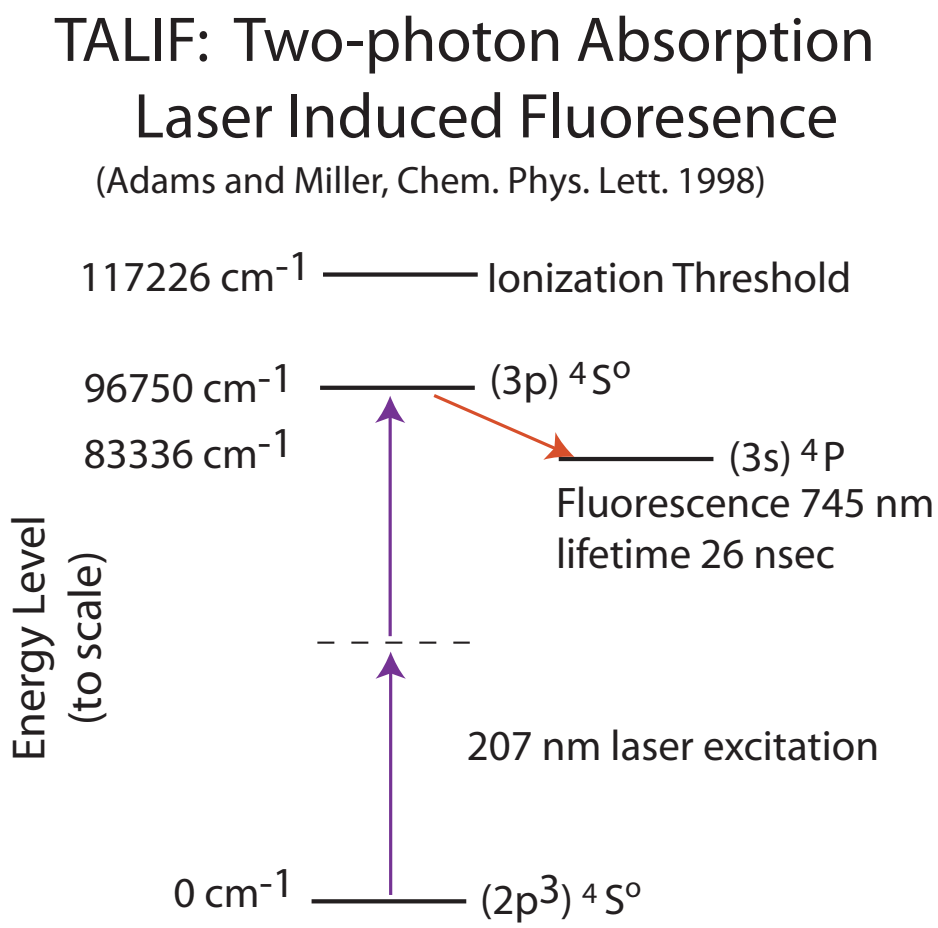

Figure 5.5: Two photon absorption laser induced fluorescence detection scheme for atomic nitrogen.

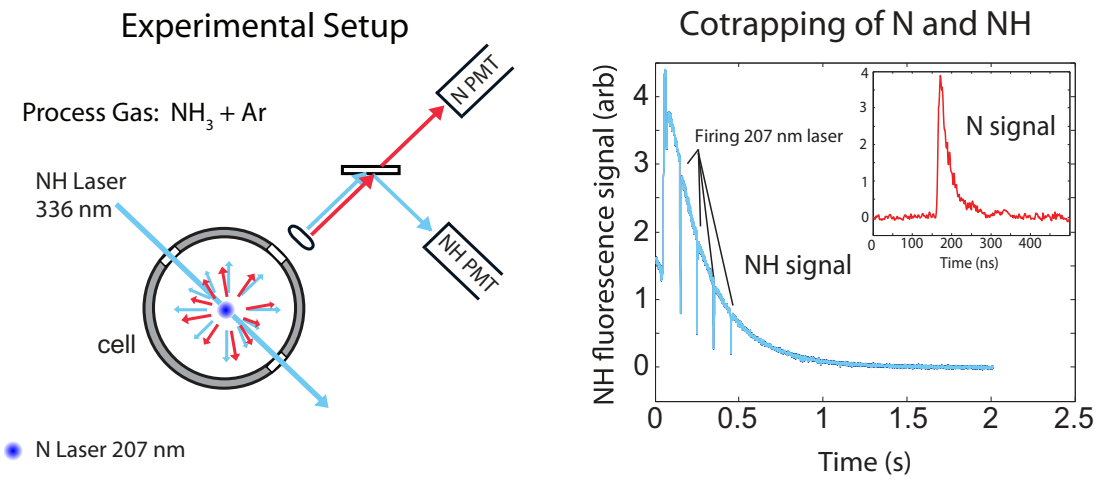

Figure 5.6: Detection geometry for codetection of NH and nitrogen. Results of codetection.

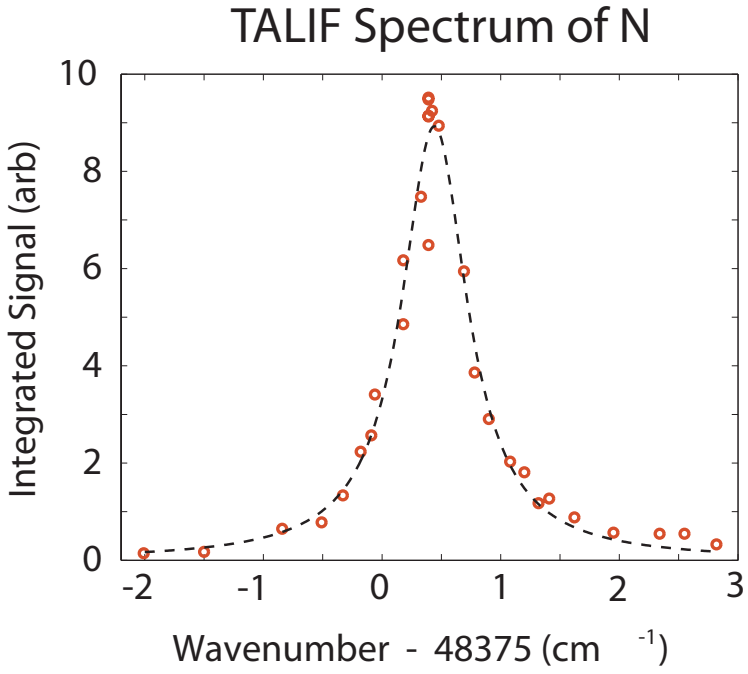

Figure 5.7: Fluorescence spectrum of atomic nitrogen.

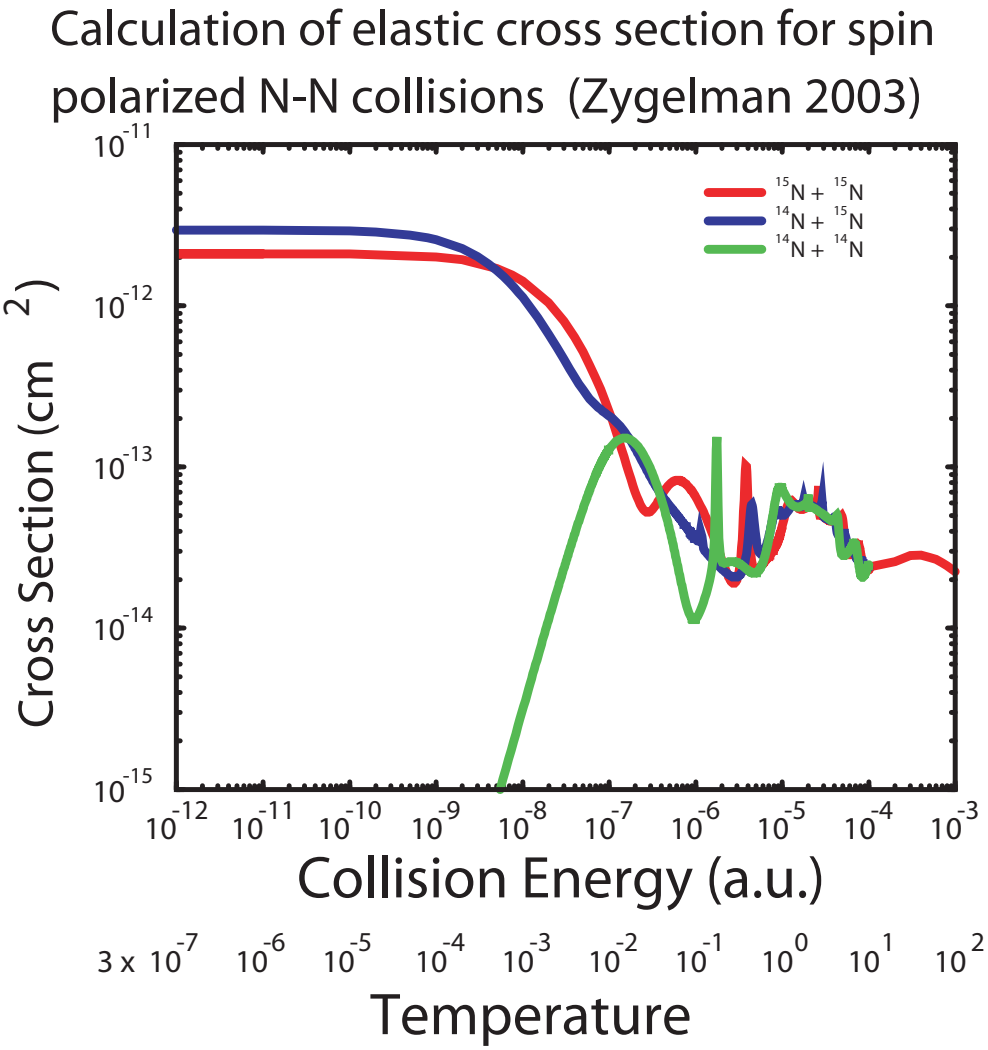

Figure 5.8: Theoretical calculation of elastic nitrogen cross-section [96].

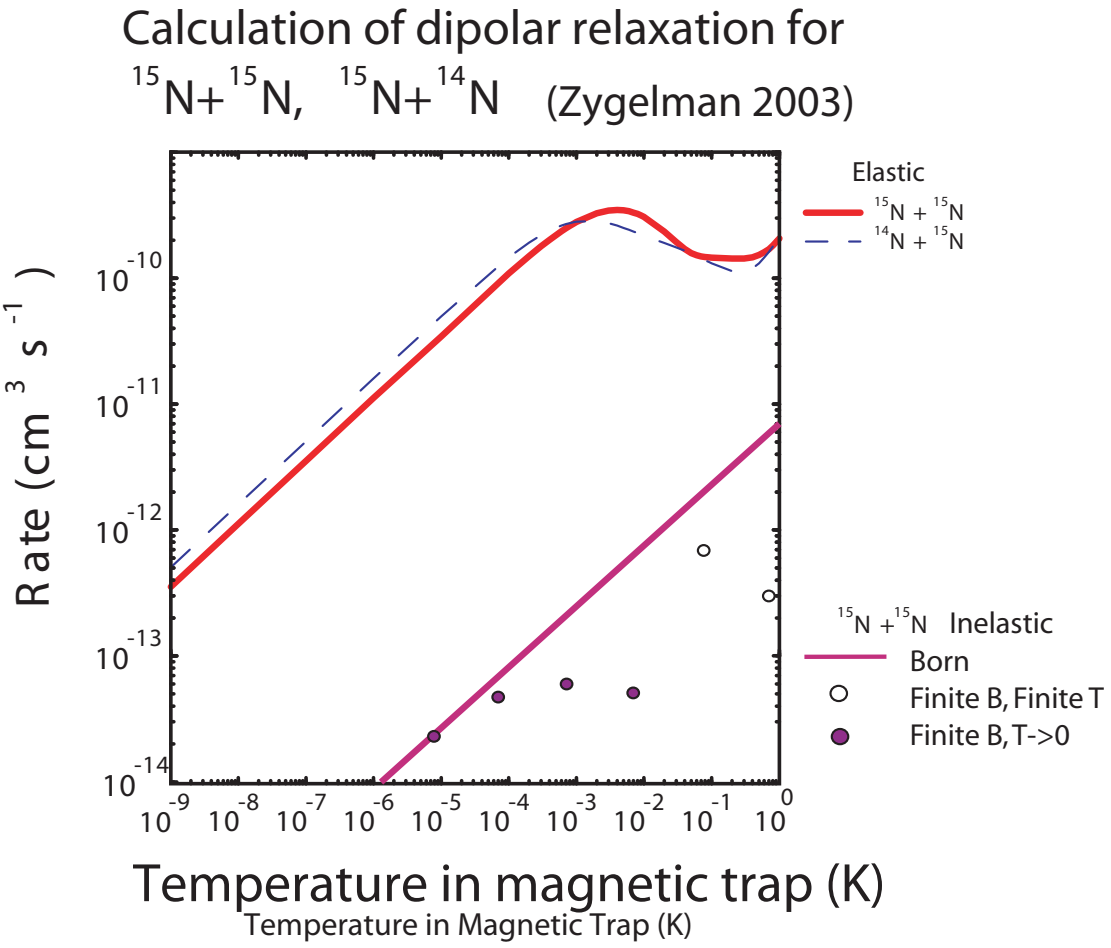

Figure 5.9: Theoretical calculation of inelastic nitrogen cross-section [96].

Bibliography

[1] K. Abdullah, C. Carlberg, E. D. Commins, H. Gould, and S. B. Ross. New experimental limit on the electron electric dipole moment. *Phys. Rev. Lett.*, **65**:2347, 1990.

[2] S. F. Adams and T. A. Miller. Two photon absorption laser induced fluorescence of atomic nitrogen by an alternative excitation scheme. *Chemical Physics Letters*, **265(4)**:305, 1998.

[3] J. B. Anderson and J. B. Fenn. Velocity distributions in molecular beams from nozzle sources. *The Physics of Fluids*, **8**:780, 1963.

[4] W. R. Anderson and D. R. Crosley. Quantum-mechanical theory of atom-molecule and molecular collisions in a magnetic field: Spin depolarization. *Chemical Physics Letters*, **62(2)**:275, 1979.

[5] W. Bernreuther and M. Suzuki. The electric dipole moment of the electron. *Rev. Mod. Phys.*, **63**:313, 1991.

[6] H. L. Bethlem, G. Berden, and G. Meijer. Decelerating neutral dipolar molecules. *Phys. Rev. Lett.*, **83**:1558, 1999.

[7] J. R. Bochinski, E. R. Hudson, H. J. Lewandowski, and J. Ye. Cold free-radical molecules in the laboratory frame. *Phys. Rev. A*, **70**:043410, 2004.

[8] J. Bohn. Molecular spin relaxation in cold atom-molecule scattering. *Phys. Rev. A*, **61**:040702, 2000.

[9] N. C. Brahms. *Trapping of 1 μ_B atoms using buffer gas loading.* PhD thesis, Harvard University, 2008.

[10] C. R. Brazier, R. S. Ram, and P. F. Bernath. Fourier transform spectroscopy of the $A^3\Pi \leftarrow X^3\Sigma$ transition of NH. *Journal of Molecular Spectroscopy*, **120**:381, 1986.

[11] W. C. Campbell. *Magnetic Trapping of Imidogen Molecules.* PhD thesis, Harvard University, 2008.

[12] W. C. Campbell, G. C. Groenenboom, Hsin-I Lu, E. Tsikata, , and J. M. Doyle. Time-domain measurement of spontaneous vibrational decay of magnetically trapped NH. *Phys. Rev. Lett.*, **100**:083003, 2008.

[13] W. C. Campbell, T. V. Tscherbul, H-I Lu, E. Tsikata, R. V. Krems, and J. M. Doyle. Mechanism of collisional spin relaxation in $^3\Sigma$ molecules. *Phys. Rev. Lett.*, **102**:013003, 2009.

[14] W. C. Campbell, E. Tsikata, H. Lu, L. D. van Buuren, and J. M. Doyle. Magnetic trapping and zeeman relaxation of NH $X^3\Sigma^-$. *Phys. Rev. Lett.*, **98**:213001, 2007.

[15] T. E. Chupp, M. E. Wagshul, K. P. Coulter, A. B. McDonald, and W. Happer. Polarized, high-density, gaseous ^{3}He targets. *Physical Review C*, **36**:2244, 1987.

[16] ACME collaboration (Harvard, Yale). Private communication. current research, 2009.

[17] E. D. Commins, S. B. Ross, D. DeMille, and B. C. Regan. Improved experimental limit on the electric dipole moment of the electron. *Phys. Rev. A*, **50**:2960, 1994.

[18] P. Courteille, R. S. Freeland, and D. J. Heinzen. Observation of a feshbach resonance in cold atom scattering. *Phys. Rev. Lett.*, **81**:69, 1998.

[19] J. Dalton, W. H. Wollaston, and T. Thomson. *Foundations of the atomic theory.* W.F. Clay, Edinburgh, 1893.

[20] R. Decarvalho. *Inelastic Scattering of Magnetically Trapped Atomic Chromium.* PhD thesis, Harvard University, 2003.

[21] R. deCarvalho, C. I. Hancox, and J. M. Doyle. Enhanced inelastic scattering rates of cold atomic chromium. *Journal of the Optical Society of America*, **20**:1131, 2003.

[22] B. Deh, C. Marzok, C. Zimmermann, and Ph. W. Courteille. Feshbach resonances in mixtures of ultracold ^{6}Li and ^{87}Rb gases. *Phys. Rev. A*, **77**:010701, 2008.

[23] B. deMarco and D. S. Jin. Onset of fermi degeneracy in a trapped atomic gas. *Science*, **285**:1703, 1999.

[24] D. DeMille. Quantum computation with trapped polar molecules. *Phys. Rev. Lett.*, **88**:067901, 2002.

[25] D. DeMille, F. Bay, S. Bickman, D. Kawall, D. Krause, S. E. Maxwell, and L. R. Hunter. Investigation of PbO as a system for measuring the electric dipole moment of the electron. *Phys. Rev. A*, **61**:052507, 2004.

[26] W. Demtroder. *Laser Spectroscopy.* Springer, 1996.

[27] R. N. Dixon. The 0-0 and 1-0 bands of the $A^3\Pi \leftarrow X^3\Sigma$ system of NH. *Canadian Journal of Physics*, **37**:1171, 1959.

[28] J. M. Doyle, J. C. Sandberg, I. A. Yu, C. L. Cesar, D. Kleppner, and T. J. Greytak. Hydrogen in the submillikelvin regime: Sticking probability on superfluid ^{4}He. *Journal of Physical Chemistry A*, **67**:603, 1991.

[29] D. Egorov, W.C. Campbell, B. Friedrich, S.E. Maxwell, E. Tsikata, L.D. van Buuren, and J.M. Doyle. Buffer gas cooling of NH via the beam loaded buffer-gas method. *European Journal of Physics*, **31**:307, 2002.

[30] D. Egorov, J. D. Weinstein, D. Patterson, B. Friedrich, and J. M. Doyle. Spectroscopy of laser-ablated buffer-gas-cooled PbO at 4 k and the prospects for measuring the electric dipole moment of the electron. *Phys. Rev. A*, **63**:030501, 2001.

[31] D. M. Egorov. *Buffer-Gas Cooling of Diatomic Molecules*. PhD thesis, Harvard University, 2004.

[32] M. S. Elioff, J. J. Valentini, and D. W. Chandler. Subkelvin cooling NO molecules via billiard-like collisions with argon. *Science*, **302**:1940, 2003.

[33] H-I Lu et al. Private communication. pending research, 2009.

[34] U. Fano. Effects of configuration interaction on intensities and phase shifts. *Physical Review*, **124**:1866, 1961.

[35] F. A. Franz. Rubidium spin relaxation in the rare gases under ultraclean conditions. *Journal of Chemical Physics*, **139**:A603, 1965.

[36] A. P. French. *Vibrations and Waves*. W. W. Norton and Co., 1966.

[37] J. J. Gilijamse, S. Hoekstra, S. A. Meek, M. Metsala, S. Y. T. van de Meerakker, and G. Meijer. The radiative lifetime of metastable CO. *Journal of Chemical Physics*, **127**:221102, 2007.

[38] J. J. Gilijamse, J. Kupper, S. Hoekstra, N. Vanhaecke, S. Y. T. van de Meerakker, and G. Meijer. Optimizing the stark-decelerator beamline for the trapping of cold molecules using evolutionary strategies. *Phys. Rev. A*, **73**:063410, 2006.

[39] R. E. Green, C. J. McCauley, E. Oberg, and F. D. Jones H. L. Horton H. H. Ryffel. *Machinery's Handbook, volume 25*. Industrial Press Inc., 1989.

[40] A. Griesmaier, J. Werner, S. Hensler, J. Stuhler, and T. Pfau. Bose-Einstein condensation of Chromium. *Phys. Rev. Lett.*, **94**:160401, 2005.

[41] M. Gupta and D. Hershbach. Making, probing and understanding Bose-Einstein condensates. *cond-mat*, **9904**:034v2, 1999.

[42] M. Gupta and D. Hershbach. A mechanical means to produce intense beams of slow molecules. *Journal of Physical Chemistry A*, **103**:10670, 1999.

[43] H. Haberland, U. Buck, and M. Tolle. Velocity distribution of supersonic nozzle beams. *Review of Scientific Instruments*, **56**:1712, 1985.

[44] Z. Hadzibabic, S. Gupta, C. A. Stan, C. H. Schunck, M. W. Zwierlein, K. Dieckmann, and W. Ketterle. Fiftyfold improvement in the number of quantum degenerate fermionic atoms. *Phys. Rev. Lett.*, **91**:160401, 2003.

[45] C Haimberger, J. Kleinert, M. Bhattacharya, and N. P. Bigelow. Formation and detection of ultracold ground-state polar molecules. *Phys. Rev. A*, **70**:021402, 2004.

[46] C. Hancox. *Magnetic Trapping of transition-metal and rare-earth atoms using buffer gas loading.* PhD thesis, Harvard University, 2005.

[47] C.I. Hancox, S.C. Doret, M.T. Hummon, L. Luo, and J.M. Doyle. Magnetic trapping of the rare-earth atoms at millikelvin temperatures. *Nature*, **431**:281, 2004.

[48] J. B. Hasted. *Physics of Atomic Collisions.* Butterworth, 1972.

[49] G. Hertzberg. *Molecular Spectra on Molecular Structure, volume 1.* Krieger Publishing Company, 1989.

[50] Y. H. Huang and G. B. Chen. A practical vapor pressure equation for helium-3 from 0.01 K to the critical point. *Cryogenics*, **46**:833–839, 2006.

[51] E. R. Hudson, C. Ticknor, B. C. Sawyer, C. A. Taatjes, H. J. Lewandowski, J. R. Bochinski, J. L. Bohn, and J. Ye. Production of cold formaldehyde molecules for study and control of chemical reaction dynamics with hydroxyl radicals. *Phys. Rev. A*, **73**:063404, 2006.

[52] J. J. Hudson, B. E. Sauer, M. R. Tarbutt, and E. A. Hinds. Measurement of the electron electric dipole moment using YbF molecules. *Phys. Rev. Lett.*, **89**:023003, 2002.

[53] S. Inouye, M. R. Andrews, J. Stenger, J. Stenger, D. M. Stamper-Kurn, and W. Ketterle. Observation of feshbach resonances in a Bose Einstein condensate. *Nature*, **392**:151, 1998.

[54] J. D. Jackson. *Classical Electrodynamics.* John Wiley, 1999.

[55] E. H. Kennard. On the thermodynamics of thermal transpiration and of the Thomson effect. *Physical Review*, **22**:617, 1923.

[56] A. J. Kerman, J. M. Sage, S. Sainis, T. Bergeman, and D. DeMille. Formation of ultracold LiCs molecules. *Phys. Rev. Lett.*, **92(3)**:033004, 2004.

[57] I. B. Khriplovich and S. K. Lamoreaux. *CP Violation Without Srangeness*. Springer-Verlag, Berlin and Heidelberg and New York, 1997.

[58] J. Kim. *Buffer-gas Loading and Magnetic Trapping of Atomic Europium*. PhD thesis, Harvard University, 1997.

[59] S. D. Kraft, P. Staanuma, J. Lange, L. Vogel, R. Wester, and M. Weidemller. Formation of ultracold LiCs molecules. *Journal of Physics B*, **39**:S993, 2006.

[60] R. V. Krems and A. Dalgarno. Disalignment transitions in cold collisions of 3P atoms with structureless targets in a magnetic field. *Phys. Rev. A*, **68**:013406, 2003.

[61] R. V. Krems, A. Dalgarno, N. Balakrishnan, and G. C. Groenenboom. Spin-flipping transitions in $^2\Sigma$ molecules induced by collisions with structureless atoms. *Phys. Rev. A*, **67**:060703, 2003.

[62] R. V. Krems, H. R. Sadeghpour, A. Dalgarno, D. Zgid, J. Klos, and G Chalasinski. Low-temperature collisions of $NH^3\Sigma^-$ molecules with He atoms in a magnetic field: An ab initio study. *Phys. Rev. A*, **68**:051401, 2003.

[63] R. V. Krems, H. R. Sadeghpour, A. Dalgarno, D. Zgid, J. Klos, and G. Chalasinski. Low-temperature collisions of $NH(X^3\Sigma^-)$ molecules with He atoms in a magnetic field: An ab initio study. *Phys. Rev. A*, **68**:051401, 2003.

[64] R. V. Krems, H. R. Sadeghpour, A. Dalgarno, D. Zgid, J. Klos, and G. Chalasinski. Quantum-mechanical theory of atom-molecule and molecular collisions in a magnetic field: Spin depolarization. *Journal of Chemical Physics*, **120**:2296, 2004.

[65] R. V. Krems, D. Zgid, G. Chalasinski, J. Klos, and A. Dalgarno. Zeeman relaxation of CaF in low-temperature collisions with helium. *Phys. Rev. A*, **66**:030702, 2002.

[66] M. W. Mancini, G. D. Telles, A. R. L. Caires, V. S. Bagnato, and L. G. Marcassa. Observation of ultracold ground-state heteronuclear molecules. *Phys. Rev. Lett.*, **92**:133203, 2004.

[67] K. Maussang, D. Egorov, J. S. Helton, S. V. Nguyen, and J. M. Doyle. Zeeman relaxation of CaF in low-temperature collisions with helium. *Phys. Rev. Lett.*, **94**:123002, 2005.

[68] H. J. Metcalf and P. van der Straten. *Laser Cooling and Trapping*. Springer, 1999.

[69] E. R. Meyer and J. L. Bohn. Prospects for an electron electric-dipole moment search in metastable ThO and ThF. *Phys. Rev. A*, **78**:010502, 2008.

[70] B. Michniak. *Enhanced Buffer Gas Loading: Cooling and Trapping of Atoms with Low Efective Magnetic Moments*. PhD thesis, Harvard University, 2004.

[71] A. J. Moerdijk, B. J. Verhaar, and A. Axelsson. Resonances in ultracold collisions of ^{6}Li, ^{7}Li and ^{23}Na. *Phys. Rev. A*, **51**:4852, 1995.

[72] B. R. Munson, D. F. Young, and T. H. Okiishi. *Fundamentals of Fluid Mechanics*. John Wiley, 2006.

[73] B. K. Newman. *Trapped atom collisions and evaporative cooling of non S-state atoms*. PhD thesis, MIT, 2008.

[74] S. Nguyen. *Buffer Gas Loading and Evaporative Cooling in the Multi-Partial-Wave Regime*. PhD thesis, Harvard University, 2006.

[75] K.-K. Ni, S. Ospelkaus, M. H. G. de Miranda, A. Peer, B. Neyenhuis, J. J. Zirbel, S. Kotochigova, P. S. Julienne, D. S. Jin, and J. Ye. A high phase-space-density gas of polar molecules. *Science*, **322**:231, 2008.

[76] M. A. Nielsen and I. Chuang. *Quantum Computation and Quantum Information*. Cambridge University Press, 2000.

[77] D. Patterson, J. Rasmussen, and J. M. Doyle. Intense atomic and molecular beams via neon buffer gas cooling. *New Journal of Physics*, publication pending, 2009.

[78] H. pauly. *Atom, molecule and cluster beams*. Springer, 2000.

[79] F. Pobell. *Matter and Methods at Low Temperatures*. Springer, 1996.

[80] B. Regan, E. D. Commins, C. J. Schmidt, and D. Demille. New limit on the electron electric dipole moment. *Phys. Rev. Lett.*, **88**:071805, 2002.

[81] H. E. Roscoe. *A new view of the origin of Daltons atomic theory*. Macmillan and co., London and New York, 1896.

[82] A. Roth. *Vacuum Technology*. North-Holland, 1990.

[83] R. Santra and C. H. Greene. Tensorial analysis of the long-range interaction between metastable alkaline-earth-metal atoms. *Phys. Rev. A*, **67**:062713, 2003.

[84] C. A. Stan, M. W. Zwierlein, C. H. Schunck, S. M. F. Raupach, , and W. Ketterle. Observation of feshbach resonances between two different atomic species. *Phys. Rev. Lett.*, **93**:143001, 2004.

[85] B. K. Stuhl, B. C. Sawyer, D. Wang, and J. Ye. Magneto-optical trap for polar molecules. *Phys. Rev. Lett.*, **101**:243002, 2008.

[86] W. Ubachs, G. Meyer, J. J. ter Meulen, and A. Dymanus. High-resolution spectroscopy on the c1$\Pi \leftarrow$ a1Δ transition in NH. *Journal of Molecular Spectroscopy*, **115**:88, 1985.

[87] W. Ubachs, J. J. ter Meulen, and A. Dymanus. High-resolution spectroscopy on the $A^3\Pi \leftarrow X^3\Sigma$ transition of NH. *Canadian Journal of Physics*, **62**:1374, 1984.

[88] J. P. Valleau and J. M. Deckers. A study of molecular interactions in molecular beams isolated from the exhaust of supersonic nozzles. *Canadian Journal of Chemistry*, **42**:225, 1964.

[89] S. Y. T. van de Meerakker, P. H. M. Smeets, N. Vanhaecke, R. T. Jongma, and G. Meijer. Deceleration and electrostatic trapping of OH radicals. *Phys. Rev. Lett.*, **94**:023004, 2005.

[90] T. G. Walker and W. Happer. Spin-exchange optical pumping of noble-gas nuclei. *Reviews of Modern Physics*, **69**:629, 1997.

[91] D. Wang, J. Qi, M. F. Stone, O Nikolayeva, B. Hattaway, S. D. Gensemer, H. Wang, W. T. Zemke, P. L. Gould, E. E. Eyler, and W. C. Stwalley. Observation of ultracold ground-state heteronuclear molecules. *European Physical Journal D.*, **31**:165, 2004.

[92] J. D. Weinstein. *Magnetic Trapping of Atomic Chromium and Molecular Calcium Monohydride*. PhD thesis, Harvard University, 2002.

[93] J. D. Weinstein, R. deCarvalho, K. Amar, A. Boca, B. C. Odom, B. Friedrich, and J. M. Doyle. Spectroscopy of buffer-gas cooled vanadium monoxide in a magnetic trapping field. *Journal of Chemical Physics*, **109**:2656, 1998.

[94] D. R. Willey, R. L. Crownover, D. N. Bittner, and F. C. De Lucia. Very low temperature spectroscopy: The pressure broadening coefficients for CO He between 4.3 and 1.7 K. *Journal 0f Chemical Physics*, **89(4)**:1923, 1988.

[95] D. R. Yarkony. On the electronic structure of the NH radical. the fine structure splitting of the $X^3\Sigma$ state and the spin-forbidden (b $^1\Sigma^+$, $a^1\Delta$)$\rightarrow$ $X^3\Sigma$, and the spin-allowed $A^3\Pi \rightarrow X^3\Sigma$ and $c^1\Pi \rightarrow$(b $^1\Sigma^+$, $a^1\Delta$), radiative transitions. *Journal of Chemical Physics*, **91(8)**:4745, 1989.

[96] Zygelman. Private communication. unpublished, 2003.

Appendix A

Procedure for radial mounting of cryogenic windows

This list describes the steps involved in mounting windows to the curved surface of a cylindrical cell. The technique described here produces windows which are (superfluid) leaktight to 10^{-8} mbar L/s. The window seal can withstand repeated magnet quenches and thermal cycling from 0.5 K to 300 K.

The cell diameter is 7.36 cm. We desire a 10 mm diameter clear area for our windows, so we use Edmund Optics 12.75 mm sapphire windows (Part No. 43631). Sapphire windows absorb deep UV (we use 207 nm light for atomic nitrogen detection). If deep UV detection is anticipated, select suitable windows; MgF_2 and Edmund Optics fused silica windows have 207 nm transmission exceeding 90%. The window thickness is 1 mm. Sapphire has excellent thermal properties, so the relative thinness of the window does not create a central hot spot. The small profile is also beneficial because we suffer minimal reduction in the radial trap depth.

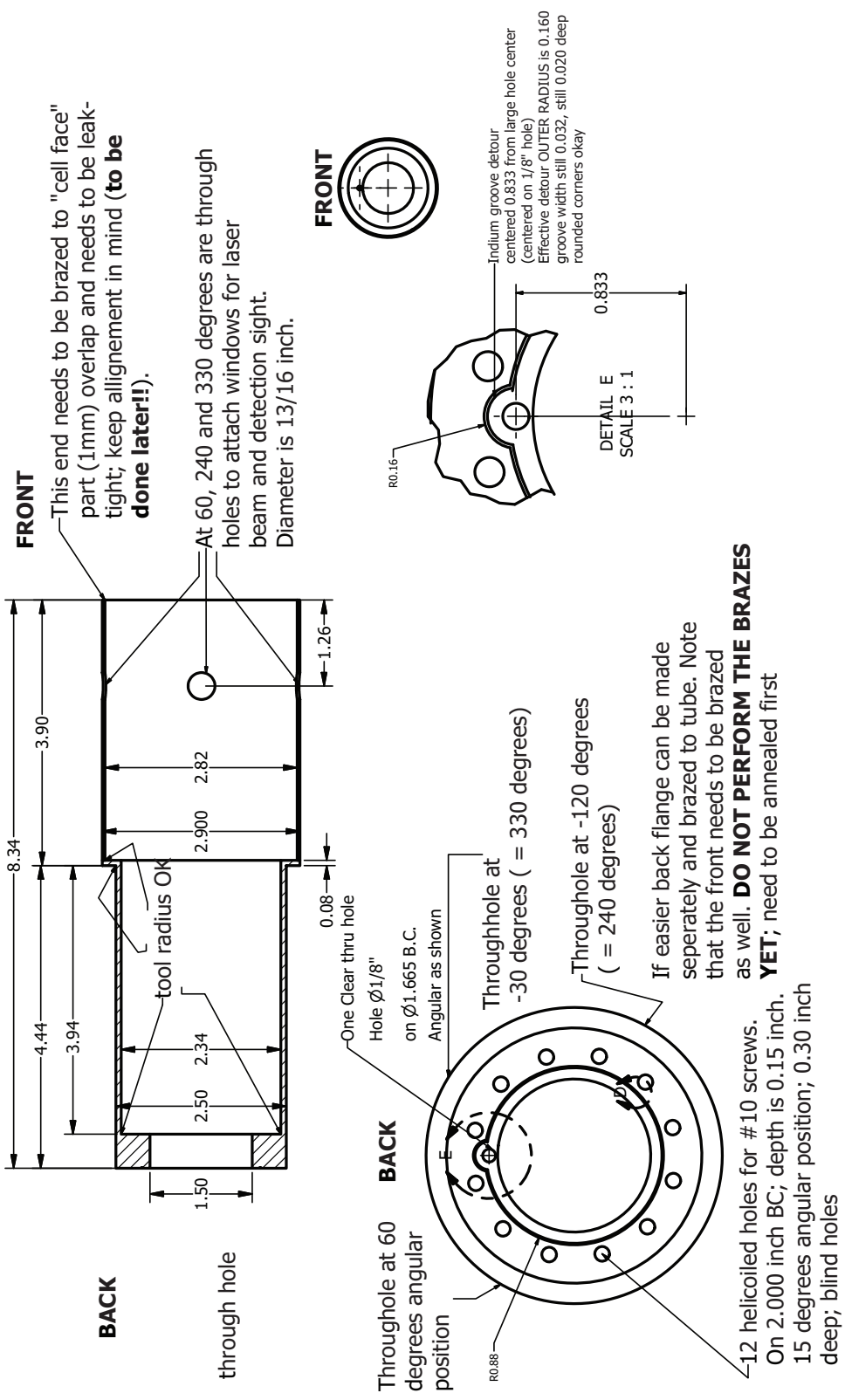

Figure A.1: Cell machine drawing. Dimensions are in inches

1. Make holes in the cell for window attachment. The holes should be large enough for the window to fit through with at least 3 mm radial clearance. For the 12.75 mm diameter window, the hole diameter is 2.0 cm.

2. Punch 1 cm diameter holes in 0.1 mm thick 3 cm by 3 cm copper foil squares.

3. Sandpaper the foil and clean it with acetone.

4. Position a foil square on top of one of the brass holders (5.04 cm diameter brass cylinder with 2.5 cm diameter hole drilled through it).

5. Position window on top of the hole in the foil. There should be a radial overlap of about 1.5 mm between window and foil.

6. Press softly on window to keep it in place. The most convenient way to do this is to let the weight of an inverted optics post (loosely held in a post holder) press the window against the foil. If an 8-32 set screw is screwed into the end of the post, the area in contact with the window will be minimized.

7. Mix Stycast 2850 epoxy with Catalyst 11 and apply it with a wooden stick to the rim of the window and the foil. A 2 mm wide ring of epoxy on the foil should surround the window.

8. Gently lift the holder with the window and foil and place the whole assembly inside an oven.

9. Heat the oven to 120 degrees Celsius for 1 hour to cure the epoxy. Stycast 2850 mixed with Catalyst 11 will not set without heating. Once cured, the epoxy

can withstand temperatures up to 200 Celsius.

DO NOT PUT FORCE ON WINDOWS AFTER THESE STEPS

10. Sandpaper the area around the holes on the cell. Clean with acetone and methanol.

11. Carefully sandpaper the area around the window on the foil (epoxy side) and clean with acetone and methanol. Do not sandpaper the epoxy.

12. Hold the cell securely in vise. Determine the exact center of the cell holes using cross wires. Repeat the center determination for the windows mounted on the foil.

13. Tape cross wires on non-epoxied side of window for alignment.

14. Cut a square of low temperature solder (InAg solder from AIM materials 97% In, 3% Ag) 3.4 cm on a side.

15. Apply flux (RMA201 paste) on the area around cell window hole and on the foil patch.

16. Place the patch of solder on the cell; adhesion to the flux should hold it in place. Cut out the solder over the cell hole with a razor blade. Smooth out the solder patch with a wooden stick to remove any ruffles.

17. Position the foil patch on top of the hole and use the cross wires to align the

window center with the cell hole center. Use 4 pieces of tape to keep patch in place once alignment is achieved.

18. Repeat steps 13 to 17 for each window.

19. Use brass rods (3 mm in diameter, 5 cm long) on both edges of the patch to clamp patch to cell without pressing the window. The rods should be parallel to the cell axis. Hold the rods in place by wrapping steel wire around the circumference of the cell and tightening it. Remove the tape which held the patches and the alignment cross wires.

20. Gently press the patch around the cell circumference using wooden sticks.

21. Heat oven to 180 degrees Celsius.

22. Place the assembled cell in the oven and heat it for twenty minutes. The solder around the patches should have melted, and the patches should lie on the cell surface with no gaps.

23. Take cell out of the oven and cool it with water.

24. Remove brass rods and steel wire.

25. Use isopropanol (non-polar solvent) and methanol (polar solvent) in turns to remove residual flux.

Appendix B

^{3}He Manual

Our helium-3 refrigerator was built by Colin Connolly. His description of the design and construction of the fridge is included here, without significant modification.

B.1 Contents

Design and Construction

. ^{3}He Fridge Parts List

. Parts Preparation

. Fridge Body Construction

. Sorption Pump (Sorb) Construction

. Gas Handling Connections

. Thermal Connections

Gas Handling System (GHS)

. GHS Components

. ^{3}He fill

. Pressure relief

. ^{3}He removal

^{3}He Fridge Operation

. Condensation Phase

. Cooling Phase

. Operation Phase

Future ^{3}He Fridge Design

B.2 Design and Construction

^{3}He Fridge Parts List:

1. Condensation Point Collar (2)
2. Burst Disk (distributor: Stafford Technical Sales, proposal #BQ032305R1; producer: BS&B Safety Systems, lot #A5070280-1)
3. Evaporator Base
4. Evaporator Housing

5. Heat Sink

6. Pump Flange

7. Pump Housing

8. Pump Tube

9. Sorption pump (Sorb)

   (a) Activated Coconut Charcoal (250 g, 8-30 mesh, Spectrum #C1221-10, pre-sifted with 42 42 wire mesh)

   (b) Bolt Guard Disc

   (c) Charcoal Can Base

   (d) Charcoal Can Fins

   (e) Charcoal Can Lower Ring

   (f) Charcoal Can Upper Ring

   (g) Wire Cloth (SS, 60 60, 53% open area, McMaster #9230T631)

10 Sorb Heater (200 W, McMaster #3618K182)

11 Thermal Link Plug

12 Tin Heat Switch (99.9985% metals basis, Alfa Aesar #11456)

13 VCR gland (4) (Swagelok #6LV-2-VCR-3-2TB7)

14 VCR female nut (4) (Swagelok #SS-2-VCR-1)

B.2.1 Parts Preparation

All copper parts were annealed in a hydrogen environment in order to improve their low-temperature conductivity. Annealing for one hour at 600 C with an H2 flow of 0.3 SCFH seemed sufficient. The Tin Heat Switch was also annealed at 200 C for 2 hours in a sealed, though not entirely oxygen-free, container.

B.2.2 Fridge Body Construction

The following steps detail how the ^{3}He fridge was actually constructed, including alterations made to the design to improve performance. Note the suggestions at the end to improve and simplify the process for the same design.

1. Braze Thermal Link Plug to Pump Flange.
2. Braze VCR Glands with VCR Nuts to Pump Flange.
3. Braze Pump Tube to Pump Housing. For all Pump Tube braze joints, minimize the amount of solder flowing on the Pump Tube away from the braze joint.
4. Face off and/or polish indium seal sealing surfaces as necessary.
5. Braze Heat Sink to Pump Tube.
6. Braze Evaporator Base to Evaporator Housing
7. Braze Evaporator Housing to Pump Tube.
8. Pre-tin Pump Tube with soft solder in a ring where it overlaps with the Condensation Point Collar.

9. Bolt on halves of Condensation Point Collar and soft solder in place.

10. Thoroughly rinse acid flux from fridge using baking soda solution.

11. Flush out inside of fridge with water and acetone multiple times to remove flux residue and clean metal surfaces.

12. With Sorb constructed and installed on Pump Flange, seal the fridge by making an indium seal between the Pump Housing and Pump Flange.

Construction suggestion: For the same design, it would be better to keep the Condensation Point Collar as one whole piece (like the Heat Sink) instead of two halves and braze it to the Pump Tube immediately following step 5 above. This will ensure a better joint and avoid soft soldering to the completed ^{3}He fridge later. The Condensation Point Collar should also have stress relief in the manner of the heat sink, i.e. fillet out to a thin section rather than rounding the corner inward. Improved condensation efficiency can also probably be improved by leaving about 2 cm of Pump Tube length between the braze joints to the Pump Housing and Heat Sink.

B.2.3 Sorption Pump (Sorb) Construction

The following steps detail how the Sorb was actually constructed, including alterations made to the design to improve performance. Note the suggestions at the end to improve and simplify the process for the same design.

1. Soft solder Charcoal Can Fins and Charcoal Can Upper Ring to Charcoal Can Base in one step.

2. Polish contact surfaces of Thermal Link Plug (brazed to Pump Flange) and underside of Charcoal Can Base. Good flatness can be achieved by sanding with the mill. Affix 600-grit sandpaper to a flat-bottomed metal piece with double-sided tape; then put the metal piece in the mill chuck and bring down spinning onto the surface to be polished. Several iterations with new sandpaper may be necessary.

3. Bolt Charcoal Can Assembly to Pump Flange with 35 in-lbs of torque, using disc springs (McMaster #9713K59) or titanium washers for additional closing force at cold temperatures.

4. Protect bolts with Bolt Guard Disc, using Mylar tape on the bolt side to prevent epoxy from dripping through #8-32 holes. An #8-32 threaded rod can be used to remove the disc to access bolts.

5. Paint all Charcoal Can Fin surfaces with Stycast 2850 epoxy (2850 FT with 24 LV catalyst, 100:7.5 ratio). Ensure good coating of all surfaces.

6. Place Charcoal Can Lower Ring on top of fins to fit snugly

7. Wrap Wire Cloth around Charcoal Can Assembly with one quarter circumference overlap. Overlap Wire Cloth 80% on gluing surfaces of Charcoal Can Lower Ring and Charcoal Can Upper Ring. Affix Wire Cloth with hose clamps to metal at top and bottom and pin down with 0.2 inch wide strips of Mylar tape at 1.0 to 1.5 inch spacing along the length of the assembly.

8. Pour in some charcoal in the center of the assembly (1/2 inch deep) and anchor

a tube of Wire Cloth at the center. The tube is 2 layers of Wire Cloth with 0.3 inch outer diameter, held in place by Mylar tape and crimped and taped shut at one end. Hold the tube in place while filling the can with charcoal, keeping the tube empty for gas flow.

9. Epoxy Wire Cloth to copper surfaces in a 1-cm band above the hose clamp at the Charcoal Can Lower Ring and below the hose clamp at the Charcoal Can Upper Ring. Be careful not to epoxy the hose clamps in place. Also add epoxy in between tape strips along the length of the assembly to hold Wire Cloth closed.

10. Epoxy a circle of Wire Cloth to Charcoal Can Lower Ring to seal charcoal inside Sorb. Wire Cloth circle should be flush with the tube in Sorb center. Add two small dots of epoxy at tube end to hold it in place, but do not block tube aperture.

11. Allow to cure for 24 hours.

12. Remove hose clamps and tape. Apply more epoxy so that all contact points between Wire Cloth and metal surfaces are held in place, as well as the entire Wire Cloth seam down the side of the Sorb. Allow 24 hours to cure.

13. Post-cure in oven at 65 C for at least 1 hour.

14. Store with desiccant until use.

Construction suggestion:

During tests there was evidence that the Sorb was becoming saturated, decreasing pumping speed and increasing the base temperature of the ^{3}He fridge. It would be difficult to get more than 250 g of charcoal into the same Pump Housing geometry; however it may be possible to improve gas flow in the current Sorb design. Good heat sinking of the charcoal can probably be sacrificed in favor of better gas access to the charcoal, especially for low heat load applications (1 mW).

B.2.4 Gas Handling Connections

The ^{3}He fridge is designed to withstand at least 10 bar of internal differential pressure. To avoid ever reaching this point, there are two pressure relief systems for recapturing ^{3}He: the relief valve and the burst disk. The relief valve is at room temperature and serves as a bypass of VX, the fill line closing valve near to the fridge. The burst disk is designed as a secondary pressure relief in the event that the fill line becomes clogged or the relief line valve is mistakenly closed. Since the burst disk is designed for a quick release of large internal pressure in the fridge, the burst line is a high-conductance 1/2 inch tube. To avoid excess fridge volume from this line, the burst disk is placed as close as possible to the fridge. The burst disk is a 1/2 inch diameter Ni 200 disk mounted in a 316LSS seal welded assembly to be used in place of a 3/4 inch VCR gasket. It was determined that a 3/16 turn was necessary beyond finger-tightening to seal the 3/4 inch VCR assembly rather than the usual 1/8 turn. Of the four VCR access points on the ^{3}He fridge Pump Flange, one is used for the fill line and one for the burst line. The other two are blanked off.

B.2.5 Thermal Connections

Cold connections must be made to three points on the ^{3}He fridge: the Sorb, the Heat Sink, and the Condensation Point. All these connections should have a very short flexible section to accommodate thermal contraction strain and not stress the annealed copper parts or Pump Tube. Thermal access to the Sorb is achieved through the Thermal Link Plug through the Pump Flange. The thermal connection to the Sorb should be minimized during Condensation Phase when the sorb is at 40 K and maximized when the Sorb is actively pumping ^{3}He during the Cooling Phase and Operation Phase. To achieve this, the Tin Heat Switch was used to passively change the thermal conductivity of the thermal connection to the Sorb. High-purity tin can exhibit an order of magnitude decrease in thermal conductivity from 4 K to 40 K. This way 100 mW can be extracted from the Sorb to a 4.2-K bath with only a 0.5-K temperature drop and keep the heat load on the bath below 1 W (instead of several watts) when the Sorb is at 40 K. The Tin Heat Switch used in testing had an area to length ratio of about 0.03 cm. Although it was annealed prior to use, it was probably strained during installation and may not have exhibited the full range of conductivity change. An active heat switch would be more ideal as long as it could maintain similar heat transfer when the Sorb is pumping. The Sorb Heater is held with Apiezon N thermally conductive grease in a tightly fitting 1/4 inch diameter hole in an annealed copper heater socket. This socket can be attached to the Thermal Link Plug with the thermal link and any thermometry, as well. The Heat Sink serves the purpose of providing an intermediate cold point between the Sorb and the Condensation Point. This avoids relying solely on the low thermal conductivity of the Pump Tube to keep

the Condensation Point cold during Condensation Phase. The Heat Sink need not be particularly well heat sunk, since there is still a 2 inch section of Pump Tube separating it from the Condensation Point. As long as this point remains below 10 K and preferably below 7 K then the condensation should be close to maximum efficiency. This implies removing 100 mW at the heat sink when in equilibrium at the end of Condensation Phase. The Condensation Point is the most important place for heat sinking on the entire fridge. Efficiency and speed of condensation are strongly correlated with how low a temperature can be achieved here during Condensation Phase. There is little to be lost in creating the strongest thermal link possible to the Condensation Point. Condensation requires extracting the enthalpy of 40 K atoms leaving the Sorb to reduce the gas temperature and pressure to the final equilibrium values, as well as removing the latent heat of vaporization from the liquefied portion. The former dominates by more than an order of magnitude, making the total amount of energy removed about 2,000 J. With a strong thermal connection there should be little difficulty in finishing Condensation Phase in 30-45 minutes of Sorb Heater voltage.

B.3 Gas Handling System (GHS)

The ^{3}He fridge was designed to test the techniques of making homemade fridges as well as create a working fridge. In this spirit, it was made modular (the indium seal and removable Sorb) and with gas access so that the ^{3}He could be removed from the fridge during testing or to put into a second-generation design. Because of this feature, the fridge was not designed to withstand the 100 bar of internal pressure from

warming up to room temperature filled with 100 STPl of ^{3}He, which must instead be vented upon warming up. Hence the gas handling system is an integral part of the fridges operation.

B.3.1 GHS Components

1. ^{3}He fridge
2. Bomb
3. Burst disk (see details in Design and Construction)
4. Cold trap
5. Dump (100 l, electropolished, Precision Cryo. DWG #050505-7)
6. Pressure gauges
   (a) Burst line mechanical gauge (Swagelok #PGI-63C-PC30-CAQX-F)
   (b) Relief line mechanical gauge (Swagelok #PGI-63C-PC30-CAQX-F)
   (c) Dump mechanical gauge (Swagelok #PGI-100C-PC15-LAOX)
   (d) Micro-Baratron (MKS #890A13TCB2GC1S)
   (e) Mini-Convectron (Helix #275905-EU)
7. Relief valve
8. Pump (external)

B.3.2 ^{3}He Fill

While the fridge is not in use at room temperature, the 100 STPl of ^{3}He is stored in the dump and warm bomb, with VN, VY and VZ closed to seal both off-panel. The rest of the GHS should be evacuated with the external pump. The ^{3}He fill of the fridge can begin at any fridge temperature, but it is convenient to fill during cooldown to 4.2 K where the filling is gradual, leaving time for the enthalpy of the 300 K gas and heat of adsorption to be steadily removed. The ^{3}He fridge is filled through a 4.2 K cold trap to remove impurities that might freeze and cause a clog.

Before ^{3}He fill:

CLOSED: VA, VB, VC, VD, VE, VF, VG, VK, VN, VX, VY, VZ

OPEN: VH, VI, VJ, VV, VW

Open VY and VN to fill GHS panel and determine initial dump pressure. With the cold trap at 4.2 K, open VC to fill the cold trap, then VB to fill the fill line, then VX to fill the fridge. Allow the fridge to cool and pump the ^{3}He from the dump. The dump pressure should drop significantly once the Sorb is below 20 K. During ^{3}He fill:

CLOSED: VA, VD, VE, VF, VG, VK, VZ

OPEN: VB, VC, VH, VI, VJ, VN, VV, VW, VX, VY

When the pressure has dropped to an acceptable value (1 mbar left in the dump is 0.1% loss of condensation efficiency), close VX and warm the cold trap. Once VX has been closed, VK and VZ should be opened for emergency pressure relief. The fridge is now filled with 100 STPl of ^{3}He and ready for operation. The paths from the dump to the relief valve and burst disk are open in case of overpressure. The dump

pressure can be monitored on the GHS gauges to l

ook for signs of overpressure venting. During operation: CLOSED: VA, VD, VE, VF, VG, VJ, VX

OPEN: VB, VC, VH, VI, VK, VN, VV, VW, VY, VZ

Its also possible to use the bomb to evacuate the fill line, cold trap, and GHS, if desired.

B.3.3 Pressure Relief

The relief valve is set to 6 bar differential pressure. The fridge has been tested to withstand pressures up to the relief pressure. If pressure cannot be vented through the relief valve, the burst disk is expected to rupture at 8.3 bar (one disk from the same lot was destructively tested to fail at this pressure at 4.2 K). The burst disk is one of 5 rated to 136 psig rupture pressure at 20 K. The PO specified 135-150 psig rupture pressure range at 4 K, however the company was unable to properly test at low temperatures. The dump pressure should be monitored to watch for overpressure venting. Small venting through the relief valve does not necessitate a ^{3}He refill, but a burst disk rupture requires that the fridge be warmed and the burst disk be replaced. If some volume vented through the relief valve needs to be put back into the fridge, this can be done by opening the fridge to the dump via the cold trap by opening VX and following the ^{3}He fill procedure above from "During ^{3}He fill."

B.3.4 ^{3}He Removal

When fridge operation is complete and the fridge is to be brought back to room temperature, the ^{3}He is allowed to flow back into the dump for storage. There are two methods designed to avoid backflow of contaminants from the dump into the cold fridge: venting the fridge through the cold trap or venting through the relief valve. When using the cold trap is not desired, its possible to simply allow the fridge to warm up with the relief line open and vent to the dump through the relief valve. Before ^{3}He removal:

CLOSED: VA, VC, VD, VE, VF, VG, VJ, VX

OPEN: VB, VH, VI, VK, VN, VV, VW, VY, VZ

Once the entire fridge has reached 20 K the pressure should begin to vent. At 60-100 K the fridge should be vented to the dump by opening VX and VA, then closing VX again. This ensures that the final room-temperature pressure in the fridge does not exceed 4-5 bar. The burst disk rupture pressure falls with increasing temperature to 7.2 bar at 200 K and 6.2 bar at 293 K, which means there is a risk of the burst disk rupturing if the fridge is allowed to warm up fully under pressure. When the fridge is warm, open VX. If using the cold trap instead to vent the fridge, the process is the same except for VB, VC and VX are always left open with VA closed. Fridge warm ($T > 200$ K) after relief valve venting:

CLOSED: VD, VC, VE, VF, VG, VJ

OPEN: VA, VB, VH, VI, VK, VN, VV, VW, VX, VY, VZ

To remove the remaining 1 bar of ^{3}He from the burst and relief lines, first close VA, VB, VY and VZ. Then cool the bomb to 4.2 K and open VC, VD and VJ. During

burst and relief lines bomb out:

CLOSED: VA, VB, VE, VF, VG, VY, VZ

OPEN: VC, VD, VH, VI, VJ, VK, VN, VV, VW, VX

Pumping with the bomb should be done until a negligible amount of ^{3}He is left outside of the bomb. The greatest ^{3}He losses (10^{-5}) will result from ^{3}He left in the fridge before the fridge is vented to air, so losses below this level should be considered acceptable. A 10^{-6} loss will result from 1 mbar left in 20 ft of 1/4 inch diameter tubing. When a small enough pressure has been reached, close VC, VD and VK. The burst and relief lines and the cold trap have now been evacuated and can be vented to air. Lastly the ^{3}He in the fridge must be evacuated. Open VA and wait for the bomb to pump ^{3}He from the Sorb. During fridge bomb out:

CLOSED: VB, VC, VD, VE, VF, VG, VK, VY, VZ

OPEN: VA, VH, VI, VJ, VN, VV, VW, VX

It can take a significant amount of time to get to small pressures in the fridge. Due to the small conductance of the VCR glands on the ^{3}He fridge Pump Flange and the large surface area of the Sorb, some ^{3}He will inevitably be lost. In testing, 24 hours of pumping with the bomb reduced the pressure in the fridge to 240 mTorr (with the bomb valve VJ closed), and further pumping did not reduce this value greatly in a reasonable amount of time. This is a loss on the order of 10^{-5}, which only begins to affect performance on the 1% level after 1000 cycles. Put another way, a 10^{-5} loss of \$15,000 of ^{3}He is 15 cents. When pumping is finished, close VX and wait a few minutes for the remainder of the GHS to reach low pressures. At this point the bomb can simply be sealed by closing VN, or vented to the dump first to keep the

storage pressure low. To vent, close VH, warm the bomb and open VY. During bomb venting:

CLOSED: VB, VC, VD, VE, VF, VG, VH, VK, VX, VZ

OPEN: VA, VI, VJ, VN, VV, VW, VY

Finally, close VY and cool the bomb again to evacuate the bomb line. After a few minutes, close VN. All the ^{3}He is now contained in the dump and bomb, and the rest of the GHS can be vented.

B.4 ^{3}He Fridge Operation

Operation of the ^{3}He fridge can be divided into three phases: Condensation Phase, Cooling Phase, and Cold Phase. At the beginning of a run, the 100 STPl of ^{3}He are adsorbed onto the charcoal Sorb. During Condensation Phase the ^{3}He atoms are driven from the Sorb by energy introduced by the Sorb Heater and condensed at the Condensation Point into liquid, which drips to the Evaporator. At the beginning of Cooling Phase, the Sorb Heater is turned off and the Sorb cools until it begins reducing the pressure in the fridge. Cold Phase begins when the Sorb and Evaporator have reached their equilibrium (coldest) temperatures and lasts until the liquid in the Evaporator has been exhausted. This ends one refrigeration cycle, at which point another cycle can be immediately started beginning with Condensation Phase.

B.4.1 Condensation Phase

The base temperature and hold time of the ^{3}He fridge are dependent on the efficiency of preparing cold liquid ^{3}He. There are two primary limiting factors de-

termining the amount of liquid ^{3}He in the Evaporator at the beginning of the Cold Phase, both of which are temperature-dependent: the volumetric efficiency and cooling efficiency. The former refers to the saturated vapor pressure of gaseous ^{3}He left in all volumes of the fridge (primarily the Sorb, Pump Tube, and Evaporator); the latter refers to the amount of liquid that must be vaporized to provide the latent heat necessary to cool the remaining liquid to the ^{3}He fridges base temperature. During Condensation Phase hot 40-K atoms leave the Sorb and bring the pressure in the fridge to about 1 to 3 bar depending on the speed of Sorb heating and strength of the Condensation Point heat sinking. These hot atoms flow through the Pump Tube past the Heat Sink and Condensation Point, which are both thermally anchored to a low temperature reservoir (less than 3 K and preferably as low as 1.5 to 2 K). Here the atoms deposit their enthalpy, which will temporarily heat the Condensation Point. At some point the flow of atoms off of the Sorb will diminish and the Condensation Point temperature will begin to fall as the gas temperature drops. When the temperature drops below the critical point of ^{3}He (3.32 K) the gas will begin to liquefy, reducing the pressure inside of the ^{3}He fridge. Reaching the critical temperature is accompanied by an increase in the cooling rate of the Condensation Point, presumably due to the declining heat capacity of the remaining gas. Condensation will continue until the pressure in the fridge has reached the saturated vapor pressure of ^{3}He. Since the vapor pressure falls exponentially with temperature, more ^{3}He will be condensed if the Condensation Point temperature (and thus the Evaporator temperature) drops significantly past the critical point. The ^{3}He that is left in the fridge in gas phase does not contribute to the cooling power of the fridge. The volumetric efficiency of

Condensation Phase gives the amount of useable liquid remaining when condensation is finished. This efficiency varies from about 80% to 95% depending on temperature and on how much ^{3}He is assumed to be left on the 40-K Sorb. Testing indicated 35 STPl remained on a 36-K Sorb at 700 mbar, which suggests that a significant amount (10-20 STPl) could stay on the Sorb at 40 K, especially at vapor pressures on the order of 1 bar (Condensation Point temperatures of 2.2 K to 3.3 K). If all the ^{3}He leaves the Sorb during Condensation Phase, then the volumetric efficiency ranges from 90% at 3.2 K to 95% at 2.2 K; if only 70% of the ^{3}He leaves the Sorb, then the efficiencies are 75% at 3.2 K and 90% at 2.2 K. Calculations from observed hold times and calculated efficiencies suggest a total desorption of 75-80% at 40 K, but the actual value is not well known. The Condensation Phase is the only time when external control is necessary. A voltage must be applied to the Sorb Heater to provide as much as 10 W initially to warm the charcoal to 40 K while providing additional heat to fuel the desorption of ^{3}He atoms. The power required to maintain the Sorb at 40 K will decrease to 4 to 4.5 W as atoms leave the Sorb. Heating the Sorb to 40 K can be done rather quickly (in 10-15 minutes), as long as the Condensation Point temperature is kept below about 6 K to prevent overpressurizing the fridge and venting gas through the relief valve. The speed of Condensation Phase depends on the strength of the thermal connection between the Condensation Point and its heat sink (i.e. pumped 4He bath, cryo-cooler, etc.), as well as the temperature of that heat sink. During testing, the Condensation Point was strongly heat sunk to a point around 2.8 K. For these conditions, a minimal Condensation Phase that reached ¿50% total efficiency (including volumetric efficiency and cooling efficiency, described below) could be per-

formed in 70 minutes. A maximal Condensation Phase with total efficiency of 65% could be performed in 2 hours. With a thermal connection half the strength of that used in testing, but sunk to a point below 2.3 K, it should be possible to condense to ¿60% efficiency in under 45 minutes and perhaps as low as 30 minutes.

B.4.2 Cooling Phase

When the Sorb Heater is turned off at the end of Condensation Phase, the Sorb temperature immediately begins to fall as heat is conducted away via the Tin Heat Switch. Meanwhile the Evaporator temperature begins to fall as the fridge pressure drops and liquid ^{3}He evaporates to maintain saturated vapor pressure. When the Sorb cools to 20 K and begins to pump strongly, then this cooling accelerates, eventually leveling out at the ^{3}He fridges base temperature. A significant fraction of the liquid ^{3}He in the Evaporator must be vaporized to provide the cooling power to lower the temperature of the remaining liquid. The latent heat of vaporization is temperature dependent, rising from zero at the critical temperature to peak near 2.1 K before dropping by a factor of about 2 from 2.1 K to 250mK. The cooling power of the liquid is thus greatest near 2.1 K and very weak near 3.32 K. The cooling rate at a given temperature is the latent heat divided by the specific heat of the liquid, which is roughly linear in temperature. This rate is used to determine the fraction of liquid remaining at the end of Cooling Phase, called the cooling efficiency. The cooling efficiency is strongly dependent on the initial liquid temperature (the Condensation Point temperature at the end of Condensation Phase), especially near 3.32K. The total efficiency is the product of the volumetric efficiency and the cooling efficiency,

and is roughly linear in the range of 3.2 K to 1.5 K, varying from 50% to 85% over that range. Cooling the Sorb takes a significant amount of time. The heat of adsorption of ^{3}He onto charcoal is about 1000 J/mole. If at the end of Condensation Phase the temperature of the Condensation Point is 2.5 K, then it will take roughly 16 STPl of evaporated ^{3}He to cool the Evaporator to its base temperature, or about 700 J of heat on the Sorb. The Sorb heat capacity has not been precisely determined, but it should take 1000-4000 J to cool the Sorb and surrounding metal from 40 K. The great majority of this heat is carried out through the Tin Heat Switch. Since the thermal conductivity of the tin increases at lower temperatures, the Sorb temperature falls roughly linearly. During testing, the Sorb cooldown took about an hour. This could be accelerated with a stronger thermal connection to cool the Sorb, but this comes at the cost of greater heat loss during Condensation Phase.

B.4.3 Cold Phase

The base temperature of the ^{3}He fridge is, in general, limited by three factors: Pump Tube conductance, Sorb pumping speed and Evaporator heat load (including parasitic heating). The conductance of the pump tube is very high and has not been noticed as a limiting factor for this fridge design. The parasitic heat load to the Evaporator is largely due to thermal conduction along the Pump Tube from the Condensation Point, which generally sits at 4.2 K. This provides about 150 W of heating. There is some evidence for another 100-200 W of parasitic heating, potentially due to poorly heat sunk electrical connections from room temperature or from 4He contamination causing superfluid film flow in the pump tube. These heat

loads are small, however, compared to the 1 mW applied heat load expected during use in experiments. Heating the evaporator vaporizes ^{3}He liquid at a steady rate, which maintains a saturated vapor pressure in the Evaporator and hence a vapor flow along the Pump Tube to the Sorb, which is expected to be at very low pressure. Each ^{3}He atom deposits its heat of adsorption on the Sorb, an amount of heat about 40 times greater than the latent heat. The heat of adsorption is carried away by copper heat sinking in the Sorb and out through the Tin Heat Switch, which has high thermal conductivity at temperatures of 4 K. If this heat sinking is not effective enough, the charcoal grains will warm until the Sorbs pumping speed is reduced. At this point there will be a non-negligible pressure near the Sorb and the Evaporator pressure will rise to maintain a constant gas flow. The liquid in the Evaporator will warm along the ^{3}He vapor pressure curve. Thus poor charcoal heat sinking limits the cooling power of the refrigerator at low temperatures. It is also possible for the charcoal to saturate when its surface area is well coated with ^{3}He. This happens first to grains near the edge of the Sorb that are best exposed to vapor. As these grains saturate, the vapor must flow deeper into the charcoal before being adsorbed. This reduces the effective conductance of the path from the Evaporator. Sorb saturation appears as a gradual rise in Evaporator temperature for a given heat load. Testing indicated that with 1 mW applied heat the Evaporator temperature rose to 400mK 3-4 hours before the liquid was exhausted, then to 500 mK with 1-2 hours remaining, and finally to 650 mK just before "running dry". When no more liquid remains in the Evaporator the temperature increases within a minute to nearly the temperature of the Condensation Point. The ^{3}He fridge test that reached a final Condensation

Point temperature of 2.9 K at the end of Condensation Phase displayed about 40 J of cooling energy before exhausting the liquid in the Evaporator. For a 1 mW applied heat load and a conservative 300 W of parasitic heat load, this corresponds to 8.5 hours of operation, or about 4.5 to 5.5 hours of operation below 400 mK. The total operation time and operation time below 400 mK can probably be increased by about 2-3 hours by bringing the Condensation Point temperature down to 2.2 K at the end of Condensation Phase.

B.5 Future ^{3}He Fridge Design

A next generation ^{3}He fridge can be improved in several ways to enhance efficiency, reduce base temperature, increase hold time, simplify operation and reduce construction cost. Some suggestions are below for general and specific applications.

B.5.1 Larger Sorb

Other ^{3}He fridge designs in the literature suggest a minimum charcoal-to-^{3}He ratio of 2.5 g/STPl. Since a large amount of ^{3}He (long hold time) and a compact geometry were both desired, the amount of charcoal in the Sorb was chosen to be this minimum; however the Sorb clearly becomes saturated towards the end of Cold Phase, causing the Evaporator to warm to unusable temperatures. It would be better to build the Sorb with a 50-100% greater charcoal-to-^{3}He ratio. In addition, better care should be taken to ensure gas access to the entire Sorb. The Charcoal Can Fins inhibit gas flow in the Sorb. Some charcoal is also buried more than 1 cm from any open surface. A fridge of similar size could be constructed with a smaller amount of ^{3}He and a more

permeable Sorb and would likely demonstrate improved Cold Phase behavior.

B.5.2 More Convenient Condensation Point Heat Sinking

Since the thermal connection to the Condensation Point is so important to the length and efficiency of Condensation Phase, the ^{3}He fridge could be improved by a design in which the Condensation Point could be easily bolted to a cold plate for dramatically improved heat sinking. Many fridge designs employ an angled Pump Tube that rises upwards out of both the Evaporator and the Pump Housing to form a "U" shape that goes through a heat exchanging Condensation Point at the top of the fridge for easy thermal anchoring. The angles reduce Pump Tube conductance, however, so this is better suited for lower expected heat loads. Improved heat sinking of the Condensation Point can also eliminate the need for a Heat Sink in the design, especially if care is taken to ensure that the Condensation Point has adequate thermal isolation from the Sorb.

B.5.3 No Gas Access

While it was useful in a diagnostic design to have gas access to the ^{3}He fridge to alter the ^{3}He content and to avoid a design capable of withstanding 100-bar internal pressures, gas access adds the unnecessary complexity of the gas handling system (GHS) and the need to evacuate the fridge in order to change its position. It would be better to build a fridge of sturdy design that can be filled from a small diameter tube which can be crimped to seal the ^{3}He inside, making the ^{3}He fridge a simple system that does not have to share plumbing access with its host experiment. This

requires important design changes, most notably a thinner-diameter or thicker-walled Pump Tube. This change will either reduce its conductance or increase the Evaporator heat load, but the overall effect will be a more useful ^{3}He fridge. A sealed design also eliminates the complexity of the high-internal-pressure indium seal.

B.5.4 Active Heat Switching

The Tin Heat Switch is useful in its simplicity, however it still allows for significant heat load from the Sorb during Condensation Phase without being as strong a thermal connection as desired during Cooling Phase and Cold Phase. An active heat switch would be ideal to switch between modes of thermal connection. Such switches can be constructed using a high surface area region that is filled with helium desorbed from a small amount of charcoal with a heater. The helium can be adsorbed quickly to turn the switch off.

B.5.5 Sorb Heater Located Opposite Heat Switch

The Sorb Heater should be located on the side of the Sorb opposite the heat switch (active or passive) so that heat applied to the Sorb goes primarily towards heating the charcoal and desorbing atoms rather than immediately being conducted away. This will make for a more energy-efficient Condensation Phase.

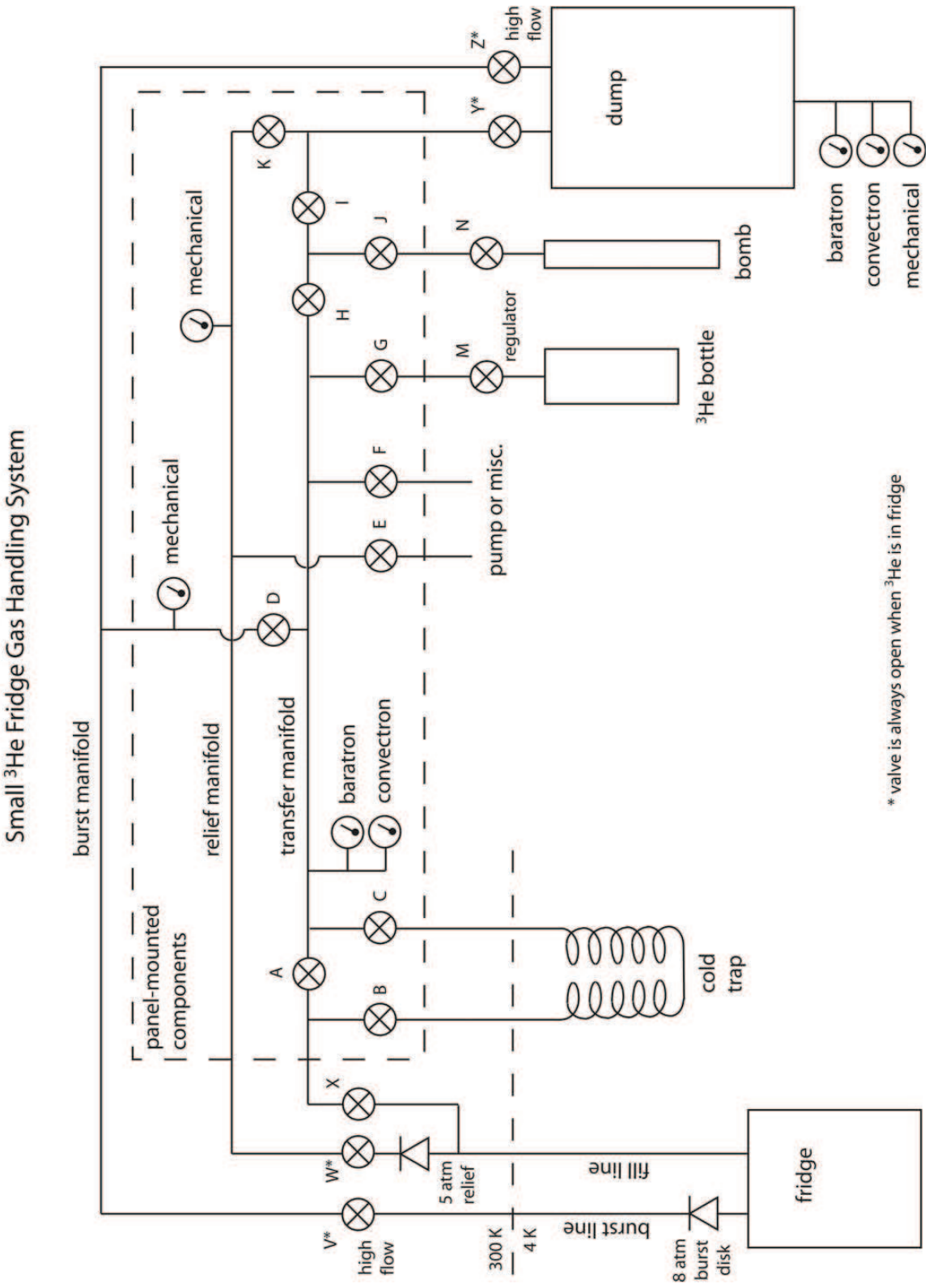

Figure B.1: Helium-3 fridge gas handling schematic.